

ENELI HÄRK

Electroreduction of complex cations
on electrochemically polished Bi(*hkl*)
single crystal electrodes



TARTU UNIVERSITY
PRESS

Institute of Chemistry, Faculty of Science and Technology, University of Tartu,
Estonia

Dissertation in physical and electrochemistry

Dissertation is accepted for the commencement of the degree of Doctor of
Philosophy in Chemistry on 24.04.2008 by the Doctoral Committee of the
Department of Chemistry, University of Tartu.

Doctoral advisor: Prof. Enn Lust, University of Tartu

Opponents: Prof. Renat R. Nazmutdinov (Kazan State Technological
University, 420015 Kazan, Republic of Tatarstan, Russia)

Prof. Andres Öpik (Tallinn University of Technology,
Tallinn, Estonia)

Commencement: 09³⁰ June 18 2008, in Tartu, 18 Ülikooli Str.,
in the University council hall

ISSN 1406–0299

ISBN 978–9949–11–870–0 (trükis)

ISBN 978–9949–11–871–7 (PDF)

Autoriõigus Eneli Härk, 2008

Tartu Ülikooli Kirjastus

www.tyk.ee

Tellimus nr. 181

CONTENTS

1. LIST OF ORIGINAL PUBLICATIONS	6
2. ABBREVIATIONS AND SYMBOLS	7
3. INTRODUCTION.....	10
4. LITERATURE OVERVIEW	12
4.1. The classical model of the reduction kinetics of the cations.....	12
4.2. Impedance spectroscopy and modelling of the charge transfer processes.....	14
4.3. Hydrogen evolution reaction kinetics	17
4.4. Fitting of impedance data.....	18
5. EXPERIMENTAL	19
6. RESULTS AND DATA ANALYSIS	21
6.1. Cyclic and rotating disc electrode voltammetry data for electroreduction of hexaamminecobalt(III) cations at Bi(<i>hkl</i>) in aqueous HClO ₄ and weakly acidified LiClO ₄ solutions	21
6.2. Kinetic analysis.....	25
6.3. Impedance spectroscopy data for electroreduction of hexaamminecobalt(III) cations at Bi(<i>hkl</i>) in aqueous HClO ₄ solutions.....	37
6.3.1. Nyquist ($-Z''$, Z')-plots and Bode plots	37
6.4. Kinetics of cathodic hydrogen evolution at the electrochemically polished Bi(001) plane.....	42
6.4.1. Modelling and parameters analysis	48
7. SUMMARY AND CONCLUSIONS	54
8. REFERENCES.....	56
9. SUMMARY IN ESTONIAN.....	60
10. ACKNOWLEDGEMENTS	64
11. PUBLICATIONS.....	65

I. LIST OF ORIGINAL PUBLICATIONS

- I R.Jäger, **E.Härk**, P.Möller, J.Nerut, K.Lust and E.Lust, The kinetics of electroreduction of hexaamminecobalt(III) cation on Bi planes in aqueous HClO_4 solutions, Journal of Electroanalytical Chemistry, 566 (2004) 217–226.
- II **E.Härk**, E.Lust, Electroreduction of Hexaamminecobalt(III) Cation on $\text{Bi}(hkl)$ Electrodes from Weakly Acidified LiClO_4 Solutions. Journal of the Electrochemical Society, 153(6) (2006) E104–E110.
- III E.Lust, J.Nerut, **E.Härk**, S.Kallip, V.Grozovski, T.Thomberg, R.Jäger, K.Lust, K.Tähnas, Electroreduction of Complex Ions at Bismuth and Cadmium Single Crystal Plane Electrodes, ESC Transactions, 1 (17) (2006) 9–17.
- IV **E.Härk**, E.Lust, Electroreduction of hexaamminecobalt(III) cations at electrochemically polished $\text{Bi}(hkl)$ using impedance spectroscopy method, (in review).
- V **E.Härk**, K.Lust, A.Jänes, E.Lust, Electrochemical impedance study of hydrogen evolution on $\text{Bi}(001)$ electrode in the HClO_4 aqueous solutions, Journal of Solid State Electrochemistry Submitted (JSEL-D-08-00102).

Author's contribution

The author performed all experiments and calculations, which were made on $\text{Bi}(111)$ and $\text{Bi}(001)$ electrodes. The author is responsible this part of manuscript, which described electroreduction of hexaamminecobalt(III) cation on $\text{Bi}(111)$ and $\text{Bi}(001)$ planes in an aqueous HClO_4 solutions [I].

The author is responsible for all electrochemical measurements, modelling, interpretation and writing the article [II, IV, V].

The author participated in the cyclic voltammetry experiments and calculations, which were made on $\text{Bi}(111)$ and $\text{Bi}(001)$ in an aqueous HClO_4 solutions and $\text{Bi}(001)$ and $\text{Bi}(01\bar{1})$ in an aqueous $\text{LiClO}_4 + \text{HClO}_4$ solutions [III].

2. ABBREVIATIONS AND SYMBOLS

a_{Ox}^0	– activity of the oxidant in the bulk solution
A	– constant characterizing the permittivity of a solvent ($A = (2\varepsilon\varepsilon_0 RT)^{-1/2}$)
ac	– alternating current
c_i, c_{Ox}^0	– concentration of the particle (ion, oxidant) in the bulk solution
cTp	– corrected Tafel plots
C	– differential capacitance
C_s	– series differential capacitance
C_{ad}	– adsorption capacitance
C_{dl}	– electrical double-layer capacitance
CPE	– constant phase element
D	– diffusion coefficient
E	– electrode potential
E^0	– equilibrium potential in the standard conditions; – formal potential
E_1^0, E_2^0	– standard redox potentials of the reactions 1 and 2
E_{min}	– potential of the minimum in the C, E -curve of the base electrolyte
E_r	– equilibrium potential
$E_{q=0}$	– zero charge potential
EC	– equivalent circuit
edl	– electrical double-layer
EP	– electrochemically polished
Eq.	– equation
F	– Faraday constant
f	– frequency of the alternating current
f_{max}	– frequency of maximum in low-frequency part of impedance complex plane plot semicircle
Fig.	– figure
$g_{\text{Ox}}; g_{\text{Red}}$	– absolute values of the specific adsorption energies of the oxidant and reductant
HER	– hydrogen evolution reaction
(hkl)	– notation of the crystallographic index
j	– imaginary unit ($j = \sqrt{-1}$)
\vec{j}	– current density of the forward reaction
j_f	– current density of the Faradaic reaction
j_k	– kinetic current density
j_0	– exchange current density

j_d	–	diffusion current density
$k_s^0 ; k_s^{(ex)}$	–	absolute and measurable rate constants of the electrochemical reaction
k_{het}	–	apparent rate constant for the heterogeneous charge transfer process
$k_f, k_b, \vec{k}_1, \overset{\leftarrow}{k}_{-1}, \vec{k}_2, \overset{\leftarrow}{k}_{-2}$	–	forward and reverse reaction rate constants
k_0, k_1^0, k_2^0	–	standard rate constant at the formal electrode potential E^0
M	–	metal
n	–	number of electrons transferred in redox reaction
oHp	–	outer Helmholtz plane
Ox	–	oxidized form of the standard system ($Ox + ne^- = Red$)
q	–	surface charge density
Q	–	CPE coefficient
R	–	universal gas constant
Red	–	reduced form of the standard system ($Ox + ne^- = Red$)
R_{ad}	–	adsorption resistance
R_{ct}	–	charge transfer resistance
R_p	–	total polarisation resistance
R_{el}	–	electrolyte resistance
r^2	–	determination coefficient
SCE	–	saturated calomel electrode
sol, ads	–	particles in solution and at adsorbed state, respectively
T	–	absolute temperature
v_1, v_2	–	rates of the reactions 1 and 2
w_a	–	average electrostatic work
zcp	–	zero charge potential
$z, (z_{Ox}, z_{Red})$	–	charge number of the particle (oxidant, reductant)
z_i	–	point charge at site i
z_{eff}	–	effective charge number of the specifically adsorbed ions
Z_f	–	Faradaic impedance
Z_{CPE}	–	impedance of CPE
Z', Z''	–	active and imaginary parts of the impedance
Z	–	magnitude of the impedance
x, y	–	molar concentration of a surface-active component and a surface-inactive electrolyte
$\alpha, \alpha_1, \alpha_2$	–	transfer coefficients
α_{app}	–	apparent transfer coefficient
α_{exp}	–	experimental transfer coefficient
α_{CPE}	–	CPE fractional exponent
γ_{\neq}	–	activity coefficient of the activated complex
Γ_i	–	Gibbs adsorption of particle i

Γ_B, Γ_s	– surface Gibbs adsorption of species B and of free adsorption sites S
Γ_{\max}	– maximal Gibbs adsorption
$\Delta c_{\text{Ox}}, \Delta c_{\text{Red}}$	– concentration fluctuations of the reacting particles in response to the ac voltage perturbation ΔE
ΔE	– amplitude of the ac potential
$\Delta \phi^{m-2}$	– potential drop across the inner-layer
ΔG_A^0	– Gibbs adsorption energy
Δj_F	– response of the Faradaic current density to the ac voltage perturbation ΔE
ε	– dielectric constant of the solvent
ε_0	– permittivity of vacuum
$\theta, (\theta_0, \theta_i)$	– surface coverage (in base electrolyte and with addition of i , respectively)
τ_{\max}	– characteristic time constant of the process
ϕ	– phase angle
ψ_1	– potential at the reaction site
ψ_d	– potential drop in the diffuse layer (outer Helmholtz plane potential)
ω	– angular frequency ($\omega = 2\pi f$); – angular velocity of the electrode

3. INTRODUCTION

The manner and extent to which the kinetics of simple electrode reactions are influenced by the nature of the metal substrate is a topic of abiding interest in electrochemistry [1].

Electroreduction kinetics of various cobalt(III) ammine complexes expected to follow outer-sphere pathway, i.e., where the reactant does not penetrate the inner solvent layer, the kinetic parameters (usually the experimental transfer coefficient) provide very useful information about the location of the reaction centre [1–13]. The substrate (electrode material) effects for the outer-sphere reactions are commonly presumed to be restricted to variations in the electrostatic work terms (double-layer effects), at least for an adiabatic process, in that the chemical and electronic properties of the metal surface should exert no direct influence on the electron transfer barrier [11–22]. It is evident from the literature that studies of the double-layer effects on the electron transfer kinetics at single crystal electrodes are important in assessing the role of the metal electronic properties on electron transfer kinetics. In recent years there has been considerable interest in fundamental studies of electron-transfer kinetics at well-defined solid single crystal electrodes [1, 5–10].

Electroreduction kinetics of $[\text{Co}(\text{NH}_3)_6]^{3+}$ have been studied at single crystal plane and polycrystal Au, Ag, Pt as well as Hg-drop electrode by many authors [1, 10, 23]. Hamelin and Weaver studied the one-electron reduction of $[\text{Co}(\text{NH}_3)_6]^{3+}$ in acidified 0.1 M NaClO_4 electrolyte, Fawcett et al. examined the same reaction in perchloric acid solutions at $\text{Au}(hkl)$ electrodes [1–5, 10].

Electroreduction of the $[\text{Co}(\text{NH}_3)_6]^{3+}$ cations has been suggested as a “model adiabatic outer-sphere” reaction and, therefore, it would give us the possibility to examine the influence of the electrical double-layer (edl) structure (i.e., dependence of edl and kinetics on the electrode material) on the electrochemical parameters for the electroreduction process at the Bi planes [1–5, 10].

The main aim of this work was to investigate the irreversible electroreduction reaction of $[\text{Co}(\text{NH}_3)_6]^{3+}$ cations at electrochemically polished $\text{Bi}(hkl)$ single crystal plane electrodes in HClO_4 and weakly acidified ($\text{pH} \sim 3.3$) aqueous LiClO_4 solutions. In the 0.01, ..., 0.1 M HClO_4 solution the hydrogen evolution reaction starts at higher negative electrode potentials and the limiting diffusion current plateaus at higher rotation velocities and scan rates were not observed [24, 25].

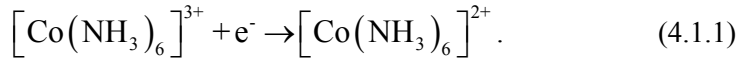
Cathodic hydrogen evolution reaction (HER) from the acidic solutions has a noticeable influence on the kinetics of electroreduction reaction of the $[\text{Co}(\text{NH}_3)_6]^{3+}$ cations on electrochemically polished Bi planes [26].

The present work also describes the influence of the crystallographic structure of the Bi single crystal plane electrodes on the charge transfer mechanism and kinetic parameters of electroreduction of the $[\text{Co}(\text{NH}_3)_6]^{3+}$ cations. The rotating disc electrode voltammetry, cyclic voltammetry and impedance spectroscopy methods have been used [27].

4. LITERATURE OVERVIEW

4.1. The classical model of the reduction kinetics of the cations

A cornerstone of Marcus theory is the notion that outer-sphere electron transfer involves separable reorganization energy components for each redox centre [28]. According to electron transfer theory, the Gibbs energy barrier is determined by three factors, namely, the inner-sphere reorganization energy, the outer-sphere reorganization energy, and the electrostatic work done to bring the reactant(s) to the reaction site. The third factor characterises the double-layer effect at electrodes. It is the most difficult to estimate because it involves a model for double-layer and assumptions about the location of the reactant within it near the electrode [29]. Electroreduction reactions of ions have extremely strong influence on the structure of edl and potential distribution near the electrode surface:



The reaction (4.1.1) is quantitatively described by the main equation of the Frumkin slow charge transfer theory for reduction

$$\vec{j} = nFk_s^{(\text{ex})} \frac{a_{\text{Ox}}^0}{\gamma_{\neq}} \exp\left[-\frac{\alpha nF(E - E^0)}{RT}\right] \text{ and} \quad (4.1.2)$$

$$k_s^{(\text{ex})} = k_s^0 \exp\left[\frac{(1-\alpha)g_{\text{Ox}} + \alpha g_{\text{Red}}}{RT}\right] \exp\left[\frac{(\alpha n - z_{\text{Ox}})F\psi_1}{RT}\right], \quad (4.1.3)$$

where k_s^0 and $k_s^{(\text{ex})}$ are the on absolute and measurable rate constants of the electrochemical reaction, respectively; α is the transfer coefficient; g_{Ox} and g_{Red} are the absolute values of the specific adsorption energies of the oxidant and reductant; a_{Ox}^0 is the activity of the oxidant in the bulk solution; z_{Ox} is the charge number of the oxidant; γ_{\neq} is the activity coefficient of the activated complex; and E^0 is the equilibrium potential at the standard conditions; R and T have their conventional meanings. In Eq. (4.1.2) the effects of the electrical double-layer are characterized by the ψ_1 potential, i.e. by the potential at the reaction site [30–32]. Double-layer effects are normally analyzed using the assumption that the reaction site located at the outer Helmholtz plane (oHp) and

the reactant and product can be represented as point charges. We assuming also the absence of the specific adsorption of reactant and products (i.e. $g_{\text{Ox}} = g_{\text{Red}} \approx 0$). The potential profile in the diffuse layer is assumed to be given by the Gouy – Chapman model. The zero charge potential (zcp) is a fundamental property of the polarizable electrode/solution interface that has been studied for many years. The value of zcp depends on the nature of metal, solvent and electrolyte. At solid electrodes the zcp is most easily found by determining the position of the diffuse layer minimum in a differential capacitance against potential curve [33]. Using differential capacitance against potential curves data obtained for base electrolyte, we can calculate the ψ_d potential values assuming that ψ_d potential can be taken equal to ψ_1 , where ψ_1 is the mean value of the potential at the plane, where the centers of charges of reacting particles are located in the transition state of the reaction [11–13, 15].

According to Gouy – Chapman theory $\psi_d = \frac{2RT}{F} \text{arcsinh} \left(\frac{q}{2A\sqrt{c}} \right)$ where q is the surface charge density in the surface inactive electrolyte solution; and $A = (2\varepsilon\varepsilon_0RT)^{-1/2}$, where the dielectric constant of the solvent is ε and ε_0 is the permittivity of vacuum.

An alternative way of writing Eq. (4.1.2) after taking the logarithm and linearizing the dependence is:

$$\ln j_k + \frac{z_{\text{Ox}}F}{RT} \psi_1 = \ln(nFk_s^0 c_{\text{Ox}}^0) - \frac{\alpha nF}{RT} (E - E_{q=0} - \psi_1), \quad (4.1.4)$$

where j_k is the kinetic current density and c_{Ox}^0 is the concentration of the oxidant in the bulk of solution. Linear dependences $\ln j_k + \frac{z_{\text{Ox}}F}{RT} \psi_1$ vs. $(E - \psi_1)$, based on Eq.(4.1.4), are called corrected Tafel plots (cTp) [34]. From the slope of the cTp it is possible to calculate the transfer coefficient and from the intercept we can calculate the rate constant for the heterogeneous reaction. According to the theory cTp's have to be linear and they must coincide if the base electrolyte concentration is varied and E is corrected with corresponding ψ_d values calculated [12, 35].

4.2. Impedance spectroscopy and modelling of the charge transfer processes

Electrochemical impedance spectroscopy (EIS) method initially applied to determination of the double-layer capacitance can be used to characterize electrode process at complex interfaces. Analysis of the system response contains information about the interface, its structure, and the reaction characteristics taking place there [36].

For the linear, casual and stable electrode system, the electrochemical impedance $Z(\omega)$ is the transfer function between the sine wave potential response function, $\Delta E(\omega)$ and the sine wave current perturbation function $\Delta I(\omega)$:

$$Z(\omega) = \Delta E(\omega) / \Delta I(\omega), \quad (4.2.1)$$

where ω is angular frequency $\omega = 2\pi f$ and f is ac frequency.

It is generally assumed that the total current density passing through the electrode/electrolyte interface is composed from the faradaic and non-faradaic part according to:

$$j_t = j_{nf} + j_f. \quad (4.2.2)$$

The faradaic part of the total current density is related to the net rate of the electron transfer reaction (if ohmic potential drop $jR \approx 0$, where R is resistance). The non-faradaic part is related to the charge density on two sides of the electrode/electrolyte interfacial region (i.e. so-called double-layer charging) [37]. The total interfacial impedance can be expressed as

$$Z_t^{-1}(\omega) = Z_{nf}^{-1}(\omega) + Z_f^{-1}(\omega). \quad (4.2.3)$$

Rate of the heterogeneous charge transfer reaction



is given by the expression

$$-j_f = nF(k_f c_{\text{Ox}} - k_b c_{\text{Red}}), \quad (4.2.5)$$

where j_f is the faradaic current density, k_f and k_b are the rate constants of forward and reverse reactions, n is the number of the electrons transferred in reaction, F is Faraday constant, c_{Ox} and c_{Red} are the concentrations of reactant (oxidizer) and product (reductant), respectively [36, 37–50].

Using impedance spectroscopy method, the current is composed of a steady-state (or direct) part (determined by the mean dc potential, E and the mean dc concentrations at the interface, c_{Ox} and c_{Red}) and an ac part Δj_f (determined by the ac perturbing signal ΔE and concentration fluctuations, Δc_{Ox} and Δc_{Red}). The faradaic impedance is given by the ratio of the Laplace transform of the ac parts of the voltage and current density [36, 38–49] respectively

$$Z_f = \{\Delta E\} / \{\Delta j_f\}. \quad (4.2.6)$$

Under equilibrium conditions the charge transfer resistance

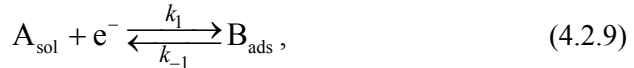
$$R_{\text{ct}} = \frac{RT}{nFj_0}, \quad (4.2.7)$$

where the exchange current density j_0 is expressed as

$$j_0 = nFk_0c_{\text{Ox}} \exp\left[-\alpha(E_r - E^0)\frac{nF}{RT}\right], \quad (4.2.8)$$

where k_0 is the potential independent rate constant of reaction and n is the number of electrons transferred.

For heterogeneous charge transfer (faradaic) reaction involving one adsorbed particle the following stages can be separated [36, 46–50]:



where the indexes sol and ads denote the particles in solution and adsorbed states, respectively. Assuming the Langmuir adsorption isotherm for B [36, 50], the rates of these reactions may be written as

$$v_1 = k_1^0 \Gamma_s a_A \exp\left[-\alpha_1(E - E_1^0)\frac{F}{RT}\right] - k_1^0 \Gamma_B \exp\left[(1 - \alpha_1)(E - E_1^0)\frac{F}{RT}\right], \quad (4.2.11)$$

$$v_2 = k_2^0 \Gamma_B \exp \left[-\alpha_2 (E - E_2^0) \frac{F}{RT} \right] - k_2^0 \Gamma_s a_C \exp \left[(1 - \alpha_2) (E - E_2^0) \frac{F}{RT} \right], \quad (4.2.12)$$

where k_1^0 and k_2^0 are the standard rate constants of these reactions; α_1 and α_2 are the transfer coefficients; Γ_B and Γ_s are the surface Gibbs adsorptions of the species B and of free adsorption sites S; a_A and a_C are the surface concentrations of A and C (assumed as equal to the bulk concentrations); E_1^0 and E_2^0 are the standard redox potentials of the reactions A and B respectively. At equilibrium potential (E_r) the net rates of both reactions are zero and the following relations are obtained:

$$\exp \left[(E_r - E_1^0) \frac{F}{RT} \right] = \frac{\Gamma_s^0 a_A}{\Gamma_B^0} = \frac{(1 - \theta_0) a_A}{\theta_0}, \quad (4.2.13)$$

$$\exp \left[(E_r - E_2^0) \frac{F}{RT} \right] = \frac{\Gamma_B^0}{\Gamma_s^0 a_C} = \frac{\theta_0}{(1 - \theta_0) a_A}, \quad (4.2.14)$$

where the index 0 indicates equilibrium conditions, and a following relation is introduced: $\Gamma_i = \theta_i \Gamma_{\max}$ (where Γ_{\max} is the maximal Gibbs adsorption [36, 50]). The total current density observed is given as

$$j_t = F(v_1 + v_2) \quad (4.2.15)$$

and the faradaic admittance is given by

$$\frac{1}{Z_f} = \frac{1}{R_{ct}} + \frac{B}{j\omega + G}, \quad (4.2.16)$$

where $j = \sqrt{-1}$ and the inverse charge transfer resistance R_{ct} is given as:

$$\frac{1}{R_{ct}} = \frac{1}{RT} \left[\alpha_1 \vec{k}_1 (1 - \theta) + (1 - \alpha_1) \overleftarrow{k}_{-1} \theta + \alpha_2 \vec{k}_2 \theta + (1 - \alpha_2) \overleftarrow{k}_{-2} (1 - \theta) \right] \quad (4.2.17)$$

and

$$B = -\frac{1}{C_{ad} R_{ct}^2} = \frac{1}{RT\Gamma_{max}} \left(-\vec{k}_1 - \vec{k}_{-1} + \vec{k}_2 + \vec{k}_{-2} \right) \times \left[\alpha_1 \vec{k}_1 (1-\theta) + (1-\alpha_1) \vec{k}_{-1} \theta - \alpha_2 \vec{k}_2 \theta - (1-\alpha_2) \vec{k}_{-2} (1-\theta) \right] \quad (4.2.18)$$

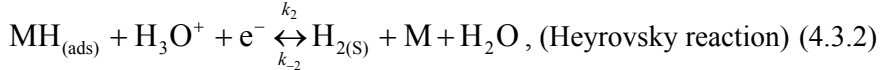
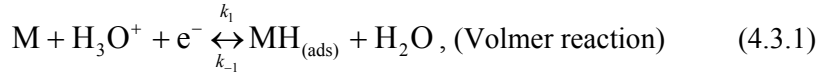
and

$$G = \frac{1}{R_{ad} C_{ad}} + R_{ct} |B| = \frac{1}{\Gamma_{max}} \left(\vec{k}_1 + \vec{k}_{-1} + \vec{k}_2 + \vec{k}_{-2} \right) = \frac{F}{\sigma_1} \left(\vec{k}_1 + \vec{k}_{-1} + \vec{k}_2 + \vec{k}_{-2} \right), \quad (4.2.19)$$

where the α_1 and α_2 are the symmetry coefficients, θ is the surface coverage. It should be noted that the quantity $F\Gamma_{max} = \sigma_1$ is the charge necessary for the total surface coverage of electrode by the reaction intermediate B . The more complicated cases, taking into account the slow diffusion step to the fractal and disc electrodes, have been discussed by Lasia in [36].

4.3. Hydrogen evolution reaction kinetics

Hydrogen evolution reaction (HER) at high cathodic overpotentials $|\eta| > 0$ from the acidic aqueous solution, to a first approximation, can be characterized by the following elementary steps [6, 11, 13, 26, 36, 51–60]:



where M is metal, H_3O^+ stands for solvated protons, $H_{2(S)}$ is the molecular hydrogen adsorbed at the surface and $MH_{(ads)}$ is the reaction intermediate, formed after electron transfer from metal M to solvated proton H_3O^+ . k_1, k_{-1}, k_2 and k_{-2} are the rate constants of corresponding reactions.

Taking into account the possible weak adsorption of reaction intermediate $MH_{(ads)}$ at the Bi electrode surface [11, 13, 51], the faradaic impedance can be mathematically simulated as Eq.(4.2.16), if we accept the so-called model for adsorption of one intermediate particle at an electrode surface [11, 13, 36, 55, 57, 59, 60].

Thus reaction (4.3.1) characterizes the formation of reaction intermediate and, depending on the chemical and crystallographic characteristics of the electrode metal, the formation of the adsorbed molecular hydrogen and

evolution probably occur through the electrochemical desorption step for Bi electrodes [61, 62].

4.4. Fitting of impedance data

Various equivalent circuits based on the various electrochemical reaction schemes have been worked out and have been tested for fitting the experimental impedance complex plane ($-Z''$ vs. Z'), Bode ($\log|Z|$ and phase angle ϕ vs. $\log f$ plots); $\log|Z''|$ vs. $\log f$ and $\log Z'$ vs. $\log f$ plots using non-linear least-squares minimization program that minimizes the sum of $(Z_m - Z_c)^2$ terms for all frequency points measured (Z_m and Z_c are the measured and calculated impedance values, respectively [63, 64]). The theoretical spectra calculated based on the arbitrarily chosen models (discussed later) have been fitted to the experimental spectra and the best-fitted case has been selected on the basis of the minimal χ^2 – function values. Additionally, the weighted sum of squares Δ^2 , as well as errors of individual parameters obtained have been analyzed [36, 37, 63, 64] keeping the number of experimental points constant for all fittings made using various equivalent circuits. The standard deviation (SD) of the fit defined as, $SD = \sqrt{\chi^2 / 2l - p}$, (where l denotes the number of points and p denotes the number of parameters of the fitting model), were calculated. Experimental impedance data for systems with weak adsorption of reactants or reaction intermediates were analyzed using the equivalent circuit (EC) (so-called Modified Armstrong-Henderson model [39] taking into account the adsorption of one intermediate particle) given in Fig. 1.

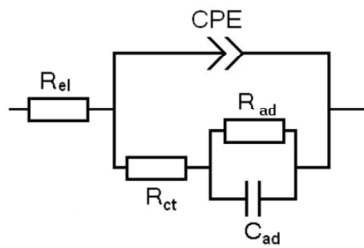


Figure 1. Modified Armstrong-Henderson model [39], where C_{dl} has been replaced by CPE, taking into account the adsorption of one intermediate particle used for fitting the experimental results: R_{el} – high – frequency solution resistance; CPE – constant phase element; R_{ct} – charge transfer resistance; R_{ad} – adsorption or partial charge transfer resistance; C_{ad} – adsorption capacitance.

5. EXPERIMENTAL

Conventional electrochemical equipment i.e. rotating disc electrode system from *Pine Instrument Company* was used for stationary and rotating disc voltammetry studies (scan rate $(5-20) \text{ mV s}^{-1}$ and rotation velocity from $(0 \text{ to } 9000) \text{ rev min}^{-1}$ were used). The impedance complex plane $-Z''$ vs. Z' (i.e., Nyquist) plots and differential capacitance vs. electrode potential dependencies have been measured using the Autolab PGSTAT 30 FRA 2 at ac frequency, f , from 0.05 Hz to $1 \cdot 10^5 \text{ Hz}$ within the region of the electrode potential $-0.85 \text{ V} < E < -0.45 \text{ V}$ vs. $\text{Hg}|\text{Hg}_2\text{Cl}_2|4\text{M KCl}(\text{SCE})$.

Electrochemically polished $\text{Bi}(hkl)$ single crystal plane electrodes were used as the working electrodes. The bismuth single crystal was grown by the modified Czochralski and Bridgman vertical methods (purity 99.99999%) at the Institute of Problems of Microelectronics Technology and Superpure Materials, Russian Academy of Sciences. Bi single crystal $\text{Bi}(hkl)$ electrode orientation has been obtained using X-ray diffraction method and the disorientation angle of plane was smaller than 0.5° . The isolation of the faces was carried out by a thin polystyrene film dissolved in toluene, covering the part of no interest, and then the sample was placed into a Teflon holder [26]. $\text{Bi}(hkl)$ single crystal electrodes were selected for detailed study in view of the very good stability (covalent bond between the Bi atoms) and wide ideal polarisation area and Bi, Cd and other metals are so-called mercury like metals with high hydrogen evolution overpotential.

Working electrode surfaces were prepared by using electrochemical polishing method ($j_{\text{pol}} \leq 1.5 \text{ A/cm}^2$) in an aqueous $\text{KI} + \text{HCl}$ solution. Thereafter the electrodes were carefully rinsed with MilliQ+ water before each set of experiments and polarized at -0.6 V vs. SCE in base electrolyte solution for 2 h.

A conventional three-electrode glass cell was used for electrochemical studies. A calomel electrode in $4 \text{ M KCl} + \text{H}_2\text{O}$ solution as the reference electrode and a large Pt counter electrode were used. The long Luggin capillary was used to connect the reference electrode to experimental part of system. The measurements were carried out at temperature $T = 298 \text{ K}$. The bubbling argon (99.999%) through or over solution were used to remove air from system during the experiment. All solutions were prepared using MilliQ+ water with resistivity $\geq 18.2 \text{ M}\Omega \text{ cm}$. Glassware was cleaned with a hot $\text{H}_2\text{SO}_4 + \text{H}_2\text{O}_2$ mixture and rinsed with MilliQ+ water before each set of measurements. HClO_4 ,

LiClO_4 , NaClO_4 and $[\text{Co}(\text{NH}_3)_6]\text{Cl}_3$ (all “Aldrich”) were of the best quality available. $[\text{Co}(\text{NH}_3)_6](\text{ClO}_4)_3$ was prepared from the corresponding chloride by precipitation with saturated sodium perchlorate and purified by triply recrystallisation of salt from water [1, 10, 23]. HClO_4 and acidified LiClO_4 were chosen as the supporting electrolytes in view of the relatively weak adsorption of perchlorate anion at bismuth. $[\text{Co}(\text{NH}_3)_6]^{3+}$ was selected for detailed study in view of the sensitivity of the supposed outer-sphere reduction kinetics to the heterogeneous reaction environment.

For the accurate determination of a precision of the experimental data, a statistical treatment of the results was carried out. A total number of the independent experiments $m \geq 4$, and at least two different electrodes with the same crystallographic orientation were used [24–27, 58]. The relative error of current density at the constant electrode potential E was not more than (5–7)%.

6. RESULTS AND DATA ANALYSIS

6.1. Cyclic and rotating disc electrode voltammetry data for electroreduction of hexaamminecobalt(III) cations at Bi(*hkl*) in aqueous HClO₄ and weakly acidified LiClO₄ solutions

The rotating disc electrode voltammetry data for the $[\text{Co}(\text{NH}_3)_6]^{3+}$ cation electroreduction at the Bi(*hkl*) electrodes in the aqueous HClO₄ solutions (from $1 \cdot 10^{-3}$ M to $1 \cdot 10^{-1}$ M) and weakly acidified LiClO₄ are displayed in Figs. 2–3.

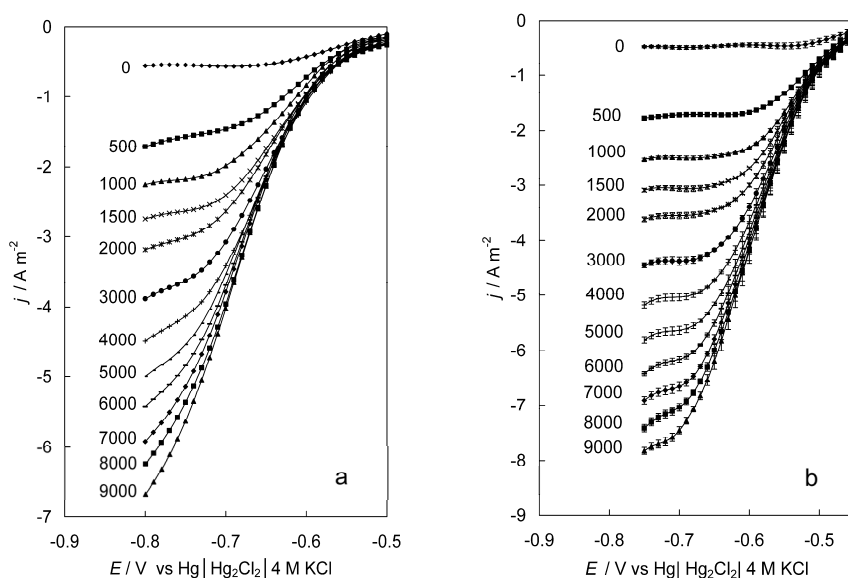


Figure 2. (a) Rotating disc voltammetry curves (scan rate 10 mVs^{-1}) for the electrochemically polished Bi(111) plane in $5 \cdot 10^{-4} \text{ M } [\text{Co}(\text{NH}_3)_6](\text{ClO}_4)_3 + 0.003 \text{ M HClO}_4$ solution at various rotation velocities $v(\text{rev min}^{-1})$, noted in figure.

(b) Rotating disc voltammetry curves (scan rate 10 mVs^{-1}) for the electrochemically polished Bi(001) plane in $5 \cdot 10^{-4} \text{ M } [\text{Co}(\text{NH}_3)_6](\text{ClO}_4)_3 + 0.003 \text{ M LiClO}_4 + 0.001 \text{ M HClO}_4$ solution at various rotation velocities $v(\text{rev min}^{-1})$, noted in figure.

Measured j vs. E plots in base electrolyte solutions show that the values of current density are practically independent of rotating speed of the electrode. However a very detailed analysis of data shows that at $E = \text{const.}$ the value of current density slightly increases with the increase of rotating speed of the electrode ($0-9000$) rev min^{-1} but these effects are very small and can be ignored to the first approximation. Unlike $\text{Au}(hkl) | \text{S}_2\text{O}_8^{2-}$ [65], $\text{Bi}(111) | \text{S}_2\text{O}_8^{2-}$ [66] and $\text{Bi}(01\bar{1}) | \text{S}_2\text{O}_8^{2-}$, hysteresis of current density between the negative and positive potential scan directions in the region of electrode potential ($-0.9 \text{ V} < E < -0.45 \text{ V}$ vs. SCE) was not observed. According to the data in Figs. 2–3 j vs. E plots can be divided into three areas. In the region of electrode potential $E < -0.6 \text{ V}$ the process is limited by the charge transfer step, from -0.6 V to -0.75 V the process is limited by the mixed kinetics (diffusion and charge transfer) and the values of current densities increase with the increase of the rotating speed of electrode. In the region of small negative surface charge densities ($E < -0.9 \text{ V}$), clear current plateaus were observed ($0-3000$) rev min^{-1}) and the values of the current density depend noticeably of the rotating velocity of $\text{Bi}(hkl)$ electrode at $E = \text{const.}$. The current of electroreduction of the $[\text{Co}(\text{NH}_3)_6]^{3+}$ cation depends noticeably on the electrode potential and on the rotation velocity (Fig. 2a), as well as on the base electrolyte composition (Fig. 2b, 3a) and $[\text{Co}(\text{NH}_3)_6]^{3+}$ cation concentrations in solution (Fig. 3b). Also the crystallographic structure of Bi plane has a influence on the electroreduction reaction rate of the hexaamminecobalt(III) cations at $\text{Bi}(hkl)$.

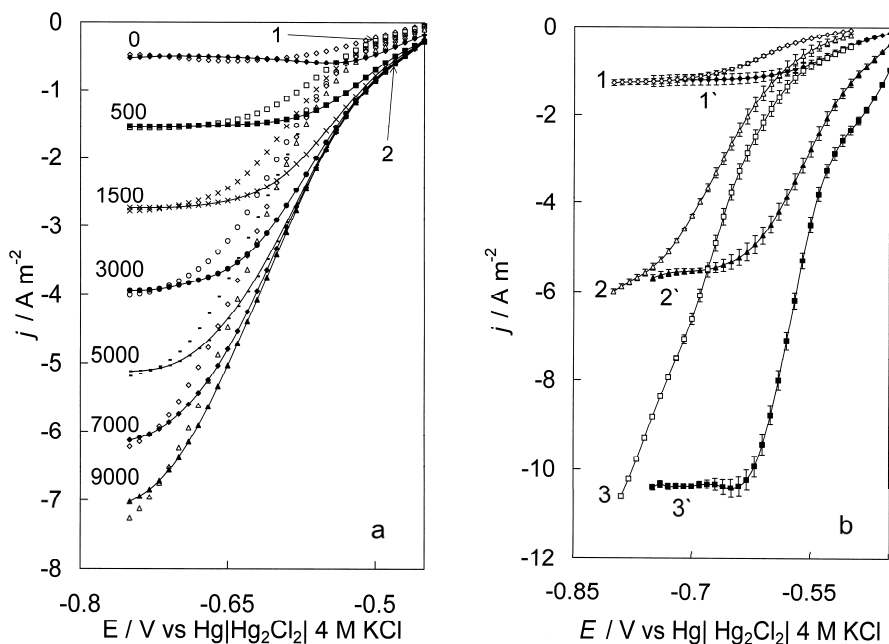


Figure 3. (a) Rotating disc voltammetry curves (scan rate 10 mVs⁻¹) for the electrochemically polished Bi(01 $\bar{1}$) plane in 5 · 10⁻⁴ M [Co(NH₃)₆](ClO₄)₃ + 0.003 M HClO₄ (open marks) and in 5 · 10⁻⁴ M [Co(NH₃)₆](ClO₄)₃ + 0.003 M LiClO₄ + 0.001 M HClO₄ (filled marks) solutions at various rotation velocities v (rev min⁻¹), noted in figure. (b) Rotating disc voltammetry curves (scan rate 10 mVs⁻¹) for the electrochemically polished Bi(001) plane at $v = 5000$ rev min⁻¹ in 0.01 M HClO₄ (1, 2, 3) and in 0.01 M LiClO₄ + 0.001 M HClO₄ (1', 2', 3') solution with different additions of [Co(NH₃)₆](ClO₄)₃ (M): 1, 1' – 0.0001; 2, 2' – 0.0005; 3, 3' – 0.001. j vs. E curves for Bi(01 $\bar{1}$).

Noticeable increase of current density takes place at $E > -0.85$ V and this is probably caused by the parallel cathodic hydrogen evolution reaction [25, 26]. The influence of the cathodic hydrogen evolution reaction has been studied and will be discussed separately. The influence of composition of the base electrolyte at fixed total electrolyte concentration is noticeable in the region of mixed kinetics (Fig. 3a), i.e., the reduction current is higher for solutions with the addition of LiClO₄ in solution, but in the region of limiting diffusion current, the reduction current is independent of the chemical composition of the

base electrolyte studied. Thus, the influence of the hydrogen evolution kinetics is not important in neutral base electrolyte solution where $[\text{Co}(\text{NH}_3)_6]^{3+}$ has been studied.

Thus, there is no quick hydrogen evolution from the weakly acidified base electrolyte solution in this limited region of the electrode potentials, and mainly the electroreduction of $[\text{Co}(\text{NH}_3)_6]^{3+}$ takes place [25]. In the region of potentials $-0.9 \text{ V} < E < -0.7 \text{ V}$ clear current plateaus were established. The limiting current density j_d at constant potential measured at the rotating electrochemically polished Bi(*hkl*) rotating disc electrode was found to fit very well to the Levich $(j \text{ vs. } \omega^{1/2})$ plot ($0.997 \leq r^2 \leq 0.999$):

$$j_d = 0.620 n_i F \nu^{-1/6} D^{2/3} \omega^{1/2} c_i, \quad (6.1.1)$$

where n_i is the number of electrons consumed in the electroreduction of the ion i ; ν is the kinematic viscosity; D is the diffusion coefficient; ω is the angular velocity of the electrode and c_i is the bulk concentration of the discharging ion. Taking $n_i = 1$ and $\nu = 0.01 \text{ cm}^2 \text{ s}^{-1}$ [2, 10, 24, 67], the values of the diffusion coefficient for the $[\text{Co}(\text{NH}_3)_6]^{3+}$ cation have been calculated ($D = 6.2 \cdot 10^{-6} \text{ cm}^2 \text{ s}^{-1}$ for Bi(111) [24] and $D = 6.6 \cdot 10^{-6} \text{ cm}^2 \text{ s}^{-1}$ for Bi(01 $\bar{1}$) [25] in the $1 \cdot 10^{-2} \text{ M}$ HClO_4 and $1 \cdot 10^{-2} \text{ M}$ $\text{LiClO}_4 + 1 \cdot 10^{-3} \text{ M HClO}_4$ solution respectively), slightly decreasing with the increase of the base electrolyte concentration, in a good agreement with the literature data [10]. Therefore, in the region of potentials $-0.85 \text{ V} < E < -0.70 \text{ V}$ the electroreduction of the $[\text{Co}(\text{NH}_3)_6]^{3+}$ cation on the electrochemically polished Bi single crystal planes is mainly limited by the rate of diffusion of the $[\text{Co}(\text{NH}_3)_6]^{3+}$ cations to the electrode surface, in a good agreement with literature data [68], where the diffusion-limited process has been observed at slow potential scan rates. For more concentrated HClO_4 solutions ($c \geq 2 \cdot 10^{-2} \text{ M}$) there is no well exposed current plateau in the $j \text{ vs. } E$ curves, likewise for more concentrated $\text{LiClO}_4 + 1 \cdot 10^{-3} \text{ M HClO}_4$ solutions. The small increase of current density at $E < -1.0 \text{ V}$ is mainly caused by the hydrogen evolution from more concentrated solutions and

blocking of the electrode surface with the adsorbed molecular hydrogen [24, 26, 51]. Quantitative analysis for more concentrated $\text{LiClO}_4 + 1 \cdot 10^{-3} \text{M HClO}_4$ and $[\text{Co}(\text{NH}_3)_6]^{3+} | \text{Bi}$ plane systems is possible in the wider potential region, compared with the aqueous HClO_4 base electrolyte system [24, 25].

6.2. Kinetic analysis

The kinetic parameters for the heterogeneous electroreduction reaction of the $[\text{Co}(\text{NH}_3)_6]^{3+}$ cation on the $\text{Bi}(001)$, $\text{Bi}(111)$ and $\text{Bi}(01\bar{1})$ planes has been established and results have been compared with the data for the $\text{Ag}(110)$, $\text{Au}(hkl)$ and Hg electrodes [1–5].

The current density j , being proportional to the rate of the heterogeneous electroreduction of the $[\text{Co}(\text{NH}_3)_6]^{3+}$ cations, occurring at high overvoltage η for the $\text{Bi}(111)$ electrode, is defined by Eq. (6.2.1)

$$\ln j \approx \ln j_k = \text{const} + \ln c_o + \frac{(\alpha n - z_{\text{Ox}}) F \psi_1}{RT} - \frac{\alpha F n E}{RT}, \quad (6.2.1)$$

where j_k is the cathodic kinetic current density; α is the transfer coefficient; z_{Ox} is the charge number of oxidizer; E is the electrode potential and the adsorption energies of oxidized and reduced forms (g_{Ox} and g_{Red} , respectively) have been taken as constants. The values of kinetic current density at constant potential were obtained from the linear Koutecky – Levich plots according to Frumkin, Aikazyan, Tedoradze and Koutecky method ($0.997 \leq r^2 \leq 0.999$) [1, 11–16, 69, 70]

$$\frac{1}{j} = \frac{1}{j_k} + \frac{1}{j_d}. \quad (6.2.2)$$

It should be noted that for the interpretation of the experimental results Eq. (6.2.2) was derived the first time by Frumkin and Aikazyan [69] and thereafter used by Frumkin and Tedoradze [70]. The apparent rate constant for the heterogeneous electroreduction reaction of the $[\text{Co}(\text{NH}_3)_6]^{3+}$ cations, k_{het} , is defined by Eq. (6.2.3):

$$j_k = nFk_{\text{het}}c_{\text{Ox}}, \quad (6.2.3)$$

where the influence of overvoltage has not been taken into account. The k_{het} vs. $\phi_m = E - E_{q=0}$ dependences are displayed in Fig. 4a,b (where ϕ_m is the rational potential and $E_{q=0}$ is the zero charge potential in the base electrolyte solution equal to -0.67 V vs. SCE for $\text{Bi}(001)$ and $\text{Bi}(01\bar{1})$ electrodes in $0.05 \text{ M LiClO}_4 + 1 \cdot 10^{-3} \text{ M HClO}_4$ aqueous solution [71, 72]) obtained at different base electrolyte concentrations for $5 \cdot 10^{-4} \text{ M } [\text{Co}(\text{NH}_3)_6]^{3+}$ system, coincide at $\phi_m = 0$.

It must be pointed out that for $\text{Bi}(hkl) | x \text{ M LiClO}_4 + 0.001 \text{ M HClO}_4 + y \text{ M } [\text{Co}(\text{NH}_3)_6]^{3+}$ system, it is possible to obtain directly the so-called double-layer corrected value of the rate constant k_{het}^0 (given in Table 1) as the Frumkin correction [11–16, 34] (i.e., the diffuse layer potential ψ_d correction) is zero at $E_{q=0}$, if we assume that the reaction site lies at the outer Helmholtz plane and discreteness of charge effects is negligible [1, 3–6, 10–13, 15, 24–28, 64, 67, 69, 70, 73, 74].

Table 1. Kinetic data for $[\text{Co}(\text{NH}_3)_6]^{3+}$ ion electroreduction on various electrodes [24, 25, 27].

Electrolyte	Electrode	α_{exp}	z_{eff}	α_{app}	$k_{\text{het}}^0 / \text{cm s}^{-1a}$
0.06 M $\text{LiClO}_4 + 0.001 \text{ M HClO}_4$	$\text{Bi}(001)$	0.55 ± 0.02	0.56 ± 0.03	0.56 ± 0.02^b	$7.1 \times 10^{-3} (\pm 0.3)^c$
	$\text{Bi}(01\bar{1})$	0.50 ± 0.02	0.53 ± 0.03	0.54 ± 0.02^b	$6.2 \times 10^{-3} (\pm 0.3)^c$
0.06 M HClO_4	$\text{Bi}(001)$	0.45 ± 0.02	0.54 ± 0.03	0.55 ± 0.02^b	$5.5 \times 10^{-3} (\pm 0.3)^c$
	$\text{Bi}(111)$	0.46 ± 0.02	-	0.56^b	$4.5 \times 10^{-3} (\pm 0.3)^c$
	$\text{Bi}(01\bar{1})$	0.44 ± 0.02	-	0.58^b	$2.1 \times 10^{-3} (\pm 0.3)^c$

^a k_{het}^0 rate constant, corrected for the electrical double layer effect and not corrected for the overvoltage values different for various electrodes.

^b α_{app} values obtained at $E_{q=0}$ with addition of $5 \cdot 10^{-4} \text{ M } [\text{Co}(\text{NH}_3)_6]^{3+}$ in base electrolyte solution.

^c k_{het}^0 values obtained at the rational electrode potential $\phi_m = 0 \text{ V}$ for $0.06 \text{ M LiClO}_4 + 0.001 \text{ M HClO}_4$ or 0.06 M HClO_4 aqueous solution with addition of $5 \cdot 10^{-4} \text{ M } [\text{Co}(\text{NH}_3)_6]^{3+}$.

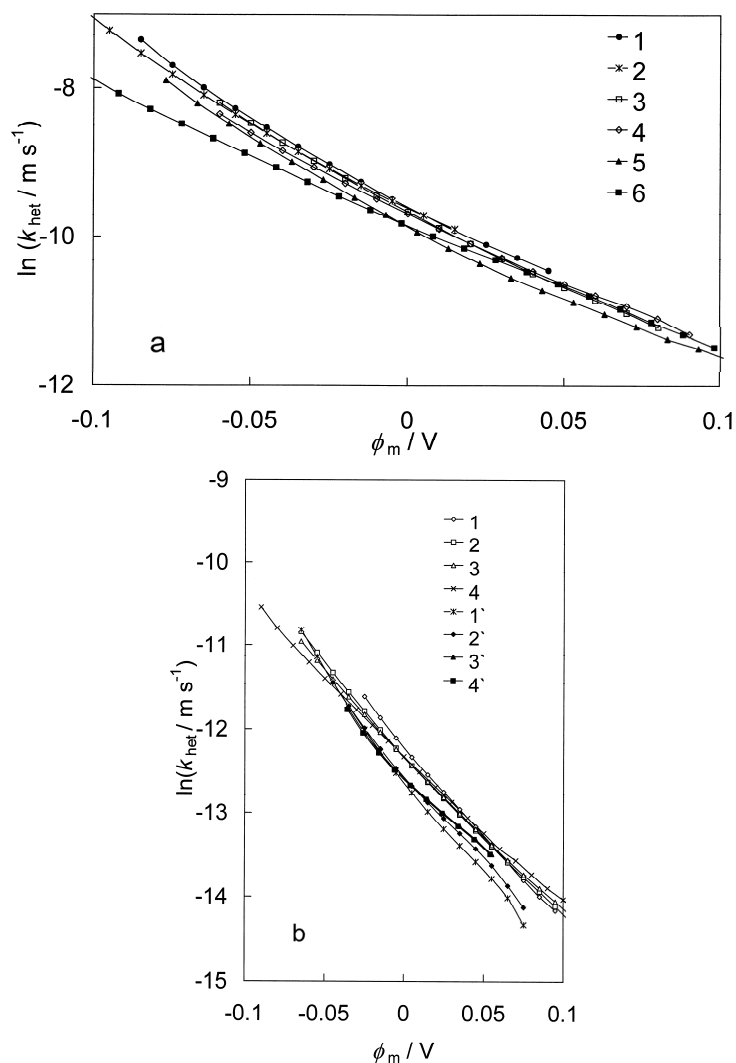


Figure 4. (a) $\ln k_{\text{het}}$ vs. rational electrode potential curves for various electrochemically polished electrodes: Bi(001) – (1; 2; 5; 6) and Bi(01 $\bar{1}$) – (3; 4) in $5 \cdot 10^{-4} \text{ M } [\text{Co}(\text{NH}_3)_6](\text{ClO}_4)_3$ with different additions of the base electrolyte : 1, 3 – $0.02 \text{ M LiClO}_4 + 0.001 \text{ M HClO}_4$ and 2, 4 – $0.06 \text{ M LiClO}_4 + 0.001 \text{ M HClO}_4$; 5 – 0.02 M HClO_4 and 6 – 0.06 M HClO_4 .

(b) $\ln k_{\text{het}}$ vs. ϕ_m vs. curves for the electrochemically polished Bi(001) electrode in $0.01 \text{ M LiClO}_4 + 0.001 \text{ M HClO}_4$ (1, 2, 3, 4) and in 0.01 M HClO_4 (1', 2', 3', 4') solutions with various additions of $[\text{Co}(\text{NH}_3)_6](\text{ClO}_4)_3$ (M): 1, 1' – 0.0005 ; 2, 2' – 0.00065 ; 3, 3' – 0.00075 ; 4, 4' – 0.001 .

Table 1 summarizes rate data for one-electron reduction of $[\text{Co}(\text{NH}_3)_6]^{3+}$ reactant in two different aqueous environments, including three different electrode interfaces and compared with other details can be found in original references [1, 10]. For more concentrated $[\text{Co}(\text{NH}_3)_6]^{3+}$ solutions ($c \geq 1 \cdot 10^{-3} \text{ M}$), the value of k_{het}^0 , obtained for the $\text{Bi}(hkl)$ planes at $\phi_m = 0$ is somewhat lower than that for less concentrated $[\text{Co}(\text{NH}_3)_6]^{3+}$ solution and the weak adsorption of the $[\text{Co}(\text{NH}_3)_6]^{3+}$ cations seems to be possible [68]. This effect is more pronounced for the electrochemically most active $\text{Bi}(01\bar{1})$ plane, taking into account the specific adsorption of cations and anions from various solutions [71, 72, 75–83]. Thus, in a good agreement with Compton et al data [68], the weak electrostatic adsorption of $[\text{Co}(\text{NH}_3)_6]^{3+}$ cation is possible, increasing with the increase of the negative surface charge density at the $\text{Bi}(hkl)$ interface [24, 25]. For all Bi planes studied, the value of the corrected rate constant at $E_{q=0}$, k_{het}^0 is practically independent of $[\text{Co}(\text{NH}_3)_6]^{3+}$ concentration if $c_{[\text{Co}(\text{NH}_3)_6]^{3+}} \leq 1 \cdot 10^{-3} \text{ M}$. The values k_{het}^0 for $\text{Bi}(hkl)$ in $x \text{ M LiClO}_4 + 0.001 \text{ M HClO}_4$ are weakly higher than those for the HClO_4 base electrolyte solutions, indicating the weak influence of the cation nature and solvation energy of ions on the electroreduction rate of the $[\text{Co}(\text{NH}_3)_6]^{3+}$ cations.

When the redox reaction is “simple“, that is, when it occurs by an outer-sphere mechanism, the kinetic parameters, especially the experimental transfer coefficient, provide information about the location of the reaction site [3]. The values of experimental transfer coefficient, α_{exp} , can be obtained from data in Fig. 4a,b which is defined as

$$\alpha_{\text{exp}} = - \frac{RT}{F} \frac{d \ln k_{\text{het}}}{dE}. \quad (6.2.4)$$

The slope of a plot of $\ln k_{\text{het}}$ against ϕ_m gives the values of α_{exp} , given in Table 1. The values of α_{exp} for

$5 \cdot 10^{-4} \text{ M } [\text{Co}(\text{NH}_3)_6]^{3+} + x \text{ M LiClO}_4 + 0.001 \text{ M HClO}_4$ system are only

somewhat higher than 0.5 and practically independent of the plane studied. Thus, to a first approximation, for more diluted $[\text{Co}(\text{NH}_3)_6]^{3+}$ solutions there are only very small deviations from the classical Frumkin slow discharge theory [1, 11–16]. These observations led to conclude that the reaction site for the $[\text{Co}(\text{NH}_3)_6]^{3+}$ complex cations is only very slightly closer to the electrode than the oHp.

The voltammetry data for rotating $\text{Bi}(hkl)$ planes have been corrected for the edl effects using, to a first approximation, the classical Frumkin approach [1, 3, 11–16, 24, 34]. The absence of the specific adsorption of base electrolyte cations and anions was assumed within the concentration range of interest in accordance with the charge density, q vs. potential curves calculated by integration from the C vs. E curves (extrapolated to ac frequency $f \rightarrow 0$) (Fig. 5) for the pure base electrolyte solution with different concentrations.

Experimental data show that the dependence of the charge density q on the potential drop across the inner-layer ($\Delta\phi^{m-2} = \phi_m - \psi_d$) is very small at different c_{LiClO_4} . Thus, it can be concluded that the specific adsorption of the ClO_4^- ions is practically absent at the Bi planes over the range of charge densities and concentrations of ClO_4^- anions studied. Double-layer effects are normally analyzed using the assumption that the reaction site located at the oHp. The potential at the oHp, ψ_d , was estimated using the Gouy-Chapman theory with consideration of the reactants and products in estimation of the diffuse layer correction

$$q^2 = A^2 \sum_i c_i \left[\exp\left(-z_i \frac{F}{RT} \psi_d\right) - 1 \right], \quad (6.2.5)$$

where q is the charge density of the electrode, c_i is the concentration of ion i whose charge is z_i ; $A^2 = 2RT\varepsilon\varepsilon_0$. If c_s and c_d are the concentrations of the supporting electrolyte and reactant, respectively then, for the 1:1 supporting electrolyte and 3:1 reactant, Eq. (6.2.5) can be rewritten as

$$q^2 / A^2 = c_s \Phi + c_d \Phi^3 + (c_s + 3c_d) / \Phi - 2c_s - 4c_d, \quad (6.2.6)$$

where $\Phi = \exp\left[-F\psi_d (RT)^{-1}\right]$. Plots of ψ_d against rational potential ϕ_m for the supporting electrolyte at different c_{LiClO_4} with addition of $[\text{Co}(\text{NH}_3)_6]^{3+}$ ions calculated according to Eq. (6.2.7) are given in Fig. 5b.

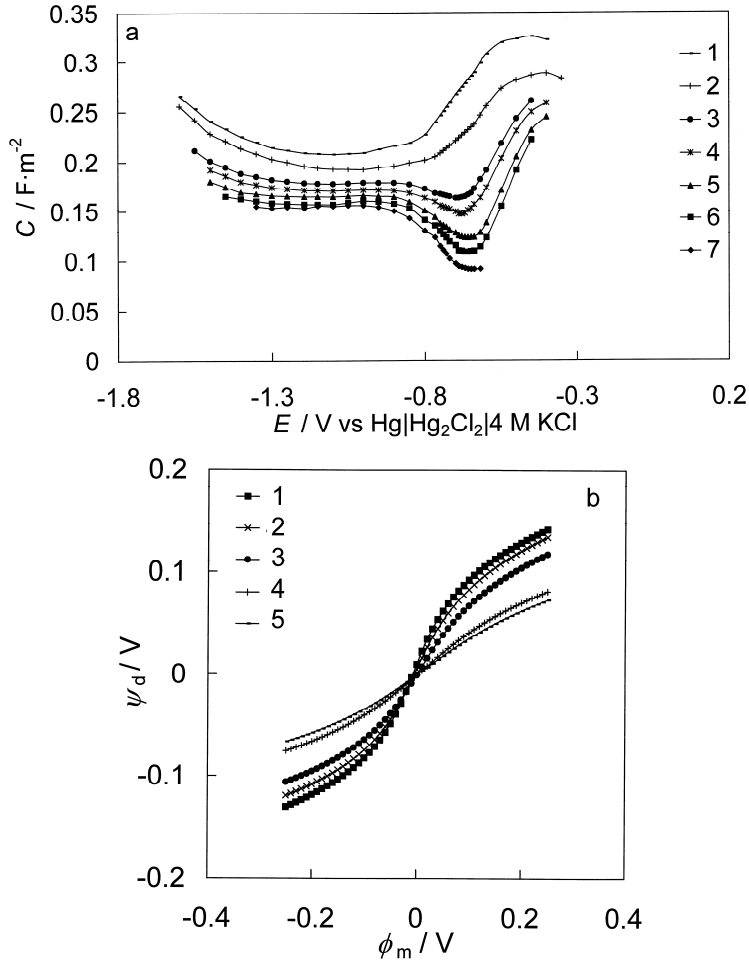


Figure 5. Differential capacitance (at $\omega = 0$) vs. electrode potential curves **(a)** and potential drop in the diffuse layer vs. rational electrode potential curves **(b)** for electrochemically polished $\text{Bi}(001)$ electrode in LiClO_4 solution with concentrations (M) (a): 1 – 0.1; 2 – 0.05; 3 – 0.01; 4 – 0.007; 5 – 0.003; 6 – 0.002; 7 – 0.001; and (b): 1 – 0.002; 2 – 0.006; 3 – 0.02; 4 – 0.04; and 5 – 0.1.

The double-layer corrected Tafel plots (cTp) [34] at $E \neq E_{q=0}$ and transfer coefficients [12], α_{app} , to a first approximation, have been obtained according to the Gouy – Chapman theory and Frumkin analysis scheme [1, 2, 10–16] using the following Eq. (6.2.7)

$$\ln k_{\text{het}} + \frac{z_{\text{eff}} F}{RT} \psi_d = \ln k_{\text{cor}}^0 - \frac{\alpha_{\text{app}} F}{RT} (\phi_m - \psi_d), \quad (6.2.7)$$

z_{eff} is the charge number of the reactant; and ψ_d is the average potential across the diffuse layer in the absence of specific adsorption of anions taken to the first approximation equal to the ψ_1 potential (mean value of the potential in the plane in which are located the centers of the charges of reacting particles in the transition state of the reaction [12].

In the case of HClO_4 base electrolyte with addition of $[\text{Co}(\text{NH}_3)_6]^{3+}$ complex cations, the cTp [34] calculated for the bismuth $(01\bar{1})$, (001) and (111) planes are presented in Figs. 6a and b. These plots represent the corrections for the double-layer, assuming that the reactant ions are the point charges with the probable effective charges $z_{\text{eff}} = 2$ (Fig. 6b) and $z_{\text{eff}} = 1$ (Fig. 6a) that are being reduced at the outer Helmholtz plane (oHp).

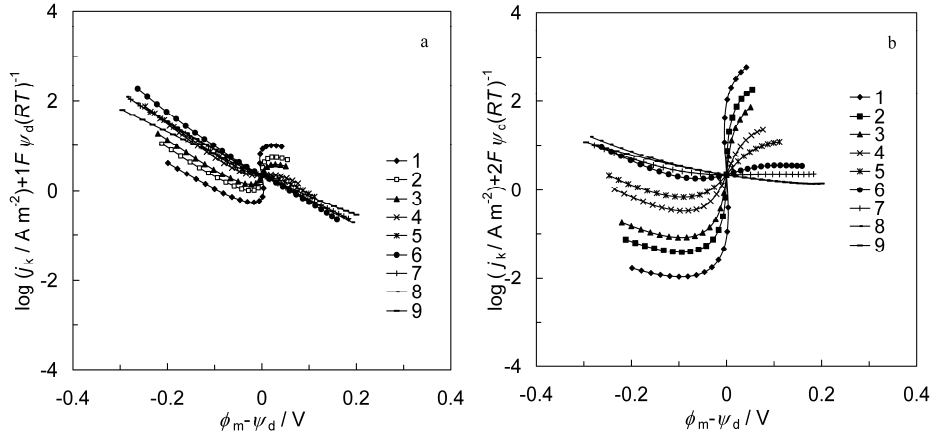


Figure 6. Corrected Tafel plots [34] calculated at **(a)** $z_{\text{eff}} = 1$ and **(b)** $z_{\text{eff}} = 2$ for $\text{Bi}(111)$ $5 \cdot 10^{-4} \text{ M } [\text{Co}(\text{NH}_3)_6]^{3+}$ in HClO_4 aqueous solution with concentrations (M): 1 – 0.001; 2 – 0.002; 3 – 0.003; 4 – 0.006; 5 – 0.01; 6 – 0.02; 7 – 0.04; 8 – 0.06; 9 – 0.1.

The cTp's [34] for the Bi planes are nonlinear in the region of $E_{q=0}$, irrespective of the assumed value of the effective charge on the reactant. In this region of potentials ($E \sim E_{q=0}$), the double-layer effect is expected to be complicated at Bi planes investigated, because the surface charge density exchanges and the species with the various effective charges can be simultaneously reduced. The experimental data in Figs. 6a and b show that the classical reaction model [12–16] is not valid for the Bi planes because the so-called “microscopic double-layer effects” i.e. the actual charge distribution within the reaction couple has not been taken into account [2, 10, 18–22]. Another reason for the effect established in Figs. 6a and b might be the fact that the reaction site is not located at the oHp thus accordingly $\psi_1 \neq \psi_d$. The cTp for $\text{Bi}(hkl) \left| x \text{M LiClO}_4 + 0.001 \text{M HClO}_4 + y \text{M} \left[\text{Co}(\text{NH}_3)_6 \right]^{3+} \right.$ have been calculated, assuming that the reactant ions are the point charges with the various probable effective charges z_{eff} that are being reduced at the oHp. For determination of the most probable effective charge value the method proposed by Fawcett [84, 85] and Boda [86] has been used. The $d(\ln k_{\text{het}})/d(\phi_m - \psi_d)$ against $(\phi_m - \psi_d)$ dependences were constructed (Fig. 7) and differentiated to obtain the z_{eff} values (given in Table 1 and Fig. 7b).

According to these data z_{eff} is independent of c_{LiClO_4} but weakly decreases with increasing c_{HClO_4} , indicating the different influence of HClO_4 and LiClO_4 base electrolyte solutions on the charge transfer kinetics. The values of z_{eff} depend on the plane studied. The positive values of z_{eff} for $\text{Bi}(hkl)$ in the dilute base electrolyte solutions show that the ion pairing is not important in determining the effective charge on the reactant at $c_{\text{ClO}_4^-} < 3 \cdot 10^{-3} \text{ M}$ [9]. Therefore, the dependence of z_{eff} on Bi plane studied shows that the inner-layer structure and comparatively weak adsorption of ClO_4^- [34, 70–72] at the $\text{Bi}(01\bar{1})$ surface have a very important role in the charge transfer characteristics of the less hydrophilic metals as Bi [66, 80, 87].

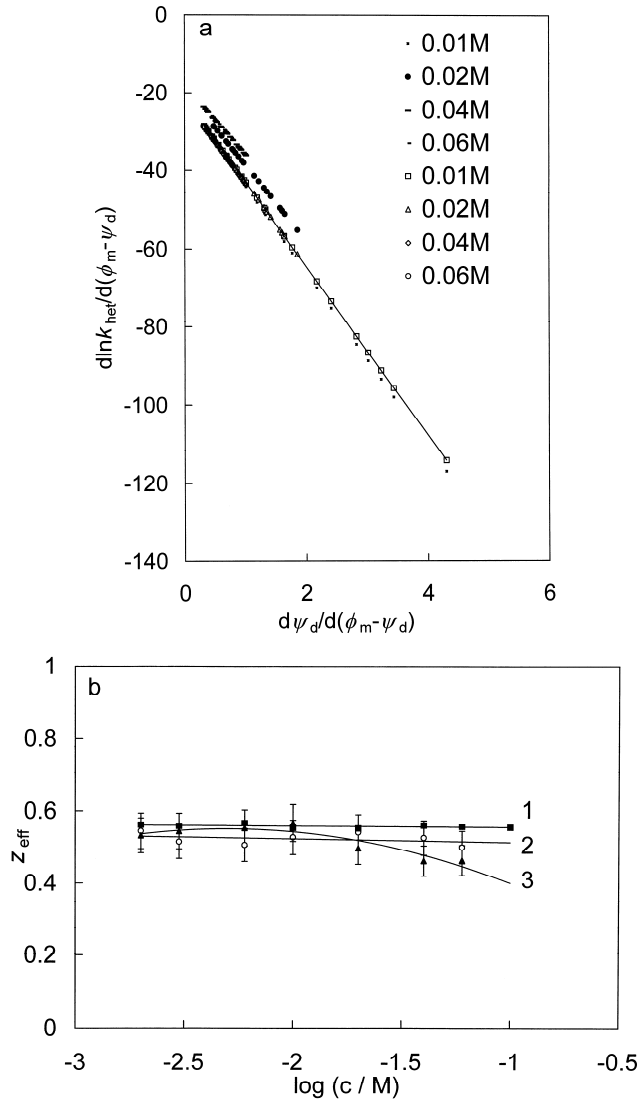


Figure 7. (a) $d(\ln k_{\text{het}}) / d(\phi_m - \psi_d)$ vs. $d\psi_d / d(\phi_m - \psi_d)$ dependences for Bi(001) (filled marks) and Bi(01 $\bar{1}$) planes (open marks) in x M LiClO₄ + 0.001 M HClO₄ + $5 \cdot 10^{-4}$ M [Co(NH₃)₆](ClO₄)₃ solution at x (M), noted in figure. **(b)** Dependence of effective charge of particle z_{eff} on base electrolyte concentration for various electrochemically polished Bi planes: for Bi(001) (1;3) and Bi(01 $\bar{1}$) (2) in $5 \cdot 10^{-4}$ M [Co(NH₃)₆](ClO₄)₃ with different additions of the base electrolyte: c M LiClO₄ + 0.001 M HClO₄ (1;2) or c M HClO₄ (3).

The cTp's for $x\text{M LiClO}_4 + 0.001\text{M HClO}_4$ solutions are linear and a good agreement of the corrected current values has been established (Fig. 8).

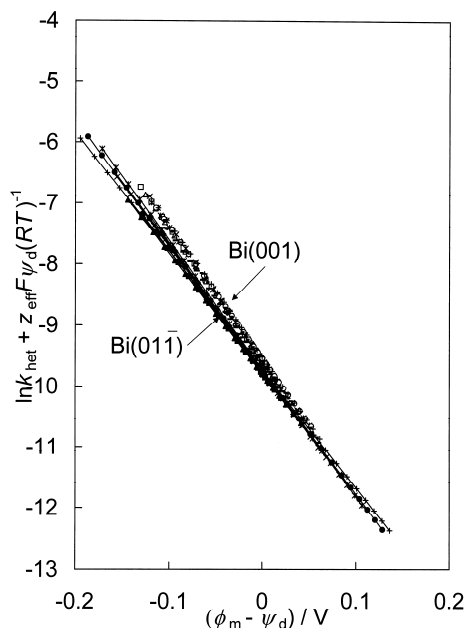


Figure 8. Corrected Tafel plots calculated at $z_{\text{eff}} = 0.52$ for various electrochemically polished Bi planes (noted in figure) in $5 \cdot 10^{-4}\text{M} [\text{Co}(\text{NH}_3)_6](\text{ClO}_4)_3 + x\text{M LiClO}_4 + 0.001\text{M HClO}_4$ aqueous solutions ($x = 0.002, \dots, 0.1$)

The forward rate constant is corrected for the corresponding value of w_a to obtain the corrected Tafel plot:

$$\ln k_{\text{het}} + z_{\text{eff}} \frac{RT}{F} \psi_d = \ln k_{\text{cor}}^0 + (z_{\text{eff}} - \alpha) \frac{F}{RT} \psi_d - w_a - \alpha \frac{F}{RT} (\phi_m - \psi_d), \quad (6.2.8)$$

where w_a is the average work of transporting the reactant and product to the reaction site, defined as

$$w_a = (1 - \alpha)w_R + \alpha w_P. \quad (6.2.9)$$

The slope of the cTp (gives the apparent charge transfer coefficient value α_{app}) is expressed as

$$\alpha_{\text{app}} = \frac{RT}{F} \frac{d \left(\ln k_{\text{het}} + z_{\text{eff}} \frac{F}{RT} \psi_d \right)}{d(\phi_m - \psi_d)} = \alpha - (z_{\text{eff}} - \alpha) \frac{d\psi_d}{d(\phi_m - \psi_d)} + \frac{RT}{F} \frac{dw_a}{d(\phi_m - \psi_d)}. \quad (6.2.10)$$

The second term on the right hand side gives the classical double-layer effect (negative contribution to α_{app}) and the third term is a part of the “true” double-layer effect, taking into account the actual charge distribution within the reaction couple. The differences between these contributions lead to the values of α_{app} , differing from the “true” value of $\alpha = 0.5$ [2, 3, 10]. According to the experimental data, the values of second term are smaller than the third term in Eq. (6.2.10) and $\alpha_{\text{app}} > 0.5$ for the Bi(001) and Bi(01 $\bar{1}$) plane | y M $[\text{Co}(\text{NH}_3)_6](\text{ClO}_4)_3$ + x M LiClO_4 + 0.001 M HClO_4 solution interfaces have been obtained (Fig. 9).

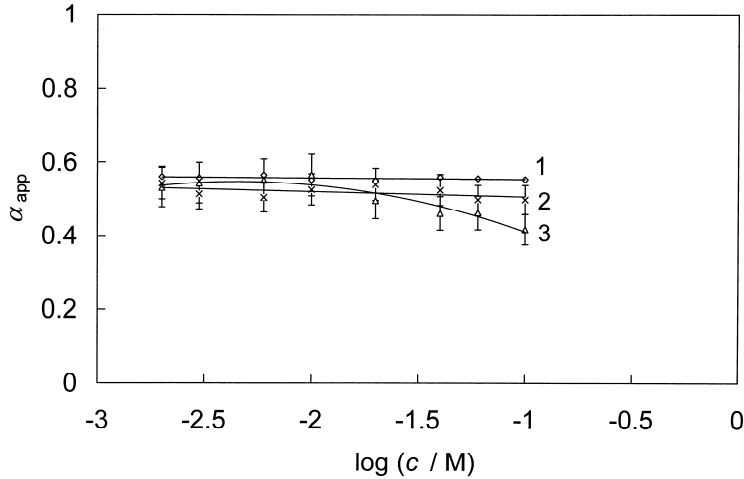


Figure 9. Dependence of apparent transfer coefficient α_{app} on $\log c$ for various electrochemically polished Bi planes: for Bi(001) (1;3) and Bi(01 $\bar{1}$) (2) in $5 \cdot 10^{-4}$ M $[\text{Co}(\text{NH}_3)_6](\text{ClO}_4)_3$ with different additions of the base electrolyte: x M LiClO_4 + 0.001 M HClO_4 (1;2) and 0.001, ..., 0.1 M HClO_4 (3).

As it was mentioned by Fawcett et al. [2, 3, 10] the detailed distribution of changes within the reactant and product in edl is unknown and only a rough estimation of α_{app} is possible through the parameter λ according to Eq. (6.2.11)

$$\alpha_{\text{app}} = \alpha - \lambda(\alpha - z_{\text{eff}}), \quad (6.2.11)$$

where λ is a fraction giving the portion of the potential drop across the inner-layer ϕ^{m-2} , which is added to ψ_d to give ψ_1 , the potential at the reaction site.

Based on Eq. (6.2.10), the apparent charge transfer coefficient is given as

$$\alpha_{\text{app}} = \alpha - (z - \alpha - z_{\text{eff}}) \frac{d\psi_d}{d(\phi_m - \psi_d)}, \quad (6.2.12)$$

where $d\psi_d/d(\phi_m - \psi_d)$ is the double-layer coefficient for $\text{Bi}(hkl)$, shown in Fig. 10.

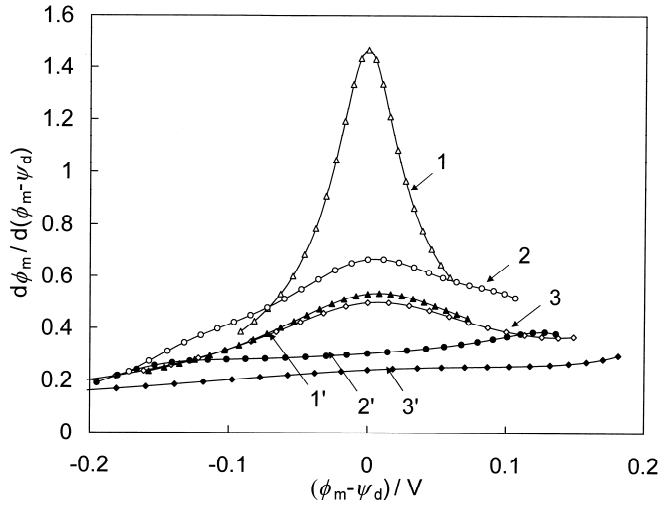


Figure 10. $d\psi_d/d(\phi_m - \psi_d)$ vs. $(\phi_m - \psi_d)$ curves for various electrochemically polished electrodes $\text{Bi}(001)$ (1;1'), $\text{Bi}(01\bar{1})$ (2;2') and $\text{Bi}(111)$ (3;3') in $5 \cdot 10^{-4} \text{ M } [\text{Co}(\text{NH}_3)_6](\text{ClO}_4)_3$ with different additions of HClO_4 (M): 0.02 (1;2;3) and 0.06 (1';2';3').

The data shows that the double-layer coefficient increases in the order of electrodes $\text{Bi}(01\bar{1}) < \text{Bi}(111) < \text{Bi}(001)$. Thus, α_{app} increases with the inner-layer capacitance (i.e. with the water adsorption energy at the electrode surface [34, 71, 72]). The values of $\alpha_{\text{app}} > 0.5$ for $\text{Bi}(001)$ and $\text{Bi}(01\bar{1})$ planes in $x \text{ M LiClO}_4 + 0.001 \text{ M HClO}_4$ (Fig. 9) indicate that the reaction site is in the inner-layer for these electrochemically more active planes. These

values indicate that the $\left[\text{Co}(\text{NH}_3)_6\right]^{3+}$ complex is probably oriented with one NH_3 group toward the Bi electrode surface at $E \sim E_{q=0}$. The dependence of α_{app} on the base electrolyte concentration and the rise of α_{app} with c_{HClO_4} indicates that the electrical double-layer structure plays a very important role for the kinetics of electroreduction of $\left[\text{Co}(\text{NH}_3)_6\right]^{3+}$ ions on Bi planes.

6.3. Impedance spectroscopy data for electroreduction of hexaamminecobalt(III) cations at Bi(hkl) in aqueous HClO_4 solutions

For more detailed analysis of reaction mechanism the electrochemical impedance spectroscopy has been used for investigation of electroreduction kinetics of the hexaamminecobalt(III) cations on the electrochemically polished Bi planes. It would be very important to verify is there an adsorption of $\left[\text{Co}(\text{NH}_3)_6\right]^{3+}$ cations on the Bi(hkl) electrode surface, explaining the deviation of this system from the simple outer-sphere reaction model established [1, 2, 4–6, 67]. Electrochemical impedance data were obtained using Autolab PGSTAT30 FRA2 system at ac frequency from $5 \cdot 10^{-2}$ Hz to $5 \cdot 10^4$ Hz within the region of electrode potential $-0.85 \text{ V} < E < -0.45 \text{ V}$ vs. Ag|AgCl|sat. KCl in H_2O .

6.3.1. Nyquist ($-Z''$, Z') -plots and Bode plots

According to the data in Figs. 11–14 the shape of the Nyquist and Bode plots depends noticeably on the electrode potential and concentration of reactant in the base electrolyte (0.001, ..., 0.1 M HClO_4) solution. At $E = -0.85 \text{ V}$ for Bi(111)| $1 \cdot 10^{-3} \text{ M } \text{HClO}_4 + y \text{ M } \left[\text{Co}(\text{NH}_3)_6\right]^{3+}$ and Bi(01 $\bar{1}$)| $1 \cdot 10^{-3} \text{ M } \text{HClO}_4 + y \text{ M } \left[\text{Co}(\text{NH}_3)_6\right]^{3+}$ systems (Fig. 12a) the Nyquist plots can be simulated by the slightly depressed semicircles and the total polarisation resistance for pure base electrolyte is noticeably lower than for solutions with addition of reactant. At higher reactant concentrations $c_{\left[\text{Co}(\text{NH}_3)_6\right]^{3+}} \geq 2.5 \cdot 10^{-4} \text{ M}$ the systematical decrease of total polarisation resistance R_p (in comparison with $2.5 \cdot 10^{-4} \text{ M } \left[\text{Co}(\text{NH}_3)_6\right]^{3+}$ + base electrolyte) takes place.

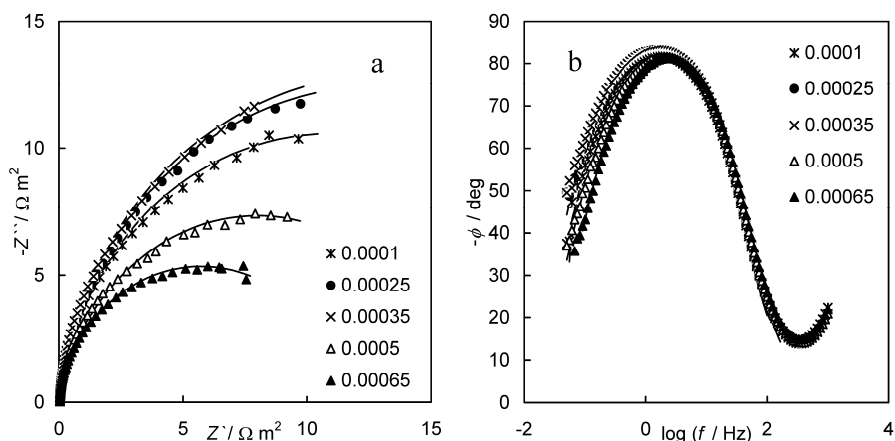


Figure 11. Plots of EIS spectra of EP Bi(111) at the electrode potential $E = -0.65$ V vs. Ag|AgCl| sat. KCl in the case of 0.001 M $HClO_4$ aqueous solution with different concentrations of $[Co(NH_3)_6]^{3+}$ (M) (noted in figure), in various coordinates: impedance complex plane plots ($-Z''$ vs. Z') (a), phase angle (b) vs. frequency dependences.

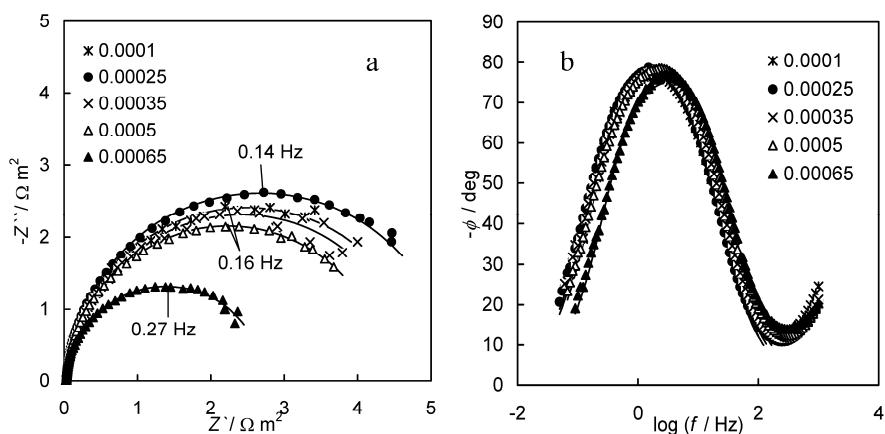


Figure 12. Plots of EIS spectra of EP Bi(011) at the electrode potential $E = -0.85$ V vs. Ag|AgCl| sat. KCl in the case of 0.001 M $HClO_4$ aqueous solution with different concentrations of $[Co(NH_3)_6]^{3+}$ (M) (noted in figure), in various coordinates: impedance complex plane plots ($-Z''$ vs. Z') (a), phase angle (b) vs. frequency dependences.

The absolute values of the so-called capacitive resistance $Z'' = \frac{1}{jC_s\omega}$ at the relaxation frequency f_{\max} decrease with the rise of reactant concentration, but the values of $|Z''|$ are noticeably higher than for the pure base electrolyte solution. The values of $|Z''|$ at $f_{\max} \sim 0.2 \text{ Hz}$ (f_{\max} is the value of the frequency at the maximum in the $-Z''$ vs. Z' curve) are practically independent of the plane studied and there is no noticeable dependence of f_{\max} on the crystallographic structure of the electrode surface as well as on $c_{[\text{Co}(\text{NH}_3)_6]^{3+}}$ in solution (Fig. 12a). The phase angle vs. $\log f$ (Bode) plots (Figs. 12b and 13c, d) show that the systematic shift of the phase angle vs. $\log f$ plots toward higher frequencies is clearly visible in the electrical double-layer formation region ($1 \text{ Hz} < f < 300 \text{ Hz}$). In the low frequency region the phase angle is practically independent of $c_{[\text{Co}(\text{NH}_3)_6]^{3+}}$, demonstrating that the adsorption equilibrium has been established already at very low reactant concentrations. Differently from the high frequency ac region the noticeable shift of the ϕ vs. $\log f$ plots for systems with addition of reactant in comparison with pure base electrolyte toward lower values of f has been observed, somewhat larger for $\text{Bi}(01\bar{1})$ than that for $\text{Bi}(111)$. For $\text{Bi}(hkl)$ planes in the region of frequency from 0.5 Hz to 10 Hz there is a small plateau with the phase angle $\phi \approx -80^\circ$ indicating that the so-called heterogeneous adsorption step is the main rate limiting process in this ac frequency region. However at lower frequencies the charge transfer is limiting step for electroreduction reaction of $[\text{Co}(\text{NH}_3)_6]^{3+}$ at $\text{Bi}(111)$ at $E = -0.85 \text{ V}$. The same rate limiting steps are valid for the $\text{Bi}(01\bar{1})$ plane too (Fig. 12b). The Nyquist plots measured at $E = -0.65 \text{ V}$ (Fig. 11) (potential region of mixed kinetics according to rotating disc electrode voltammetry data) show that differently from the data at $E = -0.85 \text{ V}$ the $-Z''$ vs. Z' plots have more complicated shape instead of semicircle, characterizing the mixed kinetic process at $\text{Bi}(hkl)$. Similarly to the data at $E = -0.85 \text{ V}$ the value of $|Z''|$ at fixed f decreases systematically with the rise of reactant concentration, but $|Z''|$ is higher than that for pure base electrolyte solution. Taking into account the complicated shape of the $-Z''$ vs. Z' plots, it is impossible to obtain correctly the so-called total polarization resistance R_p values. The phase angle

vs. $\log f$ dependences (Fig. 11b) show that differently from data at $E = -0.85$ V there is no dependency of the phase angle on reactant concentration in the high-frequency region $f > 10$ Hz, but at lower frequencies (in region of plateau and lower) the values of ϕ (at fixed ac frequency) for solutions with addition of $[\text{Co}(\text{NH}_3)_6]^{3+}$ are noticeably lower than for base electrolyte. Thus, in the region of $f < 10$ Hz there is mainly an adsorption limited process on $\text{Bi}(hkl)$. However, differently from $E = -0.85$ V the systematic increase of ϕ at $f < 1$ Hz occurs with the addition of $[\text{Co}(\text{NH}_3)_6]^{3+}$ in solution, explained with the shift of $[\text{Co}(\text{NH}_3)_6]^{3+}$ electroreduction from adsorption limited process toward mixed kinetic process with the rise of $[\text{Co}(\text{NH}_3)_6]^{3+}$ concentration in solution at lower frequencies (Fig. 11b).

The data in Fig. 13 show that at fixed f the absolute values of $|Z''|$ and $|\phi|$ are maximal in the potential region from -0.65 V to -0.55 V for $\text{Bi}(hkl)$, thus, in the region of zero charge potential $E_{q=0}$ of the $\text{Bi}(hkl)$ planes in the base electrolyte solution.

The absolute values of $|Z''|$ for the positively charged $\text{Bi}(hkl)$ electrode ($E \geq -0.55$ V) are somewhat lower compared with the data obtained at $E \sim E_{q=0}$, but the data for $E = -0.85$ V are very different from the data measured at $E = E_{q=0}$. The systematic trends of the dependence of $|Z''|$ and ϕ on E obtained for more concentrated $[\text{Co}(\text{NH}_3)_6]^{3+}$ solutions ($c_{[\text{Co}(\text{NH}_3)_6]^{3+}} \geq 5 \cdot 10^{-4}$ M) are in agreement with the results for more dilute $[\text{Co}(\text{NH}_3)_6]^{3+}$ solutions. Systematical analysis of results shows that the electroreduction reaction of $[\text{Co}(\text{NH}_3)_6]^{3+}$ is very complicated.

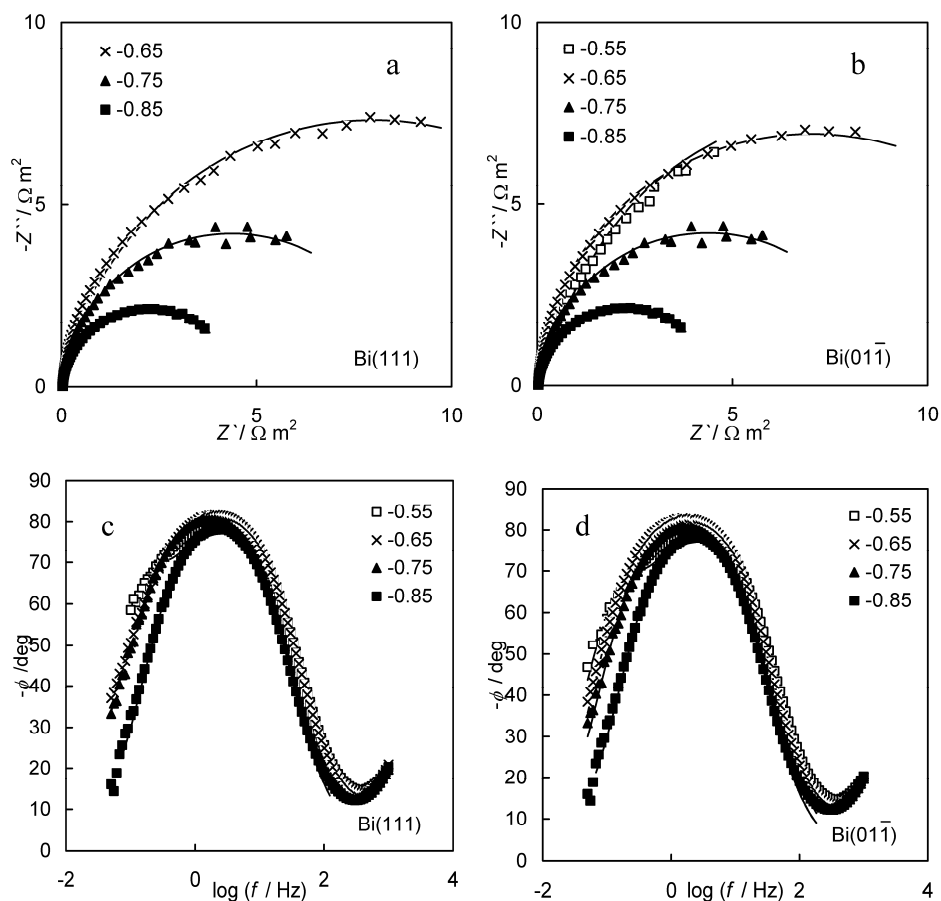


Figure 13. Plots of EIS spectra of EP Bi(111) (a, c); EP Bi(011̄) (b, d) in the 0.001 M $HClO_4$ + $5 \cdot 10^{-4}$ M $[Co(NH_3)_6]^{3+}$ aqueous solution at different electrode potentials ($E(V)$ vs. $Ag|AgCl|sat. KCl$) (noted in figure), in various coordinates: impedance complex plane plots ($-Z''$ vs. Z') (a, b), phase angle (c, d) vs. $\log f$ dependences.

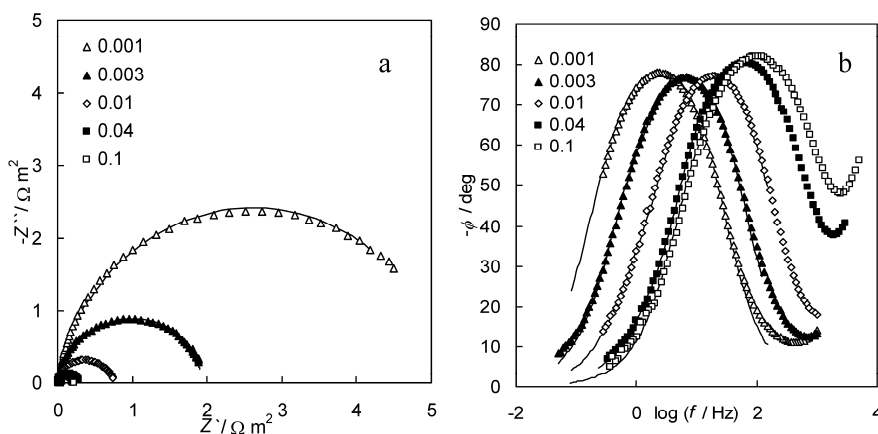


Figure 14. Plots of EIS spectra of EP Bi(111) at the electrode potential $E = -0.85$ V vs. Ag|AgCl| sat. KCl in the case of $5 \cdot 10^{-4}$ M $[\text{Co}(\text{NH}_3)_6]^{3+}$ aqueous solution with different concentrations of HClO_4 (M) (noted in figure), in various coordinates: impedance complex plane plots ($-Z''$ vs. Z') (a), phase angle (b) vs. frequency dependences.

In the 0.01,...,0.1 M HClO_4 solutions the hydrogen evolution reaction starts at higher negative electrode potentials (Fig. 14) [24, 25].

Cathodic hydrogen evolution reaction (HER) from the acidic solutions has a noticeable influence on the kinetics of electroreduction reaction of the $[\text{Co}(\text{NH}_3)_6]^{3+}$ cations on electrochemically polished Bi(hkl) planes [26].

6.4. Kinetics of cathodic hydrogen evolution at the electrochemically polished Bi(001) plane

The cathodic hydrogen evolution reaction (HER) belongs to the most often studied electrode processes. The mechanism and kinetics of HER was studied in 0.001,...,0.01 M HClO_4 on electrochemically polished Bi(001) electrode. The impedance complex plane $-Z''$ vs. Z' (i.e. Nyquist) plots and Bode plots as well as $\log(-Z'')$ vs. $\log f$ dependencies for HER have been measured using the Autolab PGSTAT 30 FRA 2 at ac frequency, f , from 0.05 Hz to $1 \cdot 10^4$ Hz within the region of the electrode potential $-0.85 \text{ V} < E < -0.45 \text{ V}$ vs. SCE combined with rotating disc electrode method (rotation velocity 150 rev min^{-1}) Figs. 15–17.

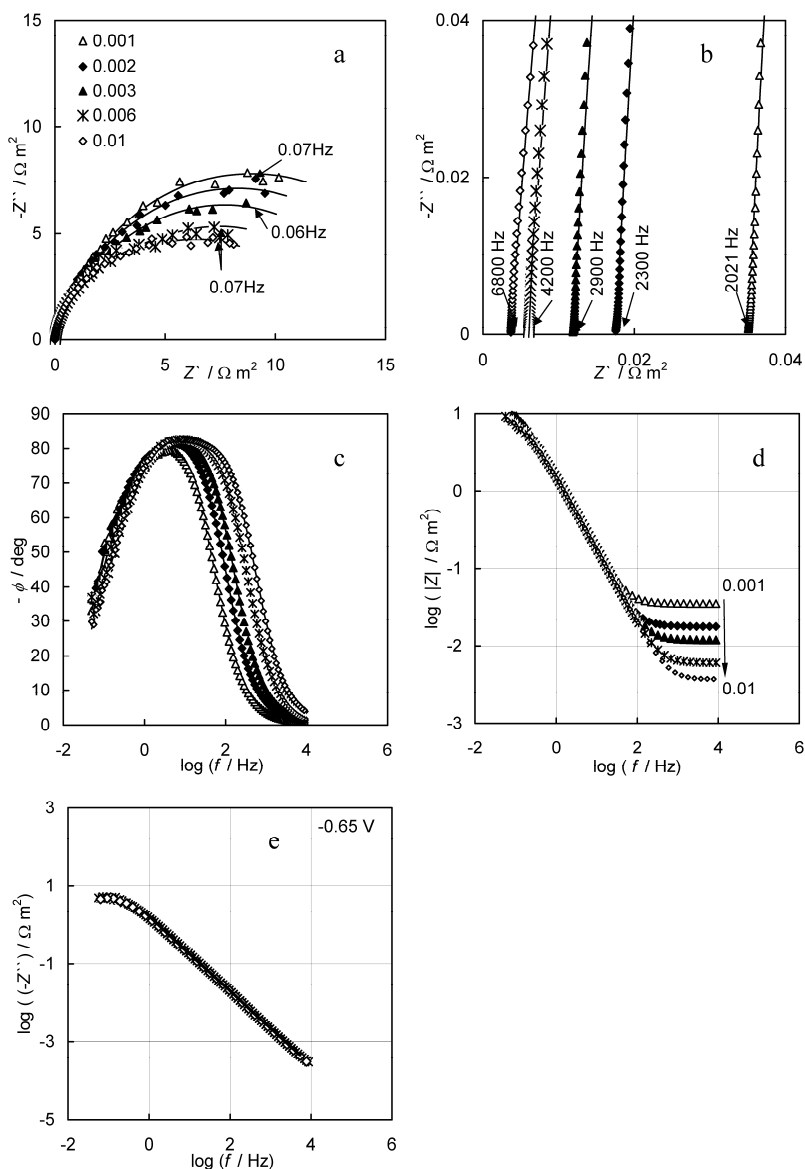


Figure 15. Plots of EIS spectra of EP Bi(001) at $v=150 \text{ rev min}^{-1}$ and at the electrode potential $E = -0.65 \text{ V}$ in the case of HClO_4 aqueous solution with different concentrations (M) (noted in figure), in various coordinates: impedance complex plane plots ($-Z''$ vs. Z') (a), zoom of the high frequency part of plot a (b); phase angle (c), $\log|Z|$ (d) and $\log(-Z'')$ (e) vs. frequency dependences, (symbols – experimental data, solid lines – calculated data according to the circuit, given in Fig. 1).

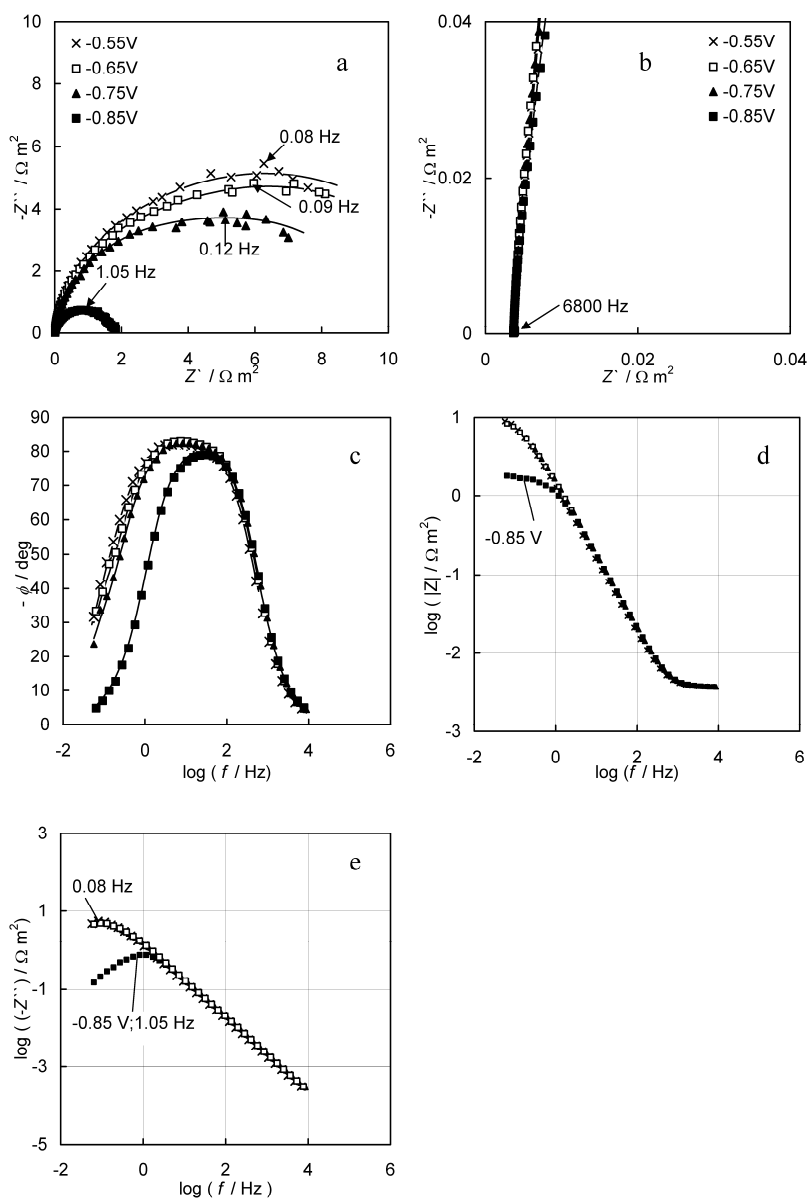


Figure 16. Plots of EIS spectra of EP Bi(001) at $\nu = 150 \text{ rev min}^{-1}$ in the 0.01 M HClO_4 aqueous solution at different electrode potentials (V) (noted in figure), in various coordinates: impedance complex plane plots ($-Z''$ vs. Z') (a); zoom of the high frequency part of plot a (b), phase angle (c), $\log|Z|$ (d) and $\log(-Z'')$ (e) vs. $\log f$ dependences, (symbols – experimental data, solid lines – calculated data according to the circuit in Fig. 1).

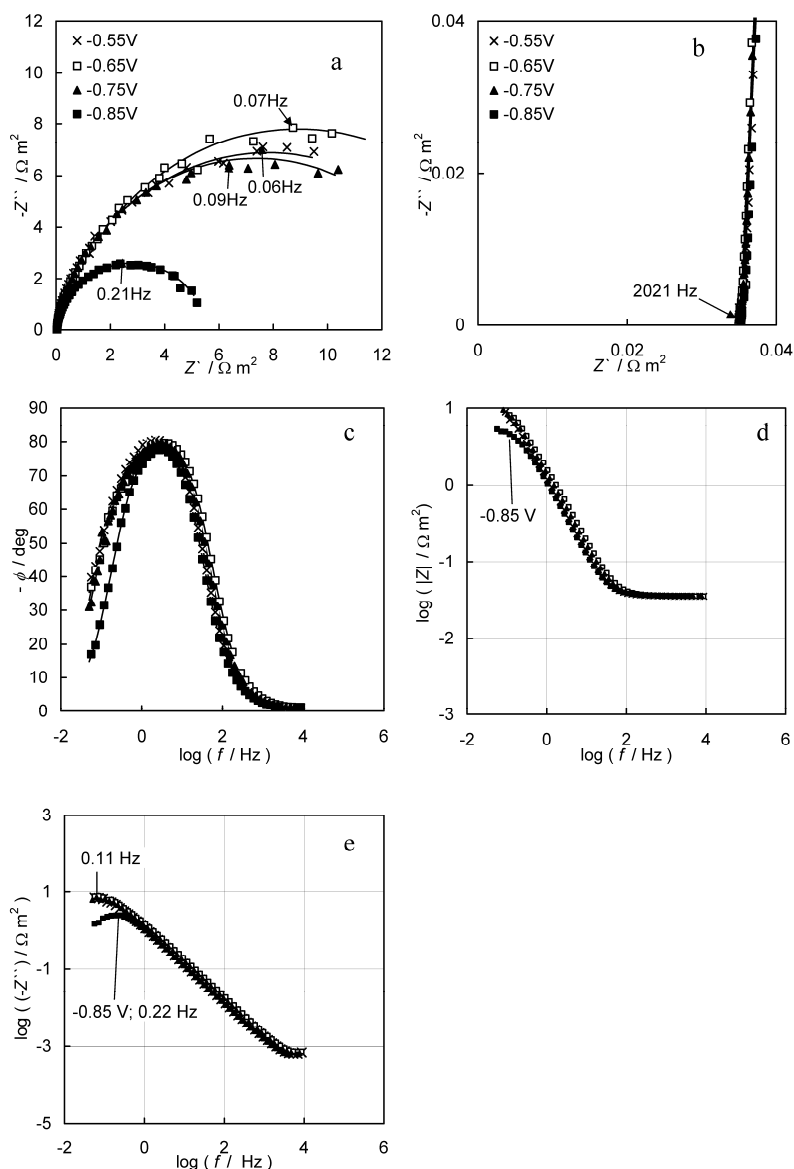


Figure 17. Plots of EIS spectra of EP Bi(001) at $\nu = 150 \text{ rev min}^{-1}$ in the 0.001 M HClO_4 aqueous solution at different electrode potentials (V) (noted in figure), in various coordinates: impedance complex plane plots ($-Z''$ vs. Z') (a); zoom of the high frequency part of plot a (b), phase angle (c), $\log|Z|$ (d) and $\log(-Z'')$ (e) vs. $\log f$ dependences, (symbols – experimental data, solid lines – calculated data according to the circuit in Fig. 1).

Bode plots (Figs. 15c, d, 16c, d and 17c, d) show clear impedance data over the total frequency range examined while the impedance complex plane data are very informative for the limited low frequency region ($f < 100 \text{ Hz}$) but higher frequency data at high extent are screened. The $\log(-Z'')$ vs. $\log f$ and $\log Z'$ vs. $\log f$ plots are very helpful for the analysis of reaction characteristics, i.e. to obtain the characteristic relaxation time(s) of low frequency process(es), as well as for CPE analysis for Bi(001) and other solid electrodes [36, 39, 72–80, 88–105]. As can be seen in Figs. 15–17 an almost capacitive-resistive behavior is observed at medium frequency region. For all concentrations studied (Figs. 15d, 16d, 17d) the $\log|Z|$ vs. $\log f$ dependences show an almost resistive response at higher frequencies $f > 1000 \text{ Hz}$. The values of $\log|Z|$, given in Fig. 15d, 16d and 17d are independent of electrode potential at frequency $f > 1 \cdot 10^3 \text{ Hz}$, thus, there is no very quick faradaic processes at the Bi(001)| $\text{HClO}_4 + \text{H}_2\text{O}$ interface. At very high frequency the values of active resistance $R_{\text{el}} = Z(\omega \rightarrow \infty)$ depend nearly linearly on c_{HClO_4} , explained by the increase of the specific conductivity of the electrolyte resistance R_{el} with the rise of c_{HClO_4} .

The data in Figs. 15e, 16e and 17e show that for dilute HClO_4 solutions ($c_{\text{HClO}_4} \leq 1 \cdot 10^{-3} \text{ M}$) at small negative electrode potentials the $\log(-Z'')$ vs. $\log f$ plots have not very well expressed maxima even at very low f and, thus, the values of characteristic relaxation time $\tau_{\text{max}} = (2\pi f_{\text{max}})^{-1}$ (f_{max} is the frequency at the maximum of the $-Z''$ vs. Z' plots) can not be calculated exactly, indicating the occurring of very slow kinetic process(es) at the Bi(001) surface. The values of total polarization resistance $R_p(\omega \rightarrow 0)$ at the electrode potentials E less negative than -0.75 V can not be determined exactly (Figs. 15a, 16a and 17a) and only at $E \leq -0.80 \text{ V}$ it is possible to calculate the values of $R_p(\omega \rightarrow 0)$, depending on c_{HClO_4} . For solutions with $c_{\text{HClO}_4} \geq 2 \cdot 10^{-3} \text{ M}$, the values of τ_{max} obtained (given in Fig. 18) depend on the electrode potential applied.

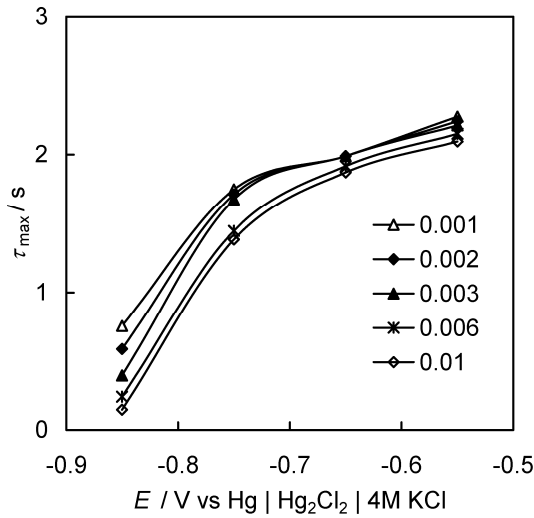


Figure 18. Characteristic relaxation time $\tau_{\max} = (2\pi f_{\max})^{-1}$ vs. electrode potential dependences for cathodic hydrogen evolution at Bi(001) in HClO_4 aqueous solution with concentrations (M), noted in figure.

According to the data given in Figs. 15–17, the total polarization resistance decreases with increasing the negative electrode potential as well as c_{HClO_4} , (i.e. with the decrease of pH). The values of τ_{\max} in Fig. 18, obtained using data in Figs. 15e, 16d and 17d, are in a good agreement with τ_{\max} , obtained from impedance complex plane plots (Figs. 15a–17a). τ_{\max} is practically independent of c_{HClO_4} at fixed potential if $E \geq -0.65 \text{ V}$, but τ_{\max} depends noticeably on E , if $c_{\text{HClO}_4} = \text{const.}$.

In the region of frequency from 1 Hz to $3 \cdot 10^3$ Hz there is a noticeable dependence of $\log|Z|$ and phase angle ϕ on $\log f$, indicating the comparatively slow electrical double-layer formation process. In this region, ϕ noticeably depends on c_{HClO_4} and only very weakly on E (Figs. 15c, 16b and 17b). The analysis of ϕ vs. $\log f$ plots shows that, in the limited region of frequencies $1 \text{ Hz} < f < 100 \text{ Hz}$, the very high negative values of phase angle, practically independent of electrode potential applied, have been observed, characteristic of the nearly ideally flat capacitive electrode, caused by the high values of resistances (R_{ad} and R_{ct}) values in parallel with the double-layer

impedance. Only at very low frequency the noticeable increase in absolute values of phase angle has been observed indicating the occurrence of the very slow charge transfer step for HER at Bi(*hkl*). At frequency $f > 100$ Hz, the values of phase angle are nearly independent of electrode potential applied. The influence of $c_{\text{H}_3\text{O}^+}$ on the position of the ϕ vs. $\log f$ plots is noticeable in the region $100 \text{ Hz} < f < 10^4 \text{ Hz}$, and with the dilution of HClO_4 solution, ϕ vs. $\log f$ plot is shifted toward lower frequencies being a simple consequence of relaxation between the resistance of electrolyte solution and electrical double-layer impedance of the Bi(001) electrode.

The analysis of the $\log(-Z'')$ vs. $\log f$ plots (Figs. 15e, 16d, 17d) shows that the deviation of the experimental system from the ideally flat surface toward constant phase element behaviour is very small [36, 37, 63, 64, 88–105] because the fractional exponent α_{CPE} for CPE with impedance $Z_{\text{CPE}} = Q^{-1}(\text{j}\omega)^{-\alpha_{\text{CPE}}}$, calculated from the slope of $\log(-Z'')$ vs. $\log f$ plots, is only somewhat lower than unity ($0.94 < \alpha_{\text{CPE}} < 0.98$), thus characteristic of the ideally flat capacitive interface [24, 39, 63, 64, 88–105].

6.4.1. Modelling and parameters analysis

The number of experimental points in the impedance spectra has been kept constant if the various ECs have been tested. The good fitting ($\chi^2 < 7 \cdot 10^{-4}$, $SD \leq 2.7 \cdot 10^{-4}$, $\Delta^2 \leq 0.2$) at $c_{\text{HClO}_4} \leq 2 \cdot 10^{-3} \text{ M}$ has been established if EC (i.e. model with one adsorbed intermediate species [36, 94], proposed by Armstrong and Henderson [39]), corresponding to the reaction steps given by Eqs. (4.3.1) and (4.3.2), has been applied. The very low SD values, calculated using method described in [64], nearly independent of the electrode potential applied, have been obtained. According to the fitting results the high frequency series resistance at $c_{\text{HClO}_4} = \text{const.}$ is independent of potential applied and thus, the calculated values of R_{el} correspond to the high frequency electrolyte resistance. In the C_{dl} vs. E curves for solutions with $c_{\text{HClO}_4} \leq 2 \cdot 10^{-3} \text{ M}$ there are characteristic diffuse layer minima at the diffuse layer minimum potential $E_{\text{min}} = -0.65 \text{ V}$ (Fig. 19a), being in a good agreement with the zero charge potential $E_{\text{q}=0}$ obtained for LiClO_4 solutions [82, 83], and therefore the C_{dl}

vs. E curves for dilute HClO_4 solutions ($c_{\text{HClO}_4} < 2 \cdot 10^{-3} \text{ M}$) can be used for classical Frumkin ψ_1 potential correction analysis [11, 13, 24, 59–62, 82].

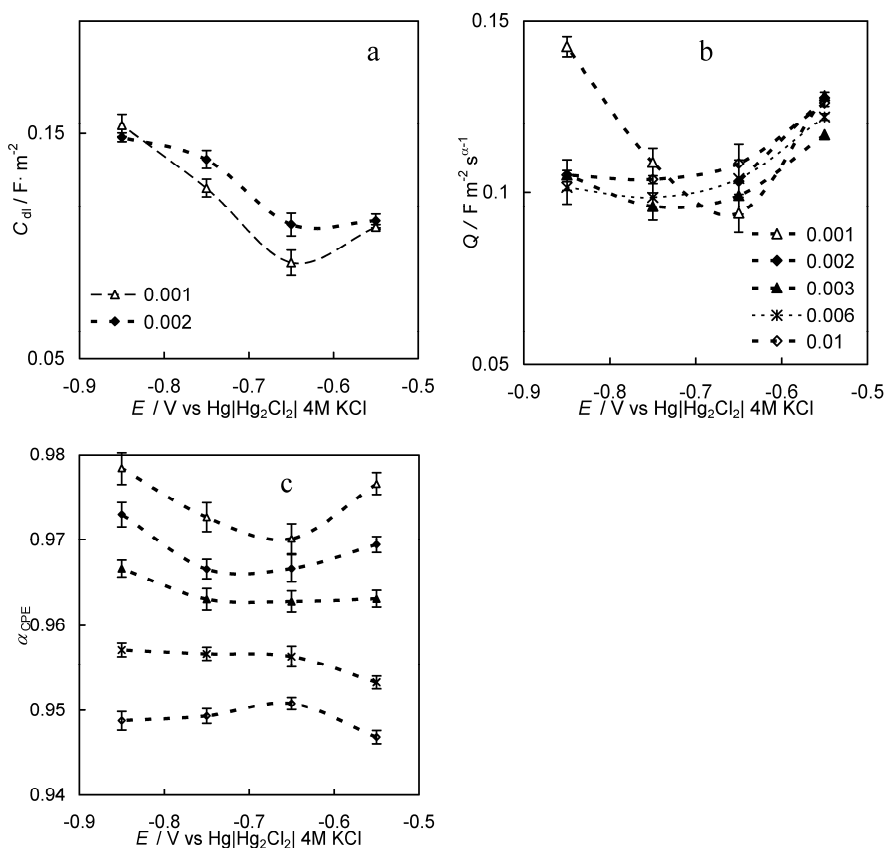


Figure 19. Dependences of C_{dl} (a) (calculated according to the Armstrong-Henderson circuit); CPE coefficient Q (b) and fractional exponent α_{CPE} (c) on the electrode potential (calculated according to the circuit in Fig. 1) for EP Bi(001) in HClO_4 aqueous solution with concentrations (M), noted in figure.

However, according to the detailed analysis in the case of solid electrodes [6, 36, 39, 82, 83, 88–102], the CPE element should be included into EC and therefore C_{dl} valid for ideally flat and energetically homogenous surface has to be replaced with CPE, taking into account the geometrical surface roughness and energetic inhomogeneity of solid surface studied, to receive EC (Fig. 1). According to the data in Figs. 15–17 a very good fit ($\chi^2 < 5 \cdot 10^{-4}$, $\Delta^2 \leq 0.01$)

has been observed if the modified Armstrong-Henderson EC has been used (solid lines – calculated impedance spectra using the model in Fig. 1; symbols – the experimental data). The results (Fig. 19b) show that the Q depends very weakly on the electrolyte concentration and Q has minimal values in dilute HClO_4 solutions near $E_{\min} = -0.65 \text{ V}$, being in a very good agreement with C_{dl} values (Fig. 19a) obtained using Armstrong-Henderson EC. The values of α_{CPE} at fixed E for dilute HClO_4 solutions are quite high ($\alpha_{\text{CPE}} \geq 0.97$) and depend weakly on c_{HClO_4} if $c_{\text{HClO}_4} \leq 2 \cdot 10^{-3} \text{ M}$. It should be mentioned that α_{CPE} decreases with the rise of c_{HClO_4} (Fig. 19c), contrary to the $\text{Bi}(001)|\text{LiClO}_4 + \text{H}_2\text{O}$ system, where α_{CPE} increases with the rise of c_{LiClO_4} [51, 82, 83]. Moreover, differently from LiClO_4 solutions, there is a very small minimum in the α_{CPE} vs. E dependence at $E = -0.65 \text{ V}$. The dependence of α_{CPE} on $c_{\text{HClO}_4} > 4 \cdot 10^{-3} \text{ M}$ indicates the very weak changes in surface energetic inhomogeneity are caused by the adsorption of reaction intermediates. However $\alpha_{\text{CPE}} \geq 0.97$ for $1 \cdot 10^{-3} \text{ M HClO}_4$ aqueous solution indicates that the deviation of $\text{Bi}(001)|\text{HClO}_4$ interface from the classical conception of ideally flat interface [82, 83, 99–101] is very weak and the influence of replacing CPE with C_{dl} on the values of other fitting parameters is comparatively small. At these conditions, to a first very rough approximation, the model of Brug et al. [95] can be used for calculation of the ideal C_{dl} values (Fig. 19a). This result can be explained by the fact that α_{CPE} for solutions with higher c_{HClO_4} ($\geq 2 \cdot 10^{-3} \text{ M}$) contains additional information concerning the influence of the weakly blocking adsorption of hydrogen on $\text{Bi}(001)$, but not only simply the surface roughness effect [6, 82, 83, 90–92].

According to the data (Fig. 20a), the charge transfer resistance decreases noticeably with increasing the negative potential, and R_{ct} is practically independent of c_{HClO_4} at $E_{\min} = -0.65 \text{ V}$, where the values of C_{dl} or Q are minimal [11, 13, 24, 59].

The calculated values of current density

$$j_{\text{sum}} = \frac{RT}{nF(R_{\text{ct}} + R_{\text{ad}})} = (2.13 \pm 0.01) \cdot 10^{-6} \text{ A cm}^{-2} \text{ at } E_{\text{q}=0} \text{ (} n \text{ is the number}$$

of electrons transferred) are in a good agreement with those obtained from the stationary Tafel measurements ($j_{\text{ct}} = 2 \cdot 10^{-6} \text{ A cm}^{-2}$ for 0.1 M HClO_4) [51].

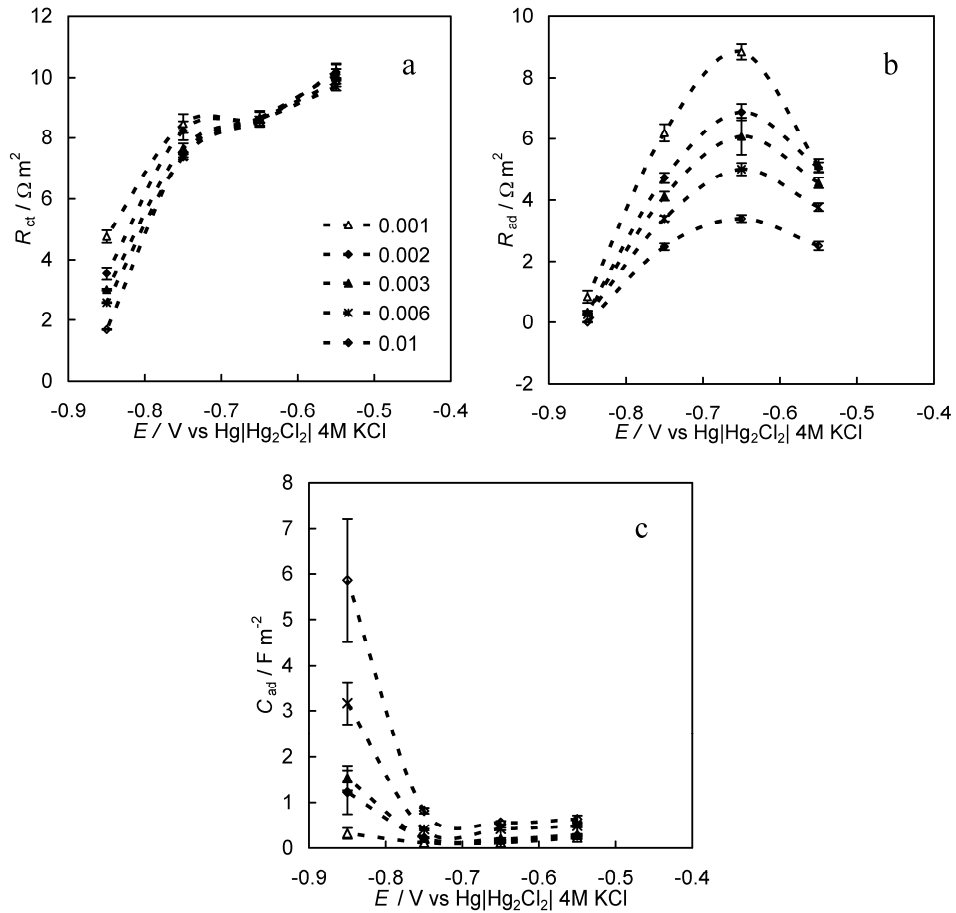


Figure 20. R_{ct} (a); R_{ad} (b) and C_{ad} (c) dependences on the electrode potential (calculated according to the equivalent circuit in Fig. 1) for EP Bi(001) in HClO₄ aqueous solution with different concentrations (M), noted in figure.

At $E > E_{min}$, there is only small decrease of R_{ct} with the rise of c_{HClO_4} caused by less pronounced classical Frumkin ψ_1 potential effect [11, 13, 24, 51, 58]. The adsorption resistance R_{ad} (Fig. 20b) depends noticeably on the electrode potential, being maximal near the E_{min} and the values of R_{ad} have a noticeable decrease with the rise of negative E . The decrease of R_{ad} with c_{HClO_4} is pronounced only in the region of small positive surface charge densities. The adsorption capacitance C_{ad} (Fig. 20c) is nearly independent of E and c_{HClO_4} at

$E > -0.7 \text{ V}$. At more negative potentials (C_{ad} noticeably increases) which is more expressed for solutions with lower pH. In concentrated HClO_4 solutions, C_{ad} is nearly 60 times higher than the values of Q at $E = -0.85 \text{ V}$ (Fig. 20c).

The attempts to use more complicated models like Ershler model (nowadays known as Frumkin-Melik-Gaikazyan-Randles circuit [92–96]) or the modified Grafov – Damaskin ECs, based on the multi-port impedance model for totally irreversible reaction discussed in detail in [102–104], did not give a better fit for the experimental data and the errors in R_{ad} and C_{ad} are very high. Thus, modified Armstrong-Henderson model (Fig. 1) is the only EC giving a good fit of the $\text{Bi}(001)|\text{HClO}_4 + \text{H}_2\text{O}$ impedance data.

The corrected Tafel plots have been calculated according to the Eq. (4.1.4). For calculation of the cTp, ψ_1 potential has been taken equal to ψ_d potential ($\psi_1 \approx \psi_d$), i.e. the reaction center has been taken to locate at the oHp with the ψ_d potential. The needful ψ_d vs. E and surface charge density q vs. E plots have been calculated using corresponding impedance data obtained for less concentrated HClO_4 solutions $c_{\text{HClO}_4} < 2 \cdot 10^{-3} \text{ M}$, where the influence of hydrogen adsorption on the values of C_{dl} or Q is weak. Calculated cTp's are nearly linear for more concentrated HClO_4 solutions ($c_{\text{HClO}_4} > 6 \cdot 10^{-3} \text{ M}$) and corrected values of current density are nearly independent of c_{HClO_4} at $E - E_{q=0} - \psi_d < 0$. Thus, the cTp's analysis method can be used for $\text{Bi}(001)|\text{HClO}_4$ interface data (Fig. 21) similarly to the systems with constant ionic strength [51, 59, 106].

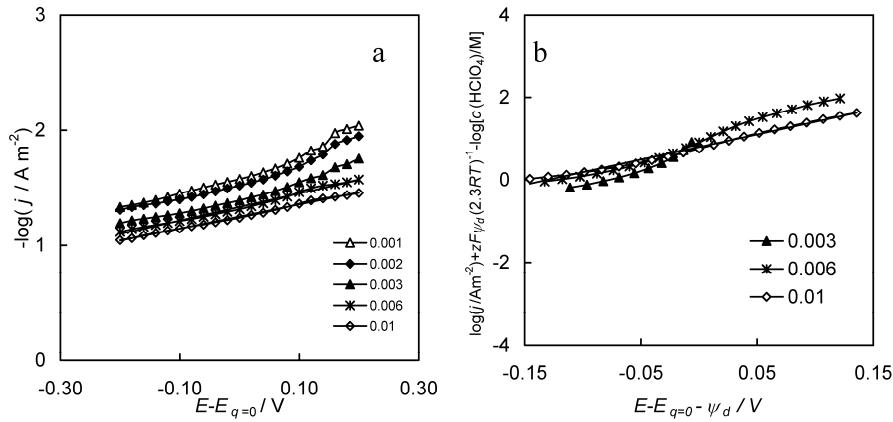


Figure 21. $-\log j$ vs. rational electrode potential $(E - E_{q=0})$ plots **(a)** and corrected Tafel plots **(b)** for EP Bi(001) in HClO_4 aqueous solution with concentrations (M), noted in figure.

It was found that the slope of cTp is equal to 0.117 V, giving the value of α equal to 0.51, in a good agreement with the data of Lust et al. for solutions with constant ionic strength [51]. If the corrected Tafel lines can be taken as representative of the kinetic mechanism [11, 13, 59–62, 106–109] then, in a good agreement with the impedance data, the slow primary discharge is the slowest rate determining step. Of course, the same slope value would be observed for slow electrochemical desorption (Heyrovsky) step, i.e. $\text{H}_3\text{O}^+ + \text{MH}_{\text{ad}} + \text{e}^- \rightarrow \text{H}_2 + \text{H}_2\text{O} + \text{M}$ step, but then the surface coverage of Bi(001) with adsorbed H_{ad} should be very high (and therefore $\theta_{\text{H}_{\text{ads}}} \rightarrow 1$) that is impossible in the case of Bi(001) [51, 61, 62]. The electroreduction reaction of H_3O^+ cations is mainly limited by the very slow charge transfer step at the Bi(001) | $\text{HClO}_4 + \text{H}_2\text{O}$ interface.

7. SUMMARY AND CONCLUSIONS

The electroreduction kinetics of the hexaamminecobalt(III) cations on electrochemically polished Bi planes has been studied by the cyclic voltammetry, rotating disc electrode and electrochemical impedance spectroscopy methods. It was found that the electroreduction of $[\text{Co}(\text{NH}_3)_6]^{3+}$ cations is limited mainly by the rate of the diffusion step in the region of the electrode potentials $-0.9 \text{ V} < E < -0.8 \text{ V}$ vs. SCE. At $E = E_{q=0}$ the value of rate constant for the heterogeneous reaction is independent of the base electrolyte concentration and, thus, the so-called corrected for the double-layer effect values of k_{het}^0 have been established. The rate constant of the heterogeneous electroreduction reaction of the $[\text{Co}(\text{NH}_3)_6]^{3+}$ complex cation on the Bi(001) and Bi(01 $\bar{1}$) planes decreases very weakly in this order of planes, i.e. with increasing adsorption activity of the ClO_4^- anions and $[\text{Co}(\text{NH}_3)_6]^{3+}$ cations on Bi(hkl). In the region of zero charge potential, the value of the experimental transfer coefficient α_{exp} obtained depends weakly on the crystallographic structure of the Bi single crystal plane studied. The values of α_{exp} are only slightly higher than 0.5 for the Bi(01 $\bar{1}$) and Bi(001) planes. The values of apparent transfer coefficient α_{app} , corrected for the double-layer effect, somewhat higher than 0.5 indicate that the reaction site is in the inner-layer for the Bi(001) and Bi(01 $\bar{1}$) planes in weakly acidified LiClO_4 solutions. Noticeably different values of the double-layer corrected rate constant and apparent charge transfer coefficients for the Bi(001), Bi(01 $\bar{1}$), Hg and Ag(110) electrodes from the data for the Au(210) and Au(111) planes have been explained by the different inner-layer structure, i.e. by the different water and probably $[\text{Co}(\text{NH}_3)_6]^{3+}$ physical adsorption energies at the metals under discussion. It should be noted that the analysis of the values of the diffuse layer potential calculated according to the Monte Carlo method as well as generalised mean spherical approximation would give more information.

Electrochemical impedance spectroscopy has been applied for investigation of the hydrogen evolution kinetics at the electrochemically polished Bi(001) plane. The mixed kinetics reaction mechanism (slow adsorption and charge transfer steps) has been established for cathodic hydrogen evolution at Bi(001)| $\text{HClO}_4 + \text{H}_2\text{O}$ interface. The charge transfer resistance R_{ct} and

adsorption capacitance C_{ad} depend noticeably on the electrode potential applied. The values of exchange current density calculated from the impedance data at zero charge potential are in a good agreement with those obtained using stationary polarization method. The adsorption resistance R_{ad} value is maximal in the region of zero charge potential. The fractional exponent of the constant phase element CPE ($\alpha_{CPE} \geq 0.94$) only very weakly depends on the HClO_4 concentration and electrode potential, and therefore, the deviation of $\text{Bi}(001)|\text{HClO}_4 + \text{H}_2\text{O}$ interface from the classical conception of ideally flat electrode is weak and CPE coefficient Q is nearly equal to the high frequency electrical double-layer capacitance C_{dl} , if $c_{\text{HClO}_4} \leq 2 \cdot 10^{-3} \text{ M}$. Similarly to the stationary polarization measurements, the electrical double-layer structure, depending strongly on the effective Debye screening length of the electrolyte ions, has a very big influence on the cathodic hydrogen evolution kinetics at the $\text{Bi}(001)$ plane from HClO_4 aqueous solution.

8. REFERENCES

- [1] A. Hamelin, M. J. Weaver, *J. Electroanal. Chem.* 209 (1986) 109.
- [2] W.R. Fawcett, in: J. Lipkowski, P.N. Ross (Eds.), *Electrocatalysis*, Wiley, New York, 1998, p. 323 (Chapter 8).
- [3] W.R. Fawcett, M. Hromadova, G.A. Tsirlina, R.R. Nazmutdinov, *J. Electroanal. Chem.* 498 (2001) 93.
- [4] M.J. Weaver, F.C. Anson, *J. Am. Chem. Soc.* 97 (1975) 4403.
- [5] A. Hamelin, M.J. Weaver, *J. Electroanal. Chem.* 223 (1987) 171.
- [6] G.J. Brug, M. Sluyters-Rehbach, J.H. Sluyters, A. Hemelin, *J. Electroanal. Chem.* 181 (1984) 245.
- [7] J. Perez, E.R. Gonzalez, H.M. Villullas, *J. Phys. Chem. B* 102 (1998) 10931.
- [8] Z. Samec, A.M. Bittner, K. Doblhofer, *J. Electroanal. Chem.* 432 (1997) 205.
- [9] W. R. Fawcett, M. Fedurco, Z. Kováčová, *J. Electrochem. Soc.* 141 (1994) L30.
- [10] M. Hromadova, W.R. Fawcett, *J. Phys. Chem. A* 104 (2000) 4356.
- [11] A.N. Frumkin, *Z. Phys. Chem.* 164 (1953) 121.
- [12] A.N. Frumkin, *Z. Elektrochem.* 59 (1955) 807.
- [13] A.N. Frumkin, in: P. Delahay (Ed.), *Advances in Electrochemistry*, vol. 1, Interscience Publ., New York, 1961, p. 65.
- [14] R. Parsons, *Surf. Sci.* 2 (1964) 418.
- [15] A.N. Frumkin, N.V. Nikolaeva-Fedorovich, N.P. Berezina, H.E. Keis, *J. Electroanal. Chem.* 58 (1975) 189.
- [16] S. Trasatti, in: H. Gerischer, C.W. Tobias (Eds.), *Advances in Electrochemistry and Electrochemical Engineering*, vol.19, Wiley, New York, 1977, p. 297.
- [17] N.V. Fedorovich, in: *Reports in Science and Technology*, vol. 14, VINITI, Moscow, 1979, p. 5 (in Russian).
- [18] R.R. Nazmutdinov, G.A. Tsirlina, Y.I. Kharkats, O.A. Petrii, M. Probst, *J. Phys. Chem. B* 102 (1998) 677.
- [19] G.A. Tsirlina, Y.I. Kharkats, R.R. Nazmutdinov, O.A. Petrii, *Russ. J. Electrochem.* 35 (1999) 19.
- [20] G.A. Tsirlina, O.A. Petrii, Y.I. Kharkats, A.M. Kuznetsov, *Russ. J. Electrochem.* 35 (1999) 1210.
- [21] R.R. Nazmutdinov, I.V. Pobelov, G.A. Tsirlina, O.A. Petrii, *J. Electroanal. Chem.* 491 (2000) 126.
- [22] I.V. Pobelov, G.A. Tsirlina, M.I. Borzenko, O.A. Petrii, *Russ. J. Electrochem.* 37 (2001) 233.
- [23] S.W. Barr, K.L. Guyer, M.J. Weaver, *J. Electroanal. Chem.* 111 (1980) 41–59.
- [24] R. Jäger, E. Härk, P. Möller, J. Nerut, K. Lust, E. Lust, *J. Electroanal. Chem.*, 566, 217 (2004).
- [25] E.Härk, E. Lust, *J. Electrochem. Soc.* 153 (2006) E104.
- [26] E.Härk, K.Lust, A.Jänes, E.Lust, Electrochemical impedance study of hydrogen evolution on Bi(001) electrode in the HClO₄ aqueous solutions, *J. Solid State Electrochem.* Submitted (JSEL-D-08-00102)
- [27] E. Lust, J. Nerut, E. Härk, R. Jäger, K. Lust, K. Tähnas, T.Thomberg, S.Kallip, V.Grozovski, *ECS Trans.* 1 (17) (2006) 9.
- [28] M.J. Weaver, *J. Electroanal. Chem.* 498 (2001) 105.
- [29] M. Muzikár, W. R. Fawcett, *J. Phys. Chem. B* 110 (2006) 2710.

- [30] B.B. Damaskin, O.A., Petrii, Vvedenie v elektrokhimicheskuyu kinetiku, Vysshaya Shkola, Moscow, 1983.
- [31] E. Gileadi, Electrode Kinetics for Chemists, Chemical Engineers and Materials Scientists, VCH Publishers, Inc., New York, Weinheim, Cambridge, 1993.
- [32] B.B. Damaskin, O.A. Petrii, G.A. Tsirlina, Elektrohimiya, Moscow, Himiya, 2001.
- [33] J.J. Calvente, N.S. Marinković, Z. Kováčková, W.R. Fawcett, J. Electroanal. Chem. 421 (1997) 49.
- [34] K. Asada, P. Delahay, A. Sundaram, J. Amer. Chem. Soc. 83 (1961) 3396.
- [35] A.N. Frumkin, G.M. Florianovich, Dokl. Akad. Nauk SSSR, 80 (1951) 907.
- [36] A. Lasia in B. E. Conway, J. O'M. Bockris, R. E. White (Ed.), Modern Aspects of Electrochemistry. vol. 32, Kluwer Academic / Plenum Publishers, New York, 1999, p. 143.
- [37] V. Horvat-Radošević, K. Kvastek, Electrochim. Acta 48 (2002) 311.
- [38] M. Sluyters-Rehbach, in: A. Bard (Eds.), vol. 4, Marcel Dekker, New York, 1970, p. 1.
- [39] R.D. Armstrong, M. Henderson, J. Electroanal. Chem. 39 (1972) 81.
- [40] M. Sluyters-Rehbach, J.H. Sluyters, in: E. Yeager, J. O. M. Bockris, B. E. Conway, S. Sarangapani (Eds.), Comprehensive Treatise of Electrochem, vol. 9, Plenum Press, New York, 1984.
- [41] I.D. Raistrick, J.R. Macdonald, D.R. Franceschetti, in: J. R. Macdonald (Ed.), Impedance Spectroscopy, Wiley, New York, 1987.
- [42] M. Sluyters-Rehbach, Pure Appl. Chem. 66 (1994) 1831.
- [43] C. Gabrielli, in: I. Rubinstein (Ed.) Physical Electrochemistry – Principles, Methods and Application (Ch.6) Marcel Dekker, New York, 1995, p. 257.
- [44] L.M. Peter, W. Dürre, P. Bindra, H. Gerischer, J. Electroanal. Chem. 71 (1976) 31.
- [45] S.A. Campbell, L.M. Peter, J. Electroanal. Chem. 364 (1994) 257.
- [46] J. Barber, S. Morin, B.E. Conway, J. Electroanal. Chem. 446 (1998) 125.
- [47] C. Deslouis, I. Epelboin, M. Keddam, J.C. Lestrade, J. Electroanal. Chem. 28 (1970) 57.
- [48] J.S. Chen, J.-P. Diard, R. Durand, C. Montella, J. Electroanal. Chem. 406 (1996) 1.
- [49] L. Bai, D.A. Harrington, B.E. Conway, Electrochim. Acta 32 (1987) 1713.
- [50] B. Breyer, H.H. Bauer, Alternating Current Polarography and Tensammetry, Wiley Interscience, New York, 1963.
- [51] K. Lust, E. Perkson, E. Lust, Russ. J. Electrochem. 36 (2000) 1257.
- [52] M. W. Breiter in E. Yeager (Ed.), Symposium on Electrode Processes, The Electrochemical Society, Wiley, New York, 1961, p. 307.
- [53] M. W. Breiter, J. Electrochem. Soc. 109 (1962) 549.
- [54] V. V. Losev, Elektrokhimija 17 (1981) 733.
- [55] A. Lasia, J. Electroanal. Chem. 593 (2006) 159.
- [56] D. Eberhardt, E. Santos, W. Schmickler, J. Electroanal. Chem. 461 (1999) 76.
- [57] A.M. Abd. El-Halim, K. Jüttner, W. J. Lorenz, J. Electroanal. Chem. 106 (1980) 193.
- [58] E. Härk, E. Lust, Electroreduction of hexaammine cobalt(III) cations at electrochemically polished Bi(*hkl*) using impedance spectroscopy method (in prep.) 2008

- [59] O.A.Petrij, R.R. Nazmutdinov, M.D. Bronshtein, G.A.Tsirlina, *Electrochim. Acta* 52 (2007) 3493.
- [60] E. Gileadi, E. Kirowa-Eisner, *Corros. Sci.* 47 (2005) 3068.
- [61] U.Palm, T.Tenno, *J.Electroanal.Chem.* 42 (1973) 457.
- [62] T.T.Tenno, U.V. Palm, *Elektrokhimiya* 18(1972) 1381.
- [63] Zview for Windows (version 2.7) Fitting Program, Scribner, Southern Pines, NC, USA
- [64] P. Zoltowski, *Solid State Ionics* 176 (2005) 1979.
- [65] Z. Samec, *J. Electrochem. Soc.* 146 (1999) 3349.
- [66] E. Lust, R. Truu, K. Lust, *Russ. J. Electrochem.* 36 (2000) 1195.
- [67] F.C. Hanson, *Anal. Chem.* 38 (1966) 54.
- [68] X. Ji, F.G. Chevallier, A.D. Clegg, M.C. Buzzeeo, R.G. Compton, *J. Electroanal. Chem.* 581 (2005) 249.
- [69] A.N. Frumkin, E.A. Aikazyán, *Dokl. Akad. Nauk SSSR*, 100 (1955) 315.
- [70] A.N. Frumkin, E. Tedoradze, *Z. Electrochem.* 62 (1958) 252.
- [71] K. Lust, M. Väärtnõu, E. Lust, *Electrochim. Acta* 45 (2000) 3543.
- [72] K. Lust, M. Väärtnõu, E. Lust, *J. Electroanal. Chem.* 532 (2002) 303.
- [73] M. Hromádová, W.R. Fawcett, *J. Phys. Chem. A* 105 (2001) 104.
- [74] T. Thomberg, J. Nerut, R. Jäger, P. Möller, K. Lust, E. Lust, *J. Electroanal. Chem.* 582 (2005) 130.
- [75] K. Lust, E. Lust, *J. Electroanal. Chem.* 552 (2003) 129.
- [76] U.V. Palm, B.B. Damaskin, *Itogi nauki i tekhniki. Elektrkhimiya*, vol. 12, p. 99, VINITI, Moscow (1977).
- [77] M. Väärtnõu, P. Pärsimägi, E. Lust, *J. Electroanal. Chem.* 407 (1996) 227.
- [78] M. Väärtnõu, E. Lust, *Electrochim. Acta* 44 (1999) 2437.
- [79] M. Väärtnõu, E. Lust, *J. Electroanal. Chem.* 469 (1999) 182.
- [80] E. Lust, A. Jänes, K. Lust, M.Väärtnõu, *Electrochim. Acta* 42 (1997) 771.
- [81] E. Lust, K. Lust, A. Jänes, *Soviet Electrochem. Engl. Tr.*, 26, 1627 (1990).
- [82] S. Trasatti, E. Lust in R. E. White, B. E. Conway and J. O'M. Bockris (Ed.), *Modern Aspects of Electrochemistry*, vol. 33, Kluwer Academic / Plenum Publishers, New York and London, 1999, p. 1.
- [83] E. Lust in A. J. Bard, M. Stratmann (Ed.), *Encyclopedia of Electrochemistry*, vol. 1, Wiley 2002, p. 188.
- [84] M. Hromádová, W.R. Fawcett, *J. Phys. Chem. B* 108 (2004) 3277.
- [85] M.Yu. Rusanova, G.A. Tsirlina, R.R. Nazmutdinov, W.R. Fawcett, *J. Phys. Chem. A* 109 (2005) 1348.
- [86] D. Boda, D. Henderson, K.Y. Chan, *J. Chem. Phys.* 110 (1999) 5346.
- [87] T. Thomberg, E. Lust, *J. Electroanal. Chem.* 485 (2000) 89.
- [88] M. E. Orazem, N. Pèbère, B. Tribollet *J. Electrochem. Soc.* 153 (2006) B129.
- [89] V. M.-W. Huang, V. Vivier, N. Pèbère, M. E. Orazem, B. Tribollet, *J. Electrochem. Soc.* 154 (2007) C81.
- [90] V. M.-W. Huang, V. Vivier, I. Frateur, M. E.Orazem, B. Tribollet, *J. Electrochem. Soc.* 154 (2007) C89.
- [91] V. M.-W. Huang, V. Vivier, N. Pèbère, M. E. Orazem, B. Tribollet, *J. Electrochem. Soc.* 154 (2007) C99.
- [92] T. Thomberg, J. Nerut, E. Lust, *J. Electroanal. Chem.* 586 (2006) 237.
- [93] J. R. Macdonald (Ed.), *Impedance Spectroscopy: Emphasizing Solid Materials and Systems*, Wiley, New York, 1987

- [94] A. Lasia in B. E. Conway, R. E. White (Ed.), *Modern Aspects of Electrochemistry*, vol. 35, Kluwer Academic / Plenum Publishers, New York, 2002, p. 1.
- [95] G. J. Brug, A. L. G. van den Eeden, M. Sluyters-Rehbach, J. H. Sluyters, J. *Electroanal. Chem.* 176 (1984) 275.
- [96] W. H. Mulder, J. H. Sluyters, *Electrochim. Acta* 33 (1988) 303.
- [97] J. C. Wang, *Electrochim. Acta* 33 (1988) 707.
- [98] R. de Levie, J. *Electroanal. Chem.* 261 (1989) 1.
- [99] P. Zoltowski, J. *Electroanal. Chem.* 443 (1998) 149.
- [100] Z. Kerner, T. Pajkossy, J. *Electroanal. Chem.* 448 (1998) 139.
- [101] T. Pajkossy, Th. Wandlowski, D. M. Kolb, J. *Electroanal. Chem.* 414 (1996) 209.
- [102] Z. B. Stoyanov, B. M. Grafov, B. S. Savova-Stoynova, V.V. Elkin, *Electrochemical Impedance*, Nauka, Moscow (1991).
- [103] B. M. Grafov, B.B. Damaskin, J. *Electroanal. Chem.* 329 (1992) 129.
- [104] B. M. Grafov, B.B. Damaskin, J. *Electroanal. Chem.* 366 (1994) 29.
- [105] G. Nurk, A. Jänes, K. Lust, E. Lust, J. *Electroanal. Chem.* 515 (2001) 17.
- [106] S. Trasatti, J. *Electroanal. Chem.* 39 (1972) 163.
- [107] L.M. Doubova, S. Trasatti, J. *Electroanal. Chem.* 467 (1999) 164.
- [108] S. Trasatti in: H. Gerischer, C.W. Tobias (Ed.), *Advances in Electrochemistry and Electrochemical Engineering*, vol.10, Wiley Interscience New York 1997, p.123.
- [109] S. Trasatti in: J.D.E. McIntyre, M.J. Weaver, E.B. Yeager (Ed.), *The Chemistry and Physics of Electrocatalysis*, vol.84-12 The Electrochemical Society, Pennington, 1984, p. 150.

9. SUMMARY IN ESTONIAN

Komplekskatioonide elektrokeemiline redutseerimine vismut (hkl) monokristalli tahkudel

Uurimistöö raames uuriti heksaammiinkoobalt(III) kompleksioonide redutseerimise seaduspärasusi elektrokeemiliselt poleeritud Bi(111), Bi(01 $\bar{1}$) ja Bi(001) monokristalli tahkudel erineva keemilise koostisega ja loomusega foonelektrolüüdi vesilahustes. Probleem on huvipakkuv, kuna arvatakse, et antud süsteemi korral on tegu nn. välissfääri elektroni ülekande adiabaatilise protsessiga. Kus reagent otseselt ei läbi metall-elektrolüüdilahus piirpinnal olevat kompaktselt vee molekulide monokihti ehk nn. tihedat kihti. Seega elektroodi keemiline iseloom ei oma otsest mõju elektroni ülekande protsessile.

Elektroodiks valiti vismut, mis on Hg sarnane metall, mille aatomite vahel on küllastatud kovalentsed sidemed ja pind on hästi elektrokeemiliselt poleeritav. Vismut elektroodil on eelnevalt uuritud erinevate ühendite adsorptsiooni impedantsspektroskoopia meetodiga. Ning leitud, et vismuti kristallograafiliselt erinevad tahud erinevad elektrokeemilise aktiivsuse poolest. Uurimustöö üheks eesmärgiks on vismuti kristallograafilise struktuuri ja keemilise loomuse mõju nn. välissfäärireaktsioonile.

Elektrokeemilise redutseerimise mehhanismi ja kineetiliste parameetrite määramiseks teostati katsed nii pöörleva ketaselektroodi kui ka impedants-spektroskoopia meetodit kasutades.

Leiti, et $[\text{Co}(\text{NH}_3)_6](\text{ClO}_4)_3$ redutseerimisprotsessi kiirus sõltub elektroodi potentsiaalst, difuusse kihi paksusest, foonelektrolüüdi keemilisest loomusest ja kontsentratsioonist ning elektroodi pöörlemiskiirusest. Segakineetika alas $-0.75 \text{ V} < E < -0.6 \text{ V}$ on reaktsiooni kiirust limiteerivateks staadiumiteks nii aeglane laenguülekanne kui ka ionide difusioon elektroodile.

Eksperimentaalselt leitud voolutiheduse j väärtusi erinevate kontsentratsioonidega foonelektrolüüdi vesilahustes kasutati piirilise difusioonivoolu määramiseks potentsiaalide alas $-0.9 \text{ V} < E < -0.7 \text{ V}$. Leitud piirilise difusioonivoolu väärtusi kasutades arvutati difusioonikoefitsiendi väärtused Bi(111) kui ka Bi(01 $\bar{1}$) monokristalli tahu jaoks vastavalt: $D = 6.2 \cdot 10^{-6} \text{ cm}^2 \text{ s}^{-1}$ ja $D = 6.6 \cdot 10^{-6} \text{ cm}^2 \text{ s}^{-1}$, mis on samas suurusjärgus kirjanduses toodud difusioonikoefitsientide väärtustega.

Kineetiliste voolude leidmiseks kasutati Koutecky-Levich'i j^{-1} vs. $(\omega^{-1/2})$ sõltuvusi, mis osutusid segakineetika alas lineaarseteks. Leiti, et kineetilise voolu väärtused kasvavad, kui $[\text{Co}(\text{NH}_3)_6](\text{ClO}_4)_3$ kontsentratsioon

kasvab. Koutecky-Levich'i sõltuvustest saadud kineetiliste voolude j_k väärtuste põhjal arvutati heterogeense reaktsiooni kiiruskonstandi k_{het} väärtused. $Bi(hkl)$ heterogeense laenguülekande kiiruskonstantide väärtused on samas suurusjärgus $Au(111)$ saadutega.

$[Co(NH_3)_6](ClO_4)_3$ redutseerimisreaktsiooni eksperimentaalsed heterogeense laenguülekande kiiruskonstantide väärtused sõltuvad foonelektrolüüdi keemilisest loomusest olles mõnevõrra väiksemad $HClO_4$ korral $Bi(hkl)$ monokristalli tahkudel. Null-laengu lähedases alas lineaarsetest $\ln k_{het}$ vs. ϕ_m sõltuvuste tõusudest arvutati eksperimentaalsed laenguülekandekoefitsiendi α_{exp} väärtused.

Elektrokeemiliselt aktiivsemal vismuti tahul $Bi(01\bar{1})$ on foonelektrolüüdi kontsentratsioonidel $c > 0.01M$ mõnevõrra väiksemad eksperimentaalsed laenguülekandekoefitsiendid, kui $Bi(001)$ tahu korral. Eksperimentaalsed laenguülekandekoefitsiendi α_{exp} väärtused sõltuvad vismuti elektrodide kristallograafilisest struktuurist ja foonelektrolüüdi keemilisest loomusest.

Leitud kineetiliste voolude ja ψ_d potentsiaalide alusel, mis leiti elektrilise kaksikkihi andmetest, koostati parandatud Tafeli sõltuvused, kasutades efektiivseid laengu väärtusi $z_{eff} = 1$ ja $z_{eff} = 2$. Parandatud Tafeli sõltuvused foonelektrolüüdi madalamatel kontsentratsioonidel ei osutunud lineaarseteks. Konstrueerides Fawcetti poolt välja pakutud sõltuvused $d(\ln k_{het})/d(\phi_m - \psi_d)$ vs. $(\phi_m - \psi_d)$, on võimalik arvutada lineaarse sõltuvuse tõusust efektiivse laengu väärtus z_{eff} . Leiti, et parandatud Tafeli sõltuvuste kuju sõltub nii foonelektrolüüdi kui ka heksaammiinkoobalt(III) kompleksiooni kontsentratsioonist ning et parandatud Tafeli sõltuvuste kuju muutub reageeriva osakese efektiivse laengu z_{eff} muutumisel. $Bi(hkl)$ korral asub heksaammiinkoobalt(III) kompleksioon elektroodi pinnale lähemal kui seda on väline Helmholtzi tasand ja selletõttu ψ_1 potentsiaali parandused on liiga suured, mis viivadki parandatud Tafeli sõltuvuste lahknemisele. Parandatud Tafeli sõltuvustest leiti formaalse laenguülekandekoefitsiendi α_{app} väärtused. Elektrokeemiliselt aktiivsematel tahkudel $Bi(001)$ ja $Bi(01\bar{1})$ on mõnevõrra kõrgemad formaalse ülekandekoefitsiendi väärtused $LiClO_4$ lisan-diga foonelektrolüütide lahuste korral. $[Co(NH_3)_6](ClO_4)_3$ redutseerimisreaktsiooni mõjutab oluliselt katoode vesiniku eraldumise protsess. Katoode

vesiniku eraldumist uuriti keskmise aktiivsusega elektrokeemiliselt poleeritud Bi(001) tahul, impedantsspektroskoopia meetodiga, mis oli kombineeritud pöörlev ketaselektroodi meetodiga. Happe vesilahustest kõrgetel ülepingetel toimuv vesiniku eraldumise protsessi võib iseloomustada järgmiste elementaarstaadiumidena:

Volmer – iseloomustab reaktsiooni vaheühendi teket, mis sõltub elektroodi metalli keemilisest loomusest ja kristallograafilisest struktuurist. Volmeri reaktsioonile järgneb adsorbeerunud molekulaarse vesiniku moodustumine mis toimub läbi elektrokeemilise desorptsiooni staadiumi mida iseloomustab Heyrovsky reaktsioon. Impedantsspektroskoopia andmete interpreteerimiseks valiti mittelineaarse regressioonianalüüsi alusel modifitseeritud Armstrong-Henderson ekvivalentskeem, mis kirjeldab reageeriva osakese adsorptsiooni ning sellele järgnevat elektroni ülekannet. Ekvivalentskeemis on elektrilise kaksikkihi mahtuvuse asemel konstantse faasinihke element, mis võtab arvesse elektroodi pinnal voolutiheduse jaotust mis on tingitud pinna ebaühtlusest (mittehomogeensusest).

Polarisatsiooniline takistus R_p ja elektrolüüdi takistus R_{el} väheneb perkloorhappe kontsentratsiooni kasvades.

Faasinurga sõltuvustel ϕ vs. $\log f$ madalsageduslikus alas on protsess segakineetiline. Elektrilise kaksikkihi mahtuvus kasvab perkloorhappe kontsentratsiooni kasvades, nihutades elektrilise kaksikkihi laadimise ala kõrgemate sageduste suunas.

Kompleksimpedants sõltuvuste $\log|Z|$ vs. $\log f$ konstrueerimine näitab et elektrilise kaksikkihi laadimine ei sõltu madal sageduslikus alas perkloorhappe kontsentratsioonist, kuid kõrgsageduslikus alas kompleksimpedants väheneb perkloorhappe kontsentratsiooni kasvades.

Karakterseid ajakonstandid on arvatud vastavalt valemile $\tau_{\max} = (2\pi f_{\max})^{-1}$ ning sõltuvad elektroodi potentsiaalst. Negatiivsematel potentsiaalidel karakterse ajakonstandi väärtused vähenevad perkloorhappe kontsentratsiooni kasvades, katoodse vesiniku eraldumise protsess on kiirem.

ϕ vs. $\log f$ sõltuvused näitavad, et katoodse vesiniku eraldumise protsess sõltub elektroodi potentsiaalst ja mehhanism on laenguülekande poolt limiteeritud madalsageduslikus alas, elektroodi potentsiaalil $E = -0.85$ V. $\log(-Z'')$ vs. $\log f$ sõltuvuste analüüs näitab süsteemi väga väikest kõrvalekallet ideaalsest mahtuvuslikust käitumisest, millele otseselt viitavad lineaarsete alade tõusudest määratud konstantse faasinihke elemendi (CPE) $(Z_{CPE} = Q^{-1}(j\omega)^{-\alpha_{CPE}})$ fraktsionaalse eksponendi α_{CPE} väärtused. Fraktsionaalse eksponendi väärtused jäävad Bi(001)|HClO₄ + H₂O süsteemi jaoks vahemikku ($0.94 < \alpha_{CPE} < 0.98$).

Parandatud Tafeli sõltuvused on konstrueeritud kasutades impedants-spektroskoopia andmeid ning vastavalt valemile

$$\ln j_k + \frac{z_{\text{Ox}} F}{RT} \psi_1 = \ln(n F k_s^0 c_{\text{Ox}}^0) - \frac{\alpha n F}{RT} (E - E_{q=0} - \psi_1). \text{ Võttes arvesse et}$$

puudub spetsiifiline adsorptsioon ning vastavalt Gouy-Chapman'i mudelile reaktsiooni tšenter asub välisel Helmholtzi tasandil $\psi_1 \approx \psi_d$. Parandatud Tafeli sõltuvused on lineaarsed kontsentreeritumate perkloorhappe lahuste korral. Lineaarse tõusu väärtused $\alpha = 0.51$. Katoodse vesiniku eraldumise reaktsioon on peamiselt limiteeritud aeglase laenguülekande staadiumi poolt $\text{Bi}(001)|\text{HClO}_4 + \text{H}_2\text{O}$ süsteemi korral.

Armstrong-Hendersoni ekvivalentskeemi üksikparameetrite analüüs näitas et laenguülekande takistus R_{ct} ja adsorptsiooni mahtuvus C_{ad} väärtused sõltuvad elektroodi potentsiaalist. Adsorptsiooni takistuse R_{ad} väärtused on kõige kõrgemad null-laengu potentsiaali alas. Konstantse faasinihke elemendi koefitsiendi Q väärtused sõltuvad elektroodi potentsiaalist ning on kasvavad null-laengu potentsiaali alas perkloorhappe kontsentratsiooni kasvades.

$\text{Bi}(001)|\text{HClO}_4 + \text{H}_2\text{O}$ süsteemi korral sõltub katoodse vesiniku eraldumise kineetika oluliselt elektrilise kaksikkihi ehitusest.

10. ACKNOWLEDGEMENTS

The present study was performed at Institute of Chemistry of the University of Tartu. The support was received from Estonian Science Foundation (grants 6696, 5213 and 5803) and Doctoral School of Material Science and Material Technology.

First and foremost I would like to express my gratitude to my supervisor Professor Enn Lust for persistent assistance and scientific guidance through the years of our collaboration.

I am very thankful to Karmen Lust who had been very helpful in preparing the manuscripts and discussing various problems of electrochemistry.

I would like to thank all my friends and colleagues for helpful discussions, inspiration and continuous support.

I deeply appreciate the unfailing support of my family during all these years.

II. PUBLICATIONS

R. Jäger, **E. Härk**, P. Möller, J. Nerut, K. Lust and E. Lust,
The kinetics of electroreduction of hexaamminecobalt(III)
Cation on Bi planes in aqueous HClO_4 solutions,
Journal of Electroanalytical Chemistry 566 (2004) 217–226.

Reprinted from Journal of Electroanalytical Chemistry, Vol 566,
R. Jäger, E. Härk, P. Möller, J. Nerut, K. Lust and E. Lust,
The kinetics of electroreduction of hexaamminecobalt(III)
cation on Bi planes in aqueous HClO_4 solutions,
pp 217–226, copyright © 2004, with permission from Elsevier Science.

E. Härk, E. Lust,
Electroreduction of Hexaamminecobalt(III) Cation on Bi(*hkl*) Electrodes
from Weakly Acidified LiClO₄ Solutions.
Journal of the Electrochemical Society, 153(6), (2006), E104–E110.

Reproduced by permission of ECS – The Electrochemical Society

III

E. Lust, J. Nerut, **E. Härk**, S. Kallip, V. Grozovski, T. Thomberg,
R. Jäger, K. Lust, K. Tähnäs,
Electroreduction of Complex Ions at Bismuth and
Cadmium Single Crystal Plane Electrodes,
ECS Transactions, 1 (17) (2006) 9–17.

Reproduced by permission of ECS – The Electrochemical Society

IV

E. Härk, E. Lust,
Electroreduction of hexaamminecobalt(III) cations at
electrochemically polished Bi(*hkl*) using
impedance spectroscopy method,

(in review)

Electroreduction of hexaamminecobalt(III) cations at electrochemically polished Bi(hkl) using impedance spectroscopy method

E. Härk, and E. Lust*

Institute of Physical Chemistry, University of Tartu, 2 Jakobi Street, 51014 Tartu, Estonia

Abstract

The electrochemical impedance spectroscopy has been used for investigation of electroreduction kinetics of the hexaamminecobalt(III) cations on the electrochemically polished Bi planes. The total charge transfer resistance obtained depends noticeably on the electrode potential and $[\text{Co}(\text{NH}_3)_6]^{3+}$ concentration. Systematical analysis of results shows that the equivalent circuit taking into account the adsorption of one reacting (or intermediate) particle is the more probable physical model of the very complicated $[\text{Co}(\text{NH}_3)_6]^{3+}$ electroreduction reaction under discussion. The charge transfer resistance, adsorption capacitance and adsorption resistance values depend on the electrode potential as well as on the reactant concentration and the adsorption and charge transfer resistance values are maximal and the adsorption capacitance values are minimal in the region of zero charge potentials for Bi single crystal (111) and (01 $\bar{1}$) planes in the base electrolyte solution with addition of $[\text{Co}(\text{NH}_3)_6]^{3+}$.

Keywords: hexaamminecobalt(III) cation, double layer effects, bismuth single crystal

1. Introduction

The electroreduction of $[\text{Co}(\text{NH}_3)_6]^{3+}$ complex cation is observed as a model reaction for theoretical analysis of the so-called simple outer-sphere reaction [1-12]. Systematical analysis of data for various metals shows that the rate constant depends noticeably on chemical nature of the electrode as well as on the base electrolyte concentration and chemical composition [4,5,7,9-11]. It was found that the rate constant of $[\text{Co}(\text{NH}_3)_6]^{3+}$ reduction for Au single crystal planes at fixed electrode potential increases in the order $\text{Au}(100) < \text{Au}(111) < \text{Au}(110) < \text{Au}(210)$ [7]. The double layer corrected rate constant values for heterogeneous reaction depend on the crystallographic structure of Au plane as well as on the base electrolyte concentration in the $\text{Au}(hkl) | [\text{Co}(\text{NH}_3)_6]^{3+} + \text{HClO}_4 + \text{H}_2\text{O}$ system [7], demonstrating the noticeable dependence of the heterogeneous reaction rate constant k_{het}^0 , corrected for the double layer effect, on the crystallographic structure of the Au electrode and k_{het}^0 decreases with reticular density of the plane [7].

After correction for the electrical double layer effect [13], the kinetic data fall on one common plot for all Au electrodes studied and a single value of the apparent transfer coefficient (α_{app}) is obtained for this electrode reaction [7]. However the reduction kinetics of hexa-aqua-iron (III) ion was studied at $\text{Au}(hkl)$ (at various concentrations of HClO_4 as the base electrolyte [8]), but differently from $[\text{Co}(\text{NH}_3)_6]^{3+} | \text{Au}(hkl)$ interface [7] the transfer coefficient α_{app} depends noticeably on the crystallographic structure of the electrode surface and α_{app} increases with reticular density of the $\text{Au}(hkl)$ planes [8]. On the other hand, the

* Corresponding author

electric double layer corrected rate constant depends on some specific properties of the electrode and the redox species, such as the zero charge potential or the electronic work function of the single crystal plane and its relation to the standard potential [3-5,7,9,10,11].

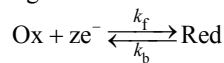
Our analysis based on cyclic voltammetry and rotating disk electrode data of $[\text{Co}(\text{NH}_3)_6]^{3+}$ electroreduction at $\text{Bi}(hkl)$ [11,14] shows that the rate constant of this heterogeneous reaction as well as charge transfer coefficient α_{app} values obtained depend on the crystallographic structure and α_{app} increases slightly with the reticular density of the plane.

Compton et al. [12] studied the electroreduction of $[\text{Co}(\text{NH}_3)_6]^{3+}$ at the polycrystalline gold disc and micro disc electrodes from 0.1 M Na_2SO_4 + 0.1 M phosphate buffer solution at different potential scan rates up to $2 \times 10^6 \text{ V} \cdot \text{s}^{-1}$. At lower potential scan rates the cyclic voltammetry is diffusion-controlled, but at higher scan rates the system undergoes a transition and thereafter the reaction kinetics is limited by the rate of adsorption process [12]. Thus, the relatively quick adsorption of $[\text{Co}(\text{NH}_3)_6]^{3+}$ seems to occur at the polycrystalline Au electrode.

Analysis of experimental data published shows that there is a noticeable dependence of k_{het}^0 on the chemical nature of the base electrolyte [4,5,7,9-11,14], i.e. on the effective solvation radius (or crystallographic radius) of the cation as well as anion studied. This conclusion is in a good agreement with Fawcett et al. results [9], where the quantum chemical calculation method has been used for the analysis of $[\text{Co}(\text{NH}_3)_6]^{3+/2+}$, $[\text{Fe}(\text{CN})_6]^{3-/4-}$ and $[\text{Fe}(\text{H}_2\text{O})_6]^{3+/2+}$ electroreduction parameters. According to calculations the influence of charge distribution in the transition metal complexes on the so-called simple heterogeneous electron transfer reaction mechanism and rate is very big [9]. It has been concluded [7-9] that the electric double layer effect for these reactions depends more on the charge density of the ligands than on the central metal ion. It was demonstrated that the effective charge of the active complex depends noticeably on the electrode potential (i.e. surface charge density σ), thus, on the diffuse layer composition and structure as well as on the orientation of the reacting complex ion. The effective positive charge of the complex cation is noticeably lower at $\sigma \geq 0$, as there are mainly solvated base electrolyte anions on the outer Helmholtz plane compensating the positive charge of central cation [9].

The main aim of this work was to investigate the electroreduction reaction of $[\text{Co}(\text{NH}_3)_6]^{3+}$ cations at the electrochemically polished $\text{Bi}(hkl)$ single crystal plane electrodes in the 0.001M HClO_4 aqueous solution, because in the $x \text{ M LiClO}_4 + y \text{ M HClO}_4$ electrolyte [14] the mixed cationic composition could influence on the electrical double layer effect. It would be very important to verify is there an adsorption of $[\text{Co}(\text{NH}_3)_6]^{3+}$ cations on the $\text{Bi}(hkl)$ electrode surface, explaining the deviation of this system from the simple outer-sphere reaction model [1-6].

Rate of the heterogeneous charge transfer reaction



is given by the expression

$$-j_F = zF(k_f c_{\text{Ox}} - k_b c_{\text{Red}}) \quad (1)$$

where j_F is the faradaic current density, k_f and k_b are the rate constants of forward and reverse reactions, z is the number of the electrons transferred in reaction, F is Faraday constant, c_{Ox} and c_{Red} are the concentrations of reactant (oxidizer) and product (reductant), respectively [15-28]. Using impedance spectroscopy method, the current is composed of a steady-state (or direct) part (determined by the mean dc potential, E , and the mean dc concentrations at the interface, c_{Ox} and c_{Red}) and an ac part Δj_F (determined by the ac perturbing signal ΔE and

concentration fluctuations, Δc_{Ox} and Δc_{Red}). The faradaic impedance is given by the ratio of the Laplace transform of the *ac* parts of the voltage and current density [15-27] respectively

$$Z_F = \{\Delta E\} / \{\Delta j_F\} \quad (2)$$

Under equilibrium conditions the charge transfer resistance

$$R_{\text{ct}} = \frac{RT}{nFj_0}, \quad (3)$$

where the exchange current density j_0 is expressed as

$$j_0 = nFk_0c_{\text{Ox}} \exp\left[-\alpha(E_r - E^0)\frac{nF}{RT}\right], \quad (4)$$

where k_0 is the potential independent rate constant of reaction and n is the number of electrons transferred.

For heterogeneous charge transfer (faradaic) reaction involving one adsorbed particle the following stages can be separated [23-28]:



where the indexes sol and ads denote the particles in solution and adsorbed states, respectively. Assuming the Langmuir adsorption isotherm for B [23, 28], the rates of these reactions may be written as

$$v_1 = k_1^0 \Gamma_s a_A \exp\left[-\alpha_1(E - E_1^0)\frac{F}{RT}\right] - k_1^0 \Gamma_B \exp\left[(1 - \alpha_1)(E - E_1^0)\frac{F}{RT}\right], \quad (5a)$$

$$v_2 = k_2^0 \Gamma_B \exp\left[-\alpha_2(E - E_2^0)\frac{F}{RT}\right] - k_2^0 \Gamma_s a_C \exp\left[(1 - \alpha_2)(E - E_2^0)\frac{F}{RT}\right], \quad (5b)$$

where k_1^0 and k_2^0 are the standard rate constants of these reactions; α_1 and α_2 are the transfer coefficients; Γ_B and Γ_s are the surface concentrations of the species B and of free adsorption sites S ; a_A and a_C are the surface concentrations of A and C (assumed as equal to the bulk concentrations); E_1^0 and E_2^0 are the standard redox potentials of the reactions A and B. At equilibrium potential (E_r) the net rates of both reactions are zero and the following relations are obtained:

$$\exp\left[(E_r - E_1^0)\frac{F}{RT}\right] = \frac{\Gamma_s^0 a_A}{\Gamma_B^0} = \frac{(1 - \theta_0)a_A}{\theta_0}, \quad (6a)$$

$$\exp\left[(E_r - E_2^0)\frac{F}{RT}\right] = \frac{\Gamma_B^0}{\Gamma_s^0 a_C} = \frac{\theta_0}{(1 - \theta_0)a_A}, \quad (6b)$$

where the index 0 indicates equilibrium conditions, and a following relation is introduced: $\Gamma_i = \theta_i \Gamma_{\text{max}}$ (where Γ_{max} is the maximal surface concentration [23, 28]).

The total current density observed is given as

$$j = F(v_1 + v_2) \quad (7)$$

and the faradaic admittance is given by

$$\hat{Y}_f = A + \frac{B}{j\omega + G}, \quad (8)$$

where the inverse charge transfer resistance is obtained as [23]

$$A = \frac{1}{R_{\text{ct}}} = \frac{1}{RT} \left[\alpha_1 \vec{k}_1 (1 - \theta) + (1 - \alpha_1) \overleftarrow{k}_{-1} \theta + \alpha_2 \vec{k}_2 \theta + (1 - \alpha_2) \overleftarrow{k}_{-2} (1 - \theta) \right] \quad (9a)$$

and

$$B = -\frac{1}{C_{ad} R_{ct}^2} = \frac{1}{RT\Gamma_{max}} \left(-\vec{k}_1 - \overleftarrow{k}_{-1} + \vec{k}_2 + \overleftarrow{k}_{-2} \right) \times \\ \times \left[\alpha_1 \vec{k}_1 (1-\theta) + (1-\alpha_1) \overleftarrow{k}_{-1} \theta - \alpha_2 \vec{k}_2 \theta - (1-\alpha_2) \overleftarrow{k}_{-2} (1-\theta) \right] \quad (9b)$$

and

$$G = \frac{1}{R_{ad} C_{ad}} + R_{ct} |B| = \frac{1}{\Gamma_{max}} \left(\vec{k}_1 + \overleftarrow{k}_{-1} + \vec{k}_2 + \overleftarrow{k}_{-2} \right) = \frac{F}{\sigma_1} \left(\vec{k}_1 + \overleftarrow{k}_{-1} + \vec{k}_2 + \overleftarrow{k}_{-2} \right) \quad (9c)$$

It should be noted that the quantity $F\Gamma_{max} = \sigma_1$ is the charge necessary for the total surface coverage of electrode by the reaction intermediate B . The more complicated cases, taking into account the slow diffusion step to the fractal and disc electrodes, have been discussed by Lasia in [23].

2. Experimental

The electrochemically polished (ECP) Bi single crystal (111) and (01 $\bar{1}$) planes were used as the working electrodes [1,29,30], and a calomel reference electrode filled with 4.0 M KCl solution (4M KCl CE), and a large Pt counter electrode completed the conventional three-electrode electrochemical cell. The cleanliness of the base electrolyte solution and the quality of the electrode surface were verified by cyclic voltammetry and impedance methods as well as by using the in situ STM/AFM method [31]. The reference electrode was connected to the cell through a long Luggin capillary filled with the same HClO₄ solution as studied. The reference electrode with two glass membranes has been inserted into the big reservoir filled with the 0.001 M HClO₄ electrolyte. Using the impedance data obtained for the base electrolyte and [Co(NH₃)₆](ClO₄)₃ systems, the absence of Cl⁻ adsorption even at $E > (-0.4 \dots -0.35)$ V (where a strong adsorption of Cl⁻ ions from the binary NaCl + H₂O system takes place [32 - 35]) as well as the absence the zero charge potential shift with the addition of [Co(NH₃)₆](ClO₄)₃ into the base electrolyte solution have been established. Thus, there is no specific adsorption of Cl⁻ ions from our systems.

Glassware was cleaned in a hot H₂SO₄ + H₂O₂ mixture and rinsed with MilliQ+ water before each set of experiments. The experiments were conducted at constant temperature $T = (298 \pm 0.1)$ K under the slight overpressure of a pure argon (99.9995%). All solutions were prepared using the so-called “nanopure water” with maximum resistivity ≥ 18.2 M Ω ·cm [29-31,36]. HClO₄, NaClO₄, and LiClO₄, (all “Aldrich”) were of the best quality available, and [Co(NH₃)₆](ClO₄)₃ was prepared from the corresponding chloride by precipitation with saturated sodium perchlorate and triply recrystallization from water [4,7]. Electrochemical impedance data were obtained using Autolab PGSTAT30 FRA2 system at ac frequency from $5 \cdot 10^{-2}$ to $5 \cdot 10^4$ Hz within the region of electrode potential -0.85 V $< E < -0.4$ V vs. Ag|AgCl|sat KCl in H₂O (future noted as Ag|AgCl). For better comparison with the data of work [11] some cyclic voltammograms (CVs) (scan rate from 5 to 200 mV·s⁻¹) and rotating disc voltammograms (scan rate from 5 to 20 mV·s⁻¹) were obtained by using the “Pine” rotating ring-disc electrode system and the data obtained were in a good agreement with the results published in [11,14].

For the accurate determination of a precision of the experimental data, a statistical treatment of the results was carried out. A total number of the independent experiments $n \geq 4$,

and at least two different electrodes with the same crystallographic orientation were used [11,36]. The relative error in imaginary part $|Z''|$ at fixed real part Z' of the impedance spectra did not exceed 7 % (Figs. 1-4).

3. Results and discussion

3.1. Nyquist ($-Z''$, Z')-plots

According to the data in Figs. 1-4 the shape of the Nyquist and Bode plots depends noticeably on the electrode potential and concentration of reactant in the base electrolyte (0.001M HClO₄) solution. At $E = -0.85$ V for Bi(111)| $1 \cdot 10^{-3}$ M HClO₄ + x M [Co(NH₃)₆]³⁺ and Bi(01 $\bar{1}$)| $1 \cdot 10^{-3}$ M HClO₄ + x M [Co(NH₃)₆]³⁺ systems (Figs. 1a and 1b) the Nyquist plots can be simulated by the slightly depressed semicircles and the total polarisation resistance for pure base electrolyte is noticeably lower than for solutions with addition of reactant. At higher reactant concentrations $c_{[\text{Co}(\text{NH}_3)_6]^{3+}} \geq 2.5 \times 10^{-4}$ M the systematical decrease of total polarisation resistance R_p (in comparison with 2.5×10^{-4} M [Co(NH₃)₆]³⁺ + base electrolyte) takes place.

The absolute values of the so-called capacitive resistance $|Z''| = \frac{1}{jC_s \omega}$ at the relaxation frequency f_{\max} decrease with the rise of reactant concentration but the values of $|Z''|$ are noticeably higher than for the pure base electrolyte solution. The values of $|Z''|$ at $f_{\max} \sim 0.2$ Hz (f_{\max} is the value of the frequency at the maximum in the $-Z''$, Z' -curve) are practically independent of the plane studied and there is no noticeable dependence of f_{\max} on the crystallographic structure of the electrode surface as well as on $c_{[\text{Co}(\text{NH}_3)_6]^{3+}}$ in solution (Fig.

1). The phase angle vs $\log f$ (Bode) plots (Figs. 2a and 2b) show that the systematic shift of the phase angle vs $\log f$ plots toward higher frequencies is clearly visible in the electrical double layer formation region (1 Hz < f < 300 Hz). In the low frequency region the phase angle is practically independent of $c_{[\text{Co}(\text{NH}_3)_6]^{3+}}$, demonstrating that the adsorption equilibrium

has been established already at very low reactant concentrations. Differently from the high ac frequency region the noticeable shift of the δ , $\log f$ - plots for systems with addition of reactant in comparison with pure base electrolyte toward lower values of f has been observed, somewhat larger for Bi(01 $\bar{1}$) than that for Bi(111). For Bi(hkl) planes in the region of frequency from 0.5 Hz to 10 Hz there is a small plateau with the phase angle $\delta \approx -80^\circ$ indicating that the heterogeneous adsorption step is the main rate limiting process in this ac frequency region. At lower frequencies the charge transfer step is limiting for electroreduction reaction of [Co(NH₃)₆]³⁺ at Bi(111) at $E = -0.85$ V. The same rate limiting steps are valid for the Bi(01 $\bar{1}$) plane too.

The Nyquist plots measured at $E = -0.65$ V (Fig.3) (potential region of mixed kinetics according to rotating disc electrode voltammetry data) show that differently from the data at $E = -0.85$ V the $-Z''$, Z' -plots have more complicated shape instead of semicircle, characterizing the mixed kinetic process at Bi(hkl). Similarly to the data at $E = -0.85$ V the value of $|Z''|$ at fixed f decreases systematically with the rise of reactant concentration, but $|Z''|$ is higher than that for pure base electrolyte solution. Taking into account the complicated shape of the $-Z''$, Z' -plots, it is impossible to obtain correctly the so-called total polarization resistance R_p values. The phase angle vs $\log f$ dependences (Fig. 4) show that differently from

data at $E = -0.85$ V there is no dependency of the phase angle on reactant concentration in the high-frequency region $f > 10$ Hz, but at lower frequencies (in region of plateau and lower) the values of δ (at fixed ac frequency) for solutions with addition of $[\text{Co}(\text{NH}_3)_6]^{3+}$ are noticeably lower than for base electrolyte. Thus, in the region of $f < 10$ Hz there is mainly an adsorption limited process at $\text{Bi}(hkl)$. However, differently from $E = -0.85$ V the systematic increase of δ at $f < 1$ Hz occurs with the addition of $[\text{Co}(\text{NH}_3)_6]^{3+}$ in solution, explained with the shift of $[\text{Co}(\text{NH}_3)_6]^{3+}$ electroreduction from adsorption limited process toward mixed kinetic process with the rise of $[\text{Co}(\text{NH}_3)_6]^{3+}$ concentration in solution at lower frequencies (Fig. 3 and 4).

The data in Figs. 5 and 6 show that at fixed f the absolute values of $|Z''|$ and $|\delta|$ are maximal in the potential region from -0.65 to -0.55 V for $\text{Bi}(hkl)$, thus, in the region of zero charge potential $E_{\sigma=0}$ of the $\text{Bi}(hkl)$ planes in the base electrolyte solution. The absolute values of $|Z''|$ for the positively charged $\text{Bi}(hkl)$ electrode ($E \geq -0.55$ V) are somewhat lower compared with the data obtained at $E \sim E_{\sigma=0}$, but the data for $E = -0.85$ V are very different from the data measured at $E = E_{\sigma=0}$. The systematic trends of the dependence of $|Z''|$ and δ on E obtained for more concentrated $[\text{Co}(\text{NH}_3)_6]^{3+}$ solutions ($c_{[\text{Co}(\text{NH}_3)_6]^{3+}} \geq 5 \times 10^{-4}$ M) are in agreement with the results for more dilute $[\text{Co}(\text{NH}_3)_6]^{3+}$ solutions (Fig. 7a and b).

3.2. Fitting results of impedance data

The experimental $-Z''$, Z' -plots and δ , $\log f$ -plots can be fitted by using the nonlinear square root least minimization method [15-24]. According to the fitting results, to the very rough approximation, the Dolin - Ershler (A circuit in Fig. 8) and Randles (C) equivalent circuits can be used for fitting the experimental results [15-18, 23, 37, 38]. However, the errors in the individual parameters are comparatively high. A noticeably better fitting has been obtained if the so-called Frumkin-Melik-Gaikazyan-Randles (in reality Ershler) [37, 38] equivalent circuit (D) has been used for analysis of the reaction mechanism (i.e. the adsorption capacitance characterizing the weak co-adsorption of $[\text{Co}(\text{NH}_3)_6]^{3+}$ cation and ClO_4^- anion is assumed). The errors in the individual parameters are quite small, however, in the case of more concentrated $[\text{Co}(\text{NH}_3)_6]^{3+}$ solutions the errors in individual parameters are comparatively high.

The equivalent circuit, taking into account one adsorbed particle (or reactant intermediate) at the electrode surface [23] (circuit B in Fig. 8), achieved a very good fit of the experimental results. Errors in the individual parameters are small and the values of the χ^2 function less than $4 \cdot 10^{-3}$ have been obtained at potentials from -0.85 to -0.55 V for the solutions with $c_{\text{base el}} = 0.001$ M. Higher χ^2 values ($\chi^2 > 6 \cdot 10^{-3}$) have been obtained for more concentrated base electrolyte solutions at potentials from -0.65 V to -0.55 V, where the simultaneous adsorption of ClO_4^- and $[\text{Co}(\text{NH}_3)_6]^{3+}$ is probable.

The results of fitting analysis, given in Figs. 9-13, show that R_{el} , C_{dl} , C_{ad} , R_{ad} and R_{ct} depend noticeably on the electrode potential as well as on $c_{[\text{Co}(\text{NH}_3)_6]^{3+}}$ in solution. The high-frequency resistance R_{el} , characterizing mainly the electrolyte resistance, is independent of the electrode potential and decreases with the rise of the ionic strength of solution. In the all potential region the electrical double layer capacitance (Fig. 10) for the base electrolyte is lower than for solutions with addition of $[\text{Co}(\text{NH}_3)_6]^{3+}$ and at $E = -0.85$ V C_{dl} is independent of $[\text{Co}(\text{NH}_3)_6]^{3+}$ addition except very concentrated reactant concentrations. In the region from -0.75 V to -0.55 V the diffuse layer minimum with characteristic minimum capacitance C_{min} and minimum potential E_{min} can be seen in a good agreement with the experimental

differential capacitance data obtained at $f = 110$ Hz. At E_{\min} the value of C_{\min} increases systematically with the rise of $c_{[\text{Co}(\text{NH}_3)_6]^{3+}}$ in solution in a good agreement with the Gouy-Chapman-Grahame model.

The charge transfer resistance R_{ct} vs potential plots (Fig. 11) have a comparatively high maximum in the region of E_{\min} where the diffuseness of the electrical double layer is maximal. At E_{\min} there is a systematic decrease in R_{ct} with the rise of $c_{[\text{Co}(\text{NH}_3)_6]^{3+}}$ in solution if $c_{[\text{Co}(\text{NH}_3)_6]^{3+}} \geq 3.5 \times 10^{-4}$ M. The charge transfer resistance is somewhat higher for Bi(01 $\bar{1}$), characterized by the higher adsorption activity of ions at this plane from aqueous base electrolyte solution [30,31,33,34]. The data in Fig.12 show that the adsorption resistance R_{ad} is maximal at E_{\min} and with the increase of absolute value of surface charge density the R_{ad} values decrease. However, in the all region of E studied the values of R_{ad} are higher than in the base electrolyte and R_{ad} decreases systematically with the rise of reactant concentration if $c_{[\text{Co}(\text{NH}_3)_6]^{3+}} \geq 2.5 \times 10^{-4}$ M. The values of R_{ad} for Bi(01 $\bar{1}$) are somewhat higher than these for the less active Bi(111) plane, in a good agreement with the R_{ct} , E -plots in Fig. 11, indicating the influence of the adsorption process on the values of R_{ct} . At $|\sigma| \geq 0$ there is no big dependence of R_{ct} and R_{ad} on $c_{[\text{Co}(\text{NH}_3)_6]^{3+}}$ in solution.

According to the data in Fig.13, the values of adsorption capacitance C_{ad} are minimal in the region of diffuse layer minimum in a good agreement with the Gouy-Chapman-Grahame model, and at $E = E_{\min}$ the values of C_{ad} are practically independent of $c_{[\text{Co}(\text{NH}_3)_6]^{3+}}$ in solution, which is in a good agreement with Gouy-Chapman-Grahame-Parsons model [11,29-37]. At negative surface charge density ($\sigma < 0$) C_{ad} increases with the rise of the reactant concentration. At positive surface charge density ($\sigma > 0$) the same is valid for the Bi(111) plane. At $E = -0.5$ V the reverse dependence of C_{ad} on the concentration of anions seems to take place for Bi(01 $\bar{1}$) explained by the stronger specific adsorption or by so-called blocking adsorption of anions at electrochemically more active Bi(01 $\bar{1}$) plane.

The dependences of kinetic parameters A , B and G (Eq. 9a-c) on the electrode potential for different Bi(hkl) planes at various additions of $[\text{Co}(\text{NH}_3)_6]^{3+}$ in the base electrolyte solution have been calculated and are given in Figs. 14 and 15. According to the fitting results C_{ad} (Fig.13) and R_{ct} (Fig. 11) are positive and, thus, B has negative values in the all regions of potential and $c_{[\text{Co}(\text{NH}_3)_6]^{3+}}$ studied (Fig. 14). The $-B$, E plots have a minimum in the region of zero charge potential and with the rise of the absolute value at surface charge density the absolute values of B decrease with the reactant concentration, expressed more noticeably at E higher than $E_{\sigma=0}$. For higher reactant concentrations ($c_{[\text{Co}(\text{NH}_3)_6]^{3+}} > 3.5 \times 10^{-4}$ M) the values of $-B$ are practically independent of $c_{[\text{Co}(\text{NH}_3)_6]^{3+}}$ if $E > E_{\min}$. According to the data in Fig. 15, the values of G are minimal at $E \sim E_{\sigma=0}$ but for Bi(111) plane at $E > E_{\sigma=0}$ the values of G rise with the $c_{[\text{Co}(\text{NH}_3)_6]^{3+}}$. For Bi(111) at $E < E_{\sigma=0}$ and for Bi(01 $\bar{1}$) electrode at $|\sigma| > 0$ the G values are maximal for base electrolyte with addition of 2.5×10^{-4} M $[\text{Co}(\text{NH}_3)_6]^{3+}$ in solution. Therefore the more pronounced specific adsorption of $[\text{Co}(\text{NH}_3)_6]^{3+}$ at electrochemically more active Bi(01 $\bar{1}$) plane is possible. However, it should be noted that the in situ FTIR spectroscopy data are inevitable for the more detailed analysis of Bi(hkl) | base electrolyte + $[\text{Co}(\text{NH}_3)_6]^{3+}$ system, in progress now in our laboratory.

4. Conclusions

The electroreduction kinetics of the hexaamminecobalt(III) cations on the electrochemically polished Bi planes has been studied by the impedance spectroscopy, cyclic voltammetry and rotating disc electrode methods. It was found that the electroreduction of $[\text{Co}(\text{NH}_3)_6]^{3+}$ cations is limited mainly by the mixed kinetics at lower ω frequencies. At moderate ω frequencies ($1 < f < 100$ Hz) the adsorption step is the main rate limiting stage.

Systematical analysis of results shows that the equivalent circuit taking into account the adsorption of one reacting (or intermediate) particle is the more probable physical model for the very complicated $[\text{Co}(\text{NH}_3)_6]^{3+}$ electroreduction reaction under discussion. The values of charge transfer resistance, adsorption capacitance, and adsorption resistance depend on the electrode potential as well as on the reactant concentration and the adsorption resistance is minimal and charge transfer resistance and adsorption capacitance are maximal in the region of zero charge potential for Bi single crystal (111) and (01 $\bar{1}$) planes in the base electrolyte solution with addition of $[\text{Co}(\text{NH}_3)_6]^{3+}$.

Acknowledgements: This work was supported in part by the Estonian Science Foundation under Project numbers 5803 and 6696.

References

- [1] F.C. Hanson, *Anal. Chem.*, **38**, 54 (1966).
- [2] M.J. Weaver and F.C. Anson, *J. Am. Chem. Soc.*, **97**, 4403 (1975).
- [3] G.J. Brug, M. Sluyters-Rehbach, J.H. Sluyters, A. Hamelin, *J. Electroanal. Chem.*, **181**, 245 (1984).
- [4] A. Hamelin, M.J. Weaver, *J. Electroanal. Chem.*, **209**, 109 (1986).
- [5] A. Hamelin, M.J. Weaver, *J. Electroanal. Chem.*, **223**, 171 (1987).
- [6] W.R. Fawcett, in *Electrocatalysis*, J. Lipkowski, P.N. Ross, Editors, p. 323 (Chapter 8), Wiley, New York (1998).
- [7] M. Hromadova, W.R. Fawcett, *J. Phys. Chem. A*, **104**, 4356 (2000).
- [8] M. Hromadova, W.R. Fawcett, *J. Phys. Chem. A*, **105**, 104 (2001).
- [9] W.R. Fawcett, M. Hromadova, G.A. Tsirlina, R.R. Nazmutdinov, *J. Electroanal. Chem.*, **498**, 93 (2001).
- [10] M.J. Weaver, *J. Electroanal. Chem.*, **498**, 105 (2001).
- [11] R. Jäger, E. Härk, P. Möller, J. Nerut, K. Lust, E. Lust, *J. Electroanal. Chem.*, **566**, 217 (2004).
- [12] X. Ji, F.G. Chevallier, A. D. Clegg, M. C. Buzzeo, R. G. Compton, *J. Electroanal. Chem.*, **581**, 249-257 (2005).
- [13] A.N. Frumkin, N.V. Nikolaeva-Fedorovich, N.P. Berezina, Kh.E. Keis, *J. Electroanal. Chem.* **58** (1975) 189.
- [14] E. Härk, and E. Lust, Electroreduction of hexaamminecobalt(III) cation on Bi(hkl) electrodes from weakly acidified LiClO₄ solutions. *J. Electrochem. Soc.* **153**, E104 (2006)
- [15] M. Sluyters-Rehbach, in: A. Bard (Eds.), vol. 4, Marcel Dekker, New York, 1970, p. 1.
- [16] R.D. Armstrong, M. Henderson, *J. Electroanal. Chem.* **39** (1972) 81.
- [17] M. Sluyters-Rehbach, J.H. Sluyters, in: E. Yeager, J. O. M. Bockris, B. E. Conway, S. Sarangapani (Eds.), *Comprehensive Treatise of Electrochem*, vol. 9, Plenum Press, New York, 1984.
- [18] I.D. Raistrick, J.R. MacDonald, D.R. Franceschetti, in: J. R. MacDonald (Eds.), *Impedance Spectroscopy*, vol., Wiley, New York, 1987.
- [19] M. Sluyters-Rehbach, *Pure Appl. Chem.* **66** (1994) 1831.
- [20] C. Gabrielli, in: I. Rubinstein (Ed.) *Physical Electrochemistry – Principles, Methods and Application* (Ch.6) Marcel Dekker, New York, 1995, p. 257.
- [21] L.M. Peter, W. Dür, P. Bindra, H. Gerischer, *J. Electroanal. Chem.* **71** (1976) 31.
- [22] S.A. Campbell, L.M. Peter, *J. Electroanal. Chem.* **364** (1994) 257.
- [23] A. Lasia, in: B. E. Conway, J. O. M. Bockris, R. E. White (Eds.), *Modern Aspects of Electrochemistry*, vol. 32, Kluwer Academic/Plenum Publishers, New York, 1999, p. 143.
- [24] J. Barber, S. Morin, B.E. Conway, *J. Electroanal. Chem.* **446** (1998) 125.
- [25] C. Deslouis, I. Epelboin, M. Keddad, J.C. Lestrade, *J. Electroanal. Chem.* **28** (1970) 57.
- [26] J.S. Chen, J.-P. Diard, R. Durand, C. Montella, *J. Electroanal. Chem.* **406** (1996) 1.
- [27] L. Bai, D.A. Harrington, B.E. Conway, *Electrochim. Acta* **32** (1987) 1713.
- [28] B. Breyer, H.H. Bauer, *Alternating Current Polarography and Tensammetry*, Wiley Interscience, New York, 1963.
- [29] E. Lust, R. Truu, K. Lust, *Russ. J. Electrochem.* **36**, 1195 (2000)
- [30] E. Lust, A. Jänes, K. Lust, M. Väärtnõu, *Electrochim. Acta* **42** (1997) 771.
- [31] S. Kallip, E. Lust, *Electrochem. Comm.*, **7**, 863 (2005).
- [32] K. Lust, M. Väärtnõu, E. Lust, *Electrochim. Acta*, **45**, 3543 (2000).
- [33] K. Lust, M. Väärtnõu, E. Lust, *J. Electroanal. Chem.*, **532**, 303 (2002).

- [34] K. Lust, E. Lust, J. Electroanal. Chem., **552**, 129 (2003).
- [35] U.V. Palm, B.B. Damaskin, Itogi nauki i tekhniki. Elektrkhimiya, vol. 12, p. 99, VINITI, Moscow (1977).
- [36] T. Thomberg, E. Lust, J. Electroanal. Chem., **485**, 89 (2000).
- [37] B.V. Ershler, Zh. Fiz. Khim. **22** (1948) 683.
- [38] T. Thomberg, J. Nerut, E. Lust, J. Electroanal. Chem., **586**, 237 (2006).
- [39] Z View for Windows (ver.2.7), Scribner, Southern Pines, NC, USA.

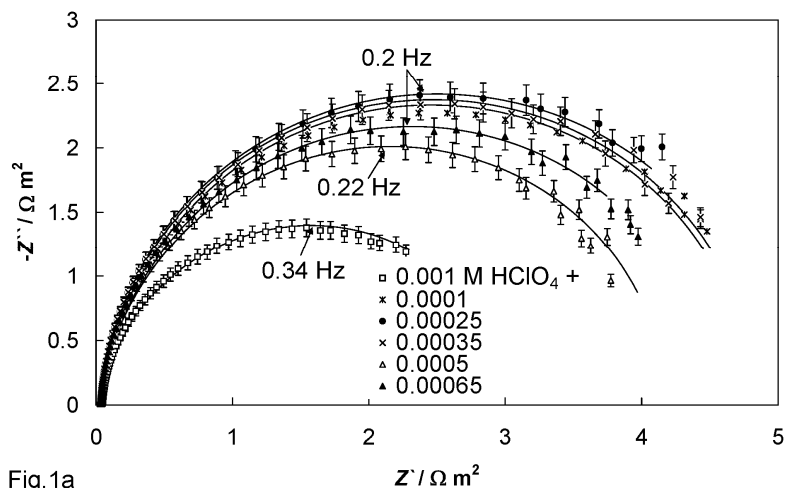


Fig.1a

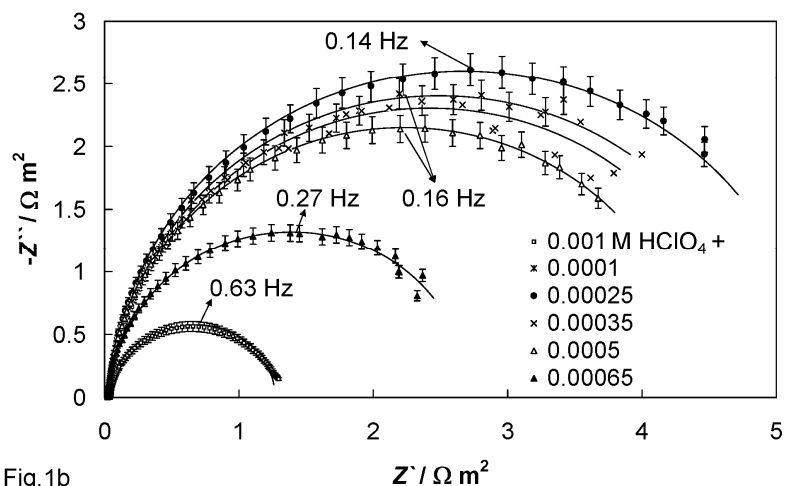


Fig.1b

Fig.1. Complex plane plots for ECP Bi(111) **(a)** and ECP Bi(011̄) **(b)** in aqueous 0.001 M HClO₄ solution with different additions of [Co(NH₃)₆](ClO₄)₃ (M), noted in figure, at the electrode potential $E = -0.85$ V vs. Ag | AgCl | sat. KCl (marks – experimental, solid lines – data calculated according to the circuit ‘B’ in Fig. 8.).

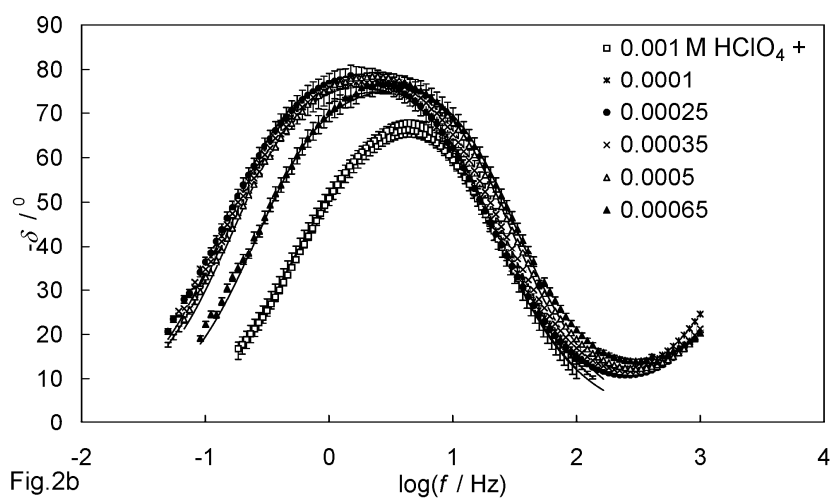
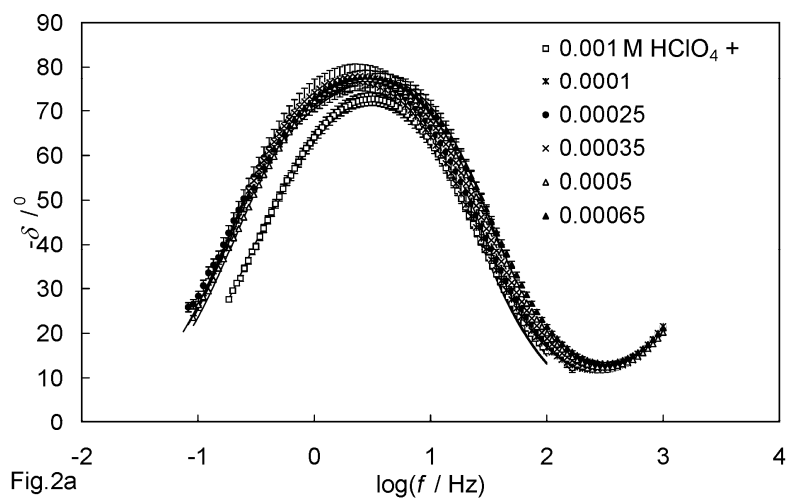


Fig.2. Phase angle (δ) vs. ac frequency plots for ECP Bi(111) (a) and ECP Bi(01 $\bar{1}$) (b) in aqueous 0.001 M HClO₄ solution with different additions of [Co(NH₃)₆](ClO₄)₃ (M), noted in figure, at the electrode potential $E = -0.85$ V vs. Ag | AgCl | sat. KCl (marks – experimental, solid lines – data calculated according to the circuit ‘B’ in Fig. 8.).

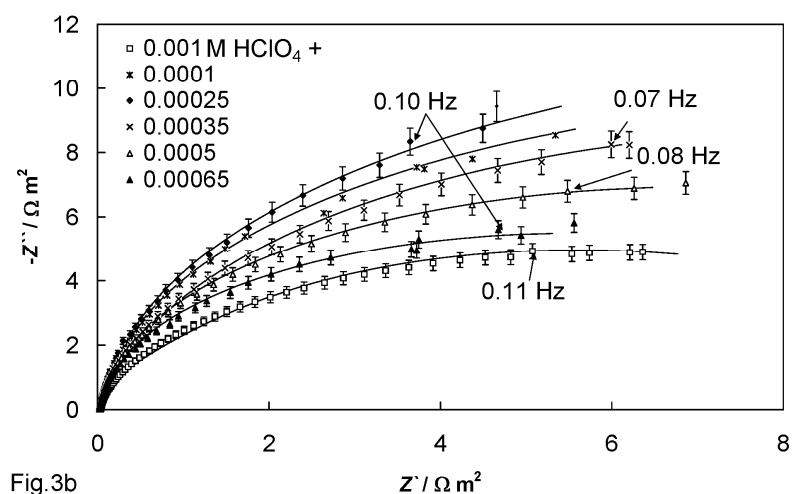
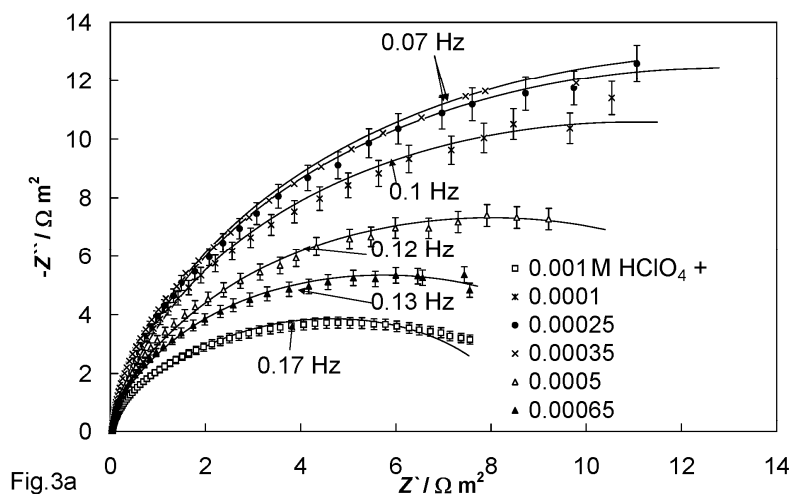


Fig.3. Complex plane plots for ECP Bi(111) (a) and ECP Bi(011̄) (b) in aqueous 0.001 M HClO₄ solution with different additions of [Co(NH₃)₆](ClO₄)₃ (M), noted in figure, at the electrode potential $E = -0.65$ V vs. Ag | AgCl | sat. KCl (marks – experimental, solid lines – data calculated according to the circuit ‘B’ in Fig. 8.).

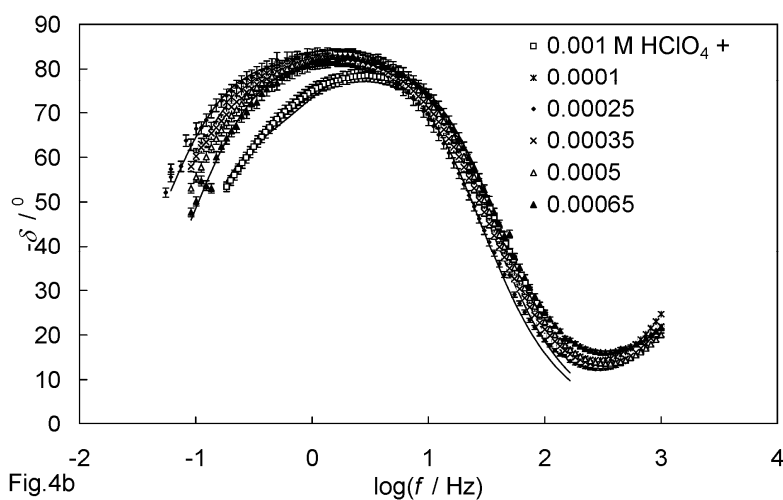
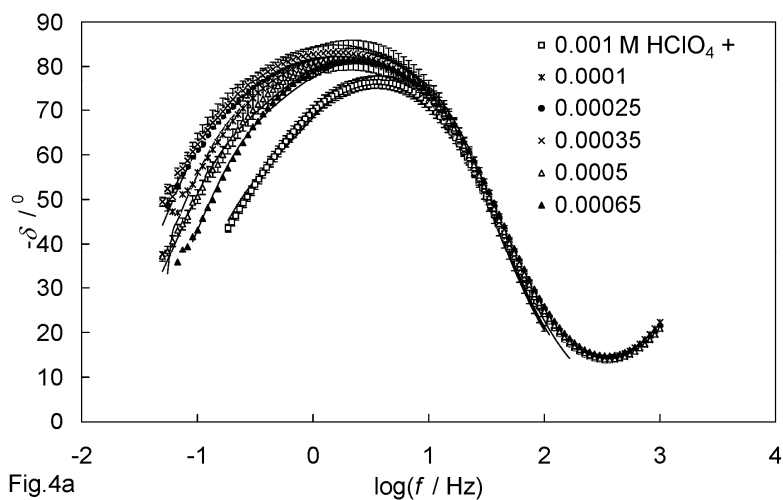


Fig.4. Phase angle (δ) vs. ac frequency plots for ECP Bi(111) (a) and ECP Bi(01 $\bar{1}$) (b) in aqueous 0.001 M HClO₄ solution with different additions of [Co(NH₃)₆](ClO₄)₃ (M), noted in figure, at the electrode potential $E = -0.65$ V vs. Ag | AgCl | sat. KCl (marks – experimental, solid lines – data calculated according to the circuit ‘B’ in Fig. 8.).

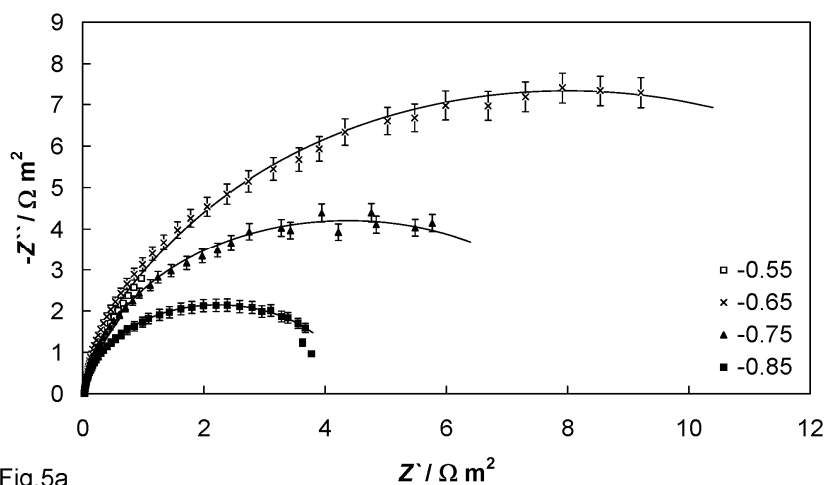


Fig.5a

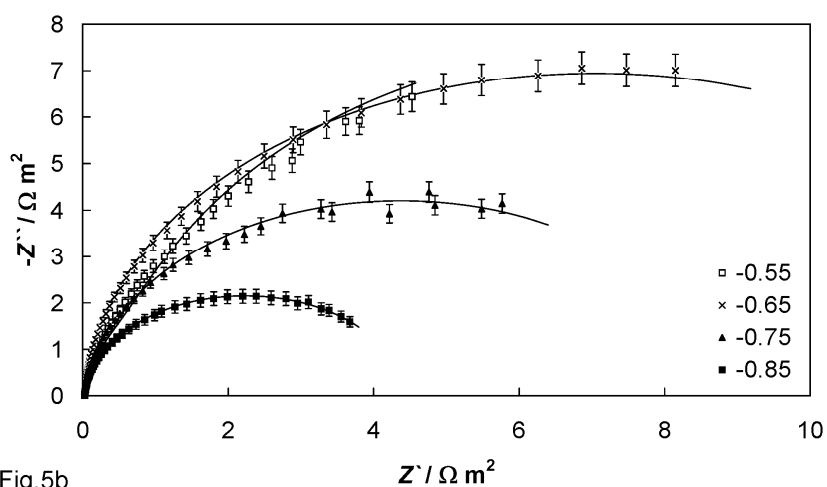


Fig.5b

Fig.5. Complex plane plots for the ECP Bi(111) (a) and ECP Bi(011̄) (b) in the 0.001 M HClO_4 + 0.0005 M $[\text{Co}(\text{NH}_3)_6](\text{ClO}_4)_3$ aqueous solution at different electrode potentials (V vs $\text{Ag} | \text{AgCl} | \text{sat. KCl}$), noted in figure, (marks – experimental, solid lines – data calculated according to the circuit ‘B’ in Fig. 8.).

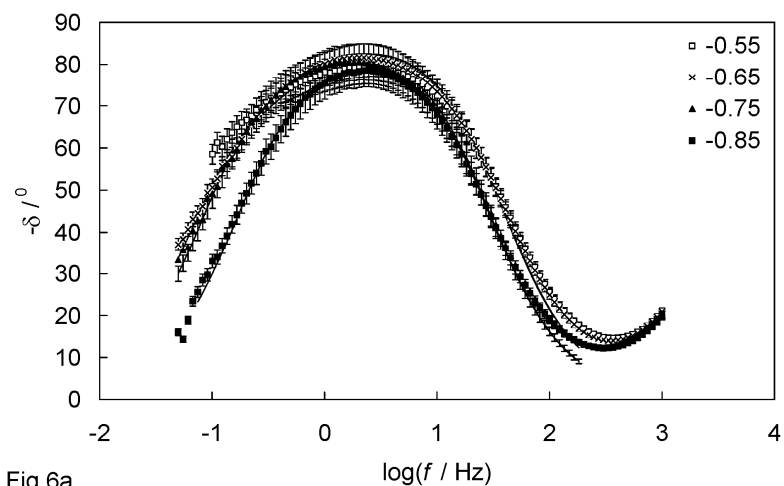


Fig.6a

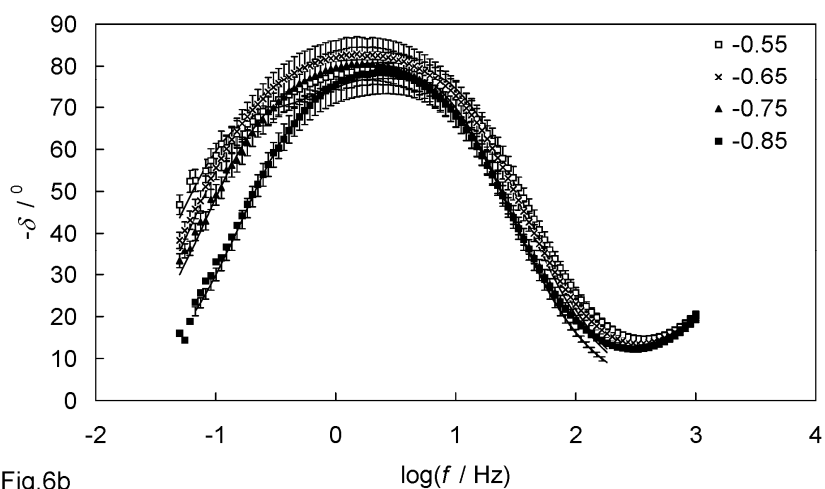


Fig.6b

Fig.6. Phase angle (δ) vs. ac frequency plots for ECP Bi(111) (a) and ECP Bi(01 $\bar{1}$) (b) in the 0.001 M HClO_4 + 0.0005 M $[\text{Co}(\text{NH}_3)_6](\text{ClO}_4)_3$ aqueous solution at different electrode potentials (V vs Ag | AgCl | sat. KCl), noted in figure, (marks – experimental, solid lines – data calculated according to the circuit ‘B’ in Fig. 8.).

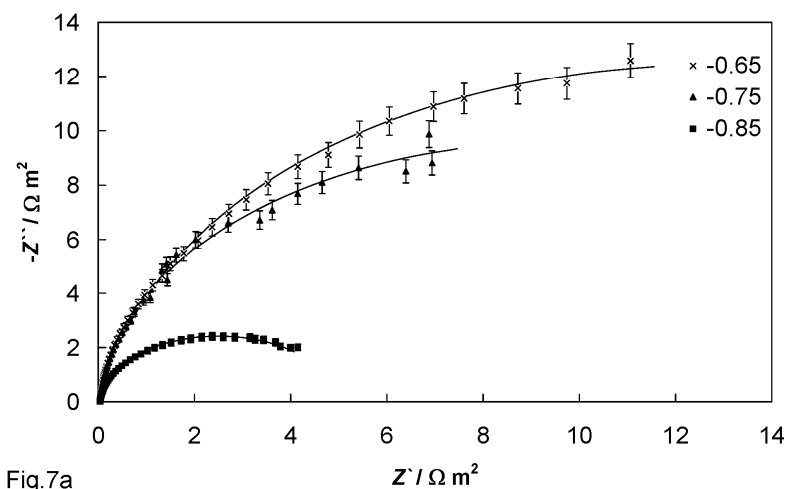


Fig.7a

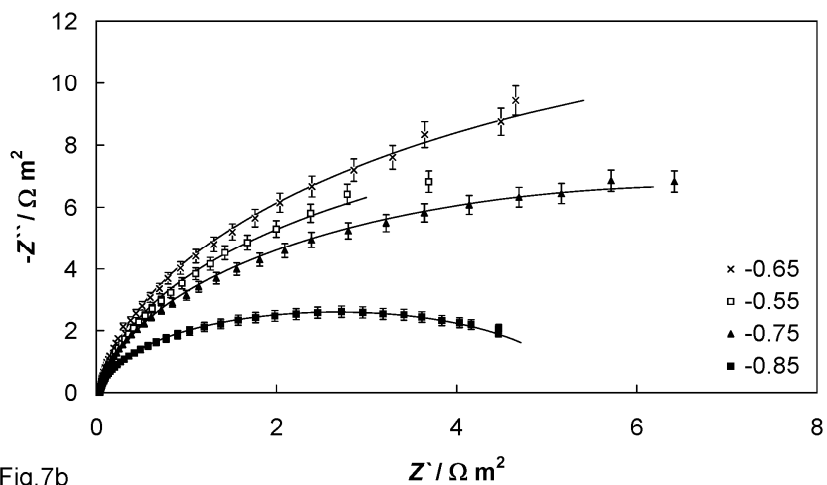


Fig.7b

Fig.7. Complex plane plots for ECP Bi(111) (a) and ECP Bi(011̄) (b) in the 0.001 M HClO₄ + 0.00025 M [Co(NH₃)₆](ClO₄)₃ aqueous solution at different electrode potentials (V vs Ag | AgCl | sat. KCl), noted in figure, (marks – experimental, solid lines – data calculated according to the circuit 'B' in Fig. 8.).

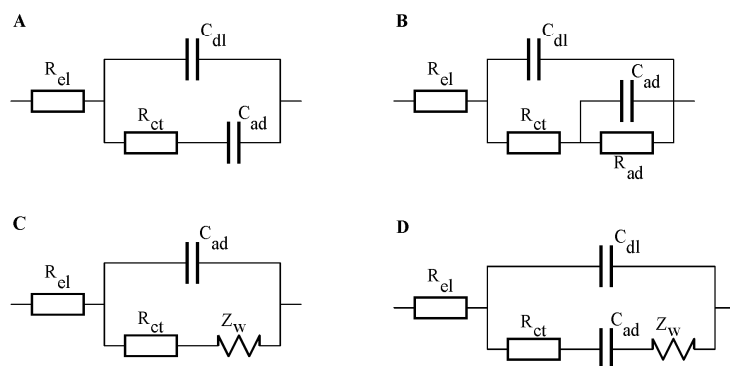


Fig.8

Fig.8. Equivalent circuits used for fitting the experimental results: Dolin-Ershler circuit (A), model taking into account adsorption of one intermediate particle (B), Randles model (C) and Frumkin–Melik-Gaikazyán–Randles model (D) (R_{el} – electrolyte solution resistance; C_{dl} – double layer capacitance; R_{ct} – charge transfer resistance; Z_w – Warburg-like diffusion impedance; R_{ad} – adsorption or partial charge transfer resistance; C_{ad} – adsorption capacitance).

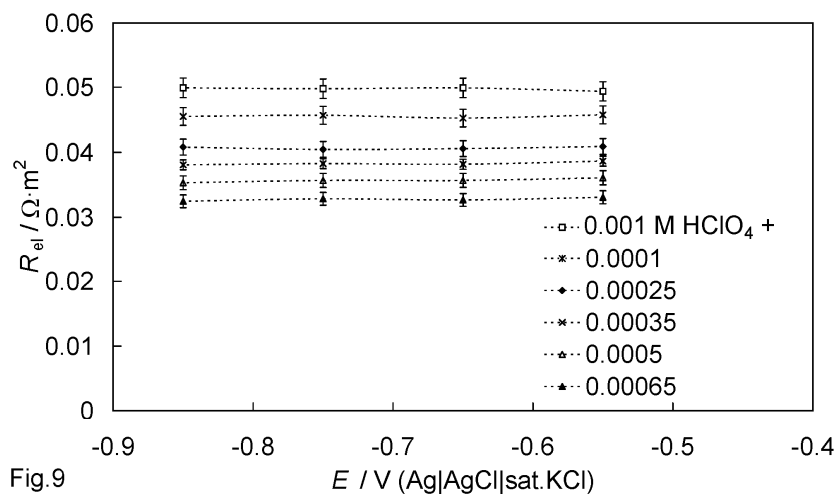


Fig.9. Dependence of electrolyte solution resistance (circuit 'B' in Fig. 8) on the electrode potential for the ECP Bi(111) plane in 0.001 M $HClO_4$ solution with different addition of $[Co(NH_3)_6](ClO_4)_3$ (M), noted in figure.

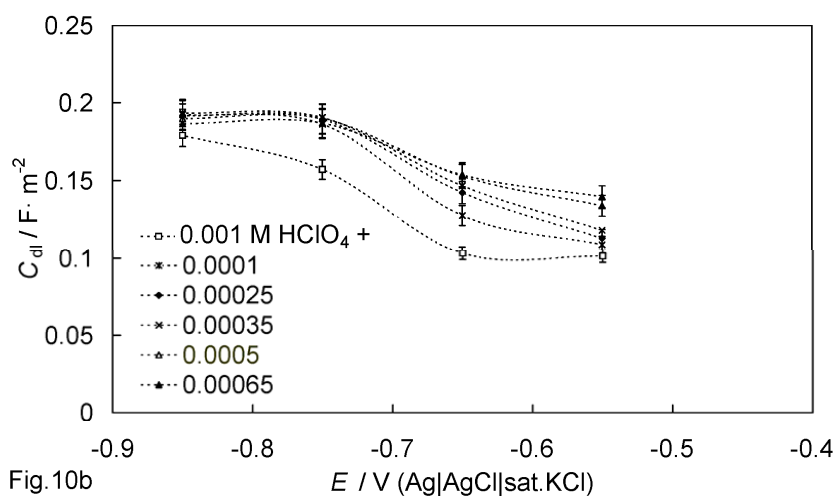
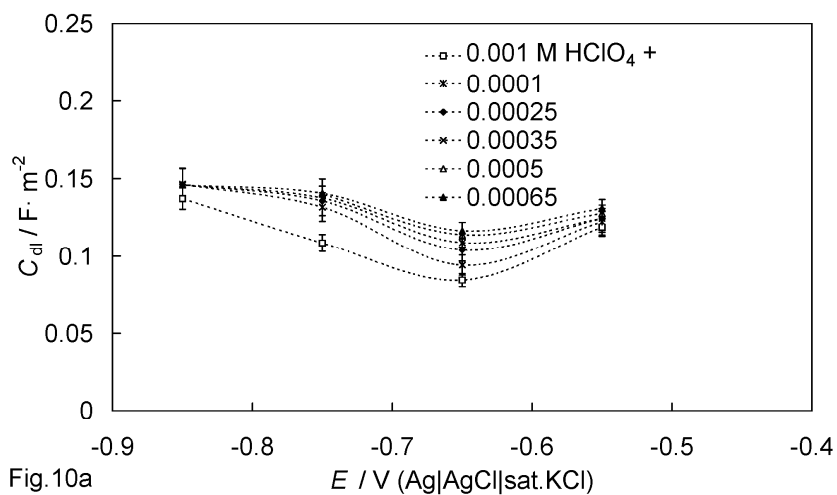


Fig.10. Dependence of double layer capacitance (circuit 'B' in Fig. 8) on the electrode potential for ECP Bi(111) (a) and ECP Bi(011̄) (b) in 0.001 M HClO₄ solution with different addition of [Co(NH₃)₆](ClO₄)₃ (M), noted in figure.

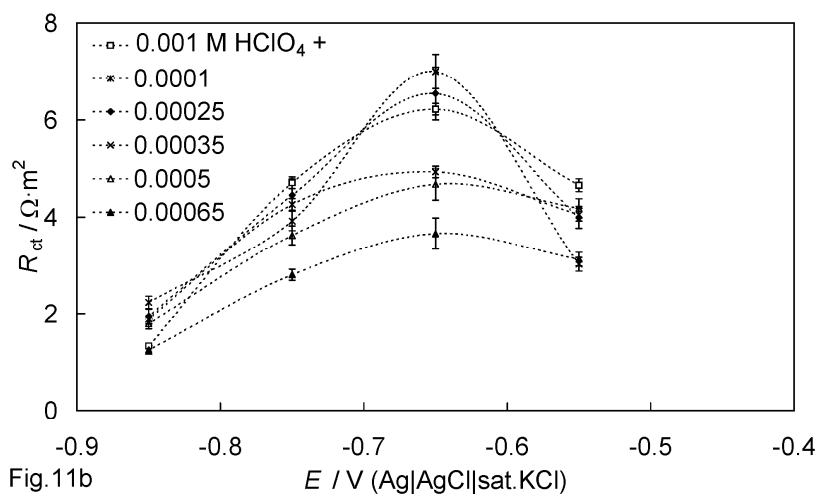
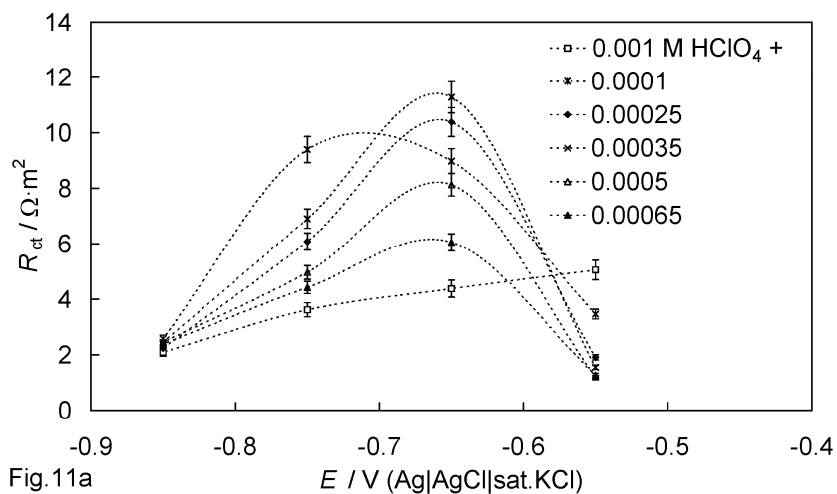


Fig.11. Dependence of charge transfer resistance (circuit 'B' in Fig. 8) on the electrode potential for ECP Bi(111) **(a)** and ECP Bi(011) **(b)** in 0.001 M HClO₄ solution with different addition of [Co(NH₃)₆](ClO₄)₃ (M), noted in figure.

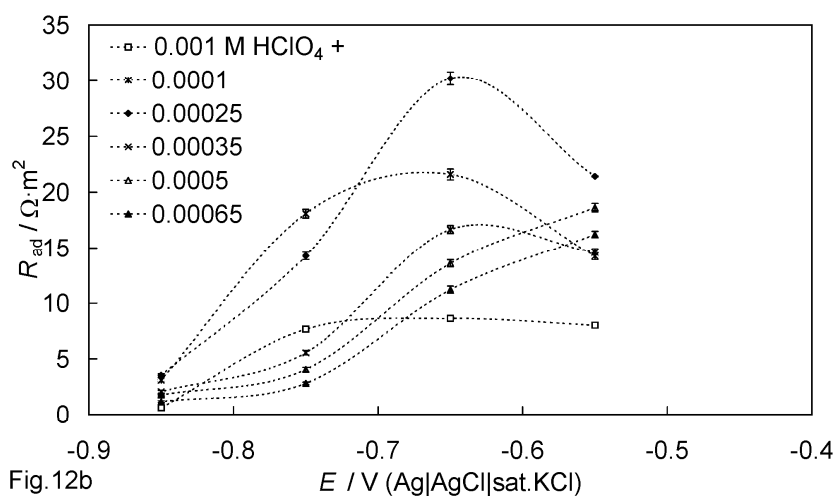
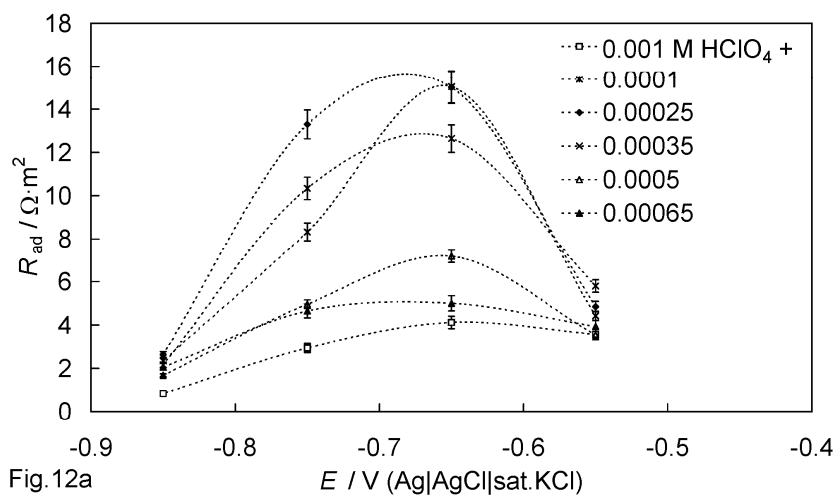


Fig.12. Dependence of adsorption resistance (circuit 'B' in Fig. 8) on the electrode potential for ECP Bi(111) (a) and ECP Bi(011) (b) in 0.001 M $HClO_4$ solution with different addition of $[Co(NH_3)_6](ClO_4)_3$ (M), noted in figure.

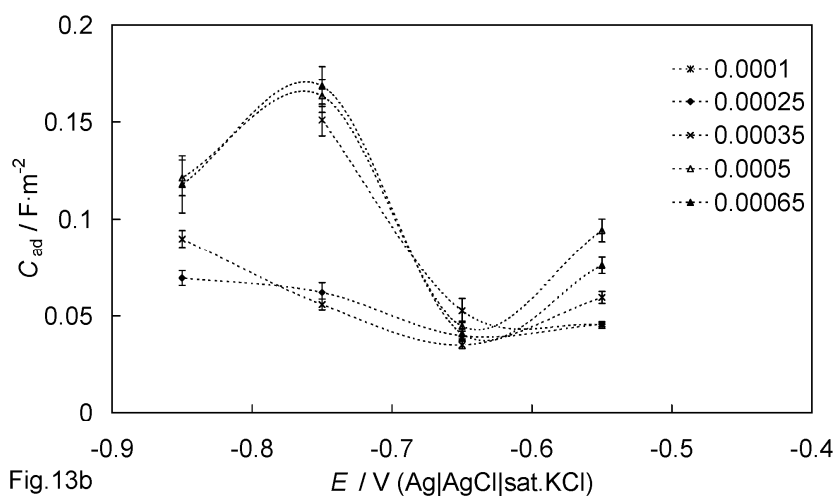
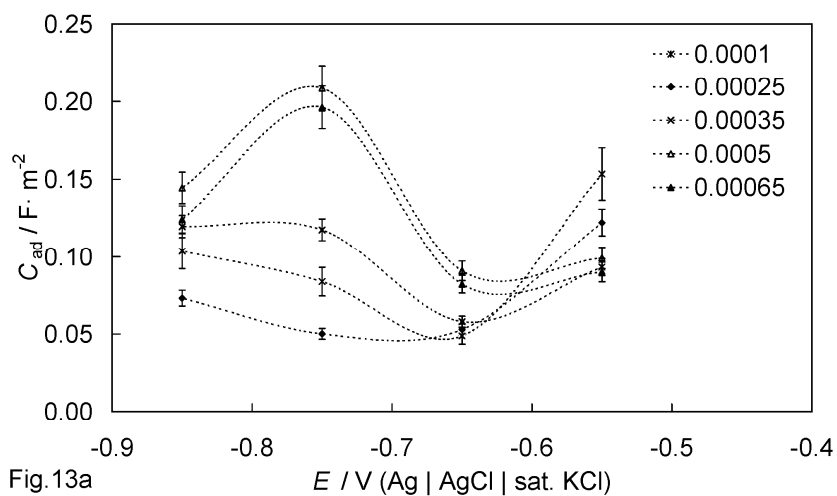


Fig.13. Dependence of adsorption capacitance (circuit 'B' in Fig. 8) on the electrode potential for ECP Bi(111) (a) and ECP Bi(011̄) (b) in 0.001 M HClO₄ solution with different addition of [Co(NH₃)₆](ClO₄)₃ (M), noted in figure.

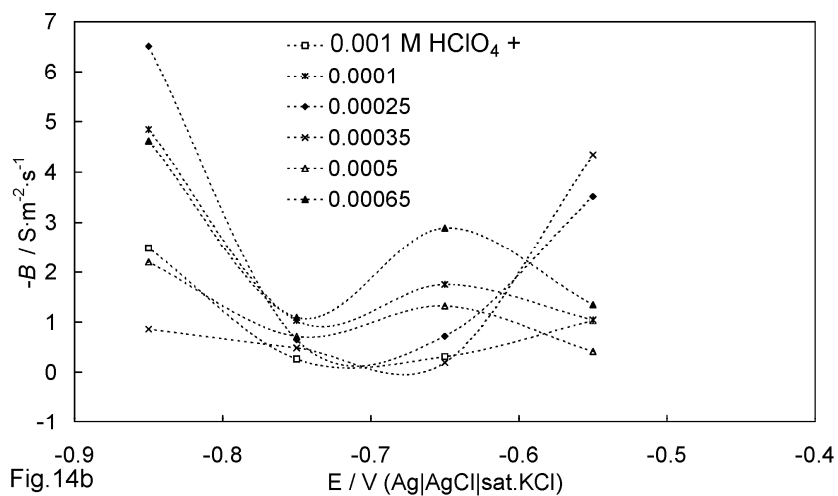
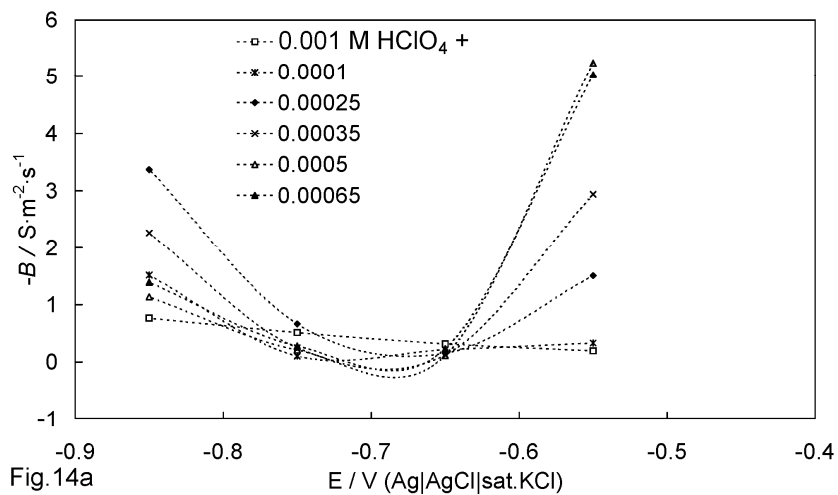


Fig.14. Dependence of the parameter B (circuit ‘B’ in Fig. 8) on the electrode potential for ECP Bi(111) (a) and ECP Bi(011) (b) in 0.001 M HClO_4 solution with different addition of $[\text{Co}(\text{NH}_3)_6](\text{ClO}_4)_3$ (M), noted in figure.

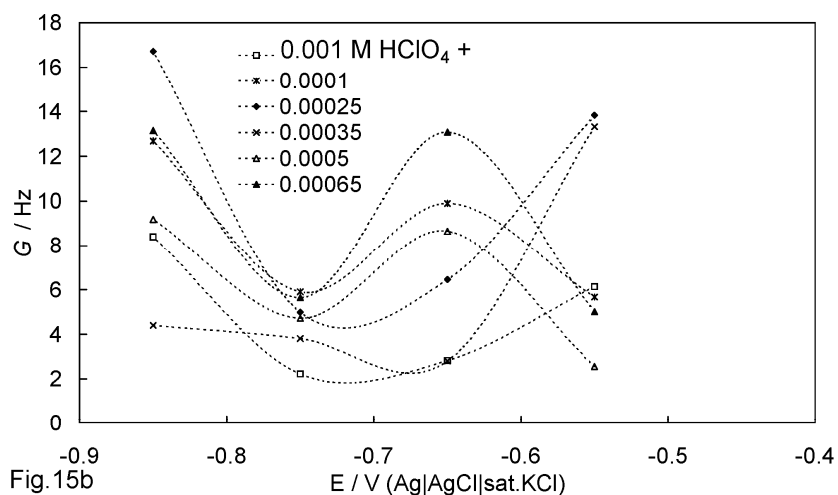
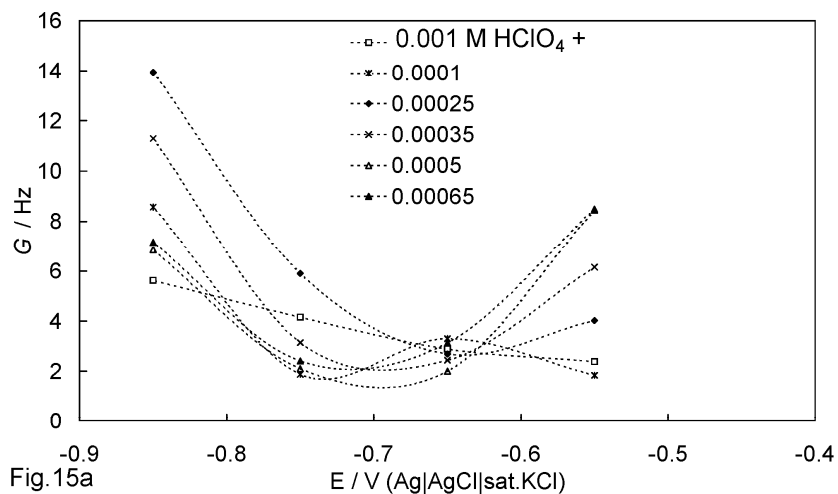


Fig.15. Dependence of the parameter G (circuit 'B' in Fig. 8) on the electrode potential for ECP Bi(111) (a) and ECP Bi(011) (b) in 0.001 M HClO_4 solution with different addition of $[\text{Co}(\text{NH}_3)_6](\text{ClO}_4)_3$ (M), noted in figure.

V

E. Härk, K. Lust, A. Jänes, E. Lust,
Electrochemical impedance study of hydrogen evolution on Bi(001)
electrode in the HClO₄ aqueous solutions,
Journal of Solid State Electrochemistry Submitted (JSEL-D-08-00102)

Electrochemical impedance study of hydrogen evolution on Bi(001) electrode in the HClO₄ aqueous solutions

Eneli Härk • Karmen Lust • Alar Jänes • Enn Lust

Abstract Electrochemical impedance spectroscopy has been applied for investigation of the hydrogen evolution kinetics at the electrochemically polished Bi(001) plane, and the complicated reaction mechanism (slow adsorption and charge transfer steps) has been established. The charge transfer resistance and adsorption capacitance values depend noticeably on the electrode potential applied. The adsorption resistance is maximal in the region of electrode potential $E_{\min} = -0.65$ V vs. (Hg|Hg₂Cl₂|4M KCl), where the minimal values of constant phase element (CPE) coefficient Q have been calculated. The fractional exponent α_{CPE} values of the CPE close to unity ($\alpha_{\text{CPE}} \geq 0.94$) and weakly dependent on the electrode potential and pH of solution ($c_{\text{HClO}_4} \leq 2 \cdot 10^{-3}$ M) have been obtained, indicating the weak deviation of Bi(001) | HClO₄ + H₂O interface from the ideally flat capacitive electrode. Q differs only very slightly from double-layer capacitance C_{dl} values in the whole region of potentials and c_{HClO_4} , investigated.

Keywords impedance · bismuth single crystal · cathodic hydrogen evolution

E.Härk · K.Lust · A.Jänes · E.Lust
Institute of Chemistry, University of Tartu,
2 Jakobi Street, 51014 Tartu, Estonia
e-mail:enn.lust@ut.ee

Introduction

The various electrochemical techniques - classical polarization measurements [1-7], potential relaxation [8-10], electrochemical impedance spectroscopy (EIS) [5, 11-14] and potential-step coulometry [15-17] have been applied for analysis of the cathodic hydrogen evolution reaction (HER) at different metal electrodes. The controversial conclusions at variously pretreated polycrystalline electrodes, assuming the formation of a Pd-H layer and formation of the supersaturated region of H₂ gas in the thin solution layer at the Pt electrode | electrolyte interface, from which molecular H₂ diffuses away [13, 18-21], have been made. The different explanations given are not surprising because the cathodic hydrogen evolution and the interaction of hydrogen atoms with Pt-metals, extensively studied using electrochemical and surface science techniques, have been found to be highly sensitive on the single-crystal plane surface structure [3-7]. The second complication is involving absorption and diffusion of hydrogen within the thin metal surface layer (almost palladium, but also rhodium, nickel and other metals and alloys) discussed by various authors [2, 18, 20-32].

The influence of the crystallographic structure of Ni(*hkl*) electrodes has been studied [33] and it was found that the hydrogen evolution overpotential increases in the order of planes (110) < (100) < (111), i.e. with the reticular density of plane [33-35].

The detailed studies at Ag(*hkl*) and Au(*hkl*) planes [36-40] show that there is a noticeable influence of the electrode surface structure on the kinetic parameters of HER. At constant electrode potential the electroreduction rate of H_3O^+ increases in the order of planes Ag(110) < Ag(100) < Ag(111) [37, 39]. A very weak dependence of the exchange current density j_0 on the surface structure of the Au(*hkl*) electrode has been observed, and j_0 increases in the order Au(110) < Au(100) < Au(111). The data for Au(*hkl*) planes are controversial [36, 40], explained by the strong influence of the surface reconstruction phenomenon of the Au interface on the kinetic parameters of hydrogen evolution [34, 35, 41-45].

A very limited amount of experimental data for single crystal planes of so-called Hg-like metals (Bi, Cd, Sb, [1, 33, 35, 46, 47]) (i.e. of metals with high hydrogen evolution overpotential [48-53]) has been performed. The discharge of hydronium ion with formation of adsorbed intermediate $\text{H}_3\text{O}^+ + \text{e}^- + \text{M} = \text{MH}_{\text{ads}} + \text{H}_2\text{O}$ is well known to be the rate-controlling step of HER at the mercury and bismuth electrodes [43, 46-53].

The noticeable influence of the crystallographic structure of the Bi(111), Bi(001) and Bi(01 $\bar{1}$) single crystal planes on the kinetic parameters of HER has been observed in the $(1-x)\text{MHClO}_4 + x\text{MLiClO}_4$ solutions (where x is the mole fraction of LiClO_4) [1]. The remarkable dependence of the Tafel constant, an apparent transfer coefficient α and j_0 on the Bi(*hkl*) surface structure as well as on the composition of the electrolyte has been established and discussed [1, 34, 35, 46]. Noticeable deviation from the simplified version of the classical Frumkin discharge model, ignoring specific adsorption of reactant, intermediate particles and product [4], has been observed [1]. In addition, influence of pH of the supporting electrolyte solution $(1-x)\text{MHClO}_4 + x\text{MLiClO}_4$ on the electroreduction kinetics of the $[\text{Co}(\text{NH}_3)_6]^{3+}$ cations has been observed [45-47], impossible to explain taking into account that solvated protons are not involved in the molecular mechanism of the electroreduction process of the hexaamminecobalt(III) complex cations at Bi(*hkl*) planes.

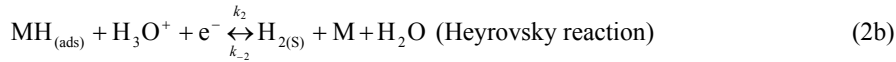
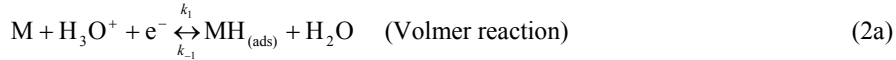
The main aim of this work was to study the kinetics of HER at the electrochemically polished (EP) Bi(001) single crystal plane in diluted solutions of HClO_4 , using EIS [54-59] and classical methods, and to compare the results with those obtained by the classical Tafel overvoltage measurement method for $(1-x)\text{MHClO}_4 + x\text{MLiClO}_4$ solutions with constant ionic strength [1]. These data are useful for the more detailed analysis of the $[\text{Co}(\text{NH}_3)_6]^{3+}$ electroreduction reaction mechanism, taking into account that simultaneous HER and $[\text{Co}(\text{NH}_3)_6]^{3+}$ electroreduction reactions probably occur on the Bi(*hkl*) planes at more negative potentials than the zero charge potential [1, 34, 35, 46, 47].

Theoretical introduction

It is generally accepted that the total current density j_t passing through the electrode | electrolyte interface consists of the non-faradic (i.e. so-called double-layer charging) j_{nf} and faradic j_f parts. and applying the *ac* potential perturbation $\Delta E(\omega)$, (ω is angular frequency, $\omega=2\pi f$, where f is *ac* frequency) the total interfacial impedance can be expressed as

$$Z_t^{-1}(\omega) = Z_{nf}^{-1}(\omega) + Z_f^{-1}(\omega), \quad (1)$$

if ohmic potential drop $jR \approx 0$, where R is ohmic resistance. HER at high cathodic overpotentials $\eta \ll 0$ from the acidic aqueous solution, to a first approximation, can be characterized by the following elementary steps [1, 13, 18, 19, 27, 28, 36, 37, 40, 46-51]:



where M is metal, H_3O^+ stands for solvated protons, $H_{2(S)}$ is the molecular hydrogen adsorbed at the surface and $MH_{(ads)}$ is the reaction intermediate, formed after electron transfer from metal M to solvated proton H_3O^+ . k_1 , k_{-1} , k_2 and k_{-2} are the rate constants of corresponding reactions.

Taking into account the possible weak adsorption of reaction intermediate $MH_{(ads)}$ at the Bi electrode surface [1, 48, 49], the faradaic impedance can be mathematically simulated as Eq.(3a), if we accept the so-called model for adsorption of one intermediate particle at an electrode surface [27, 28, 38-40, 48-51]:

$$\frac{1}{Z_f} = \frac{1}{R_{ct}} + \frac{B}{j\omega + G} \quad (3a)$$

where $j = \sqrt{-1}$ and the inverse charge transfer resistance R_{ct} is given as:

$$\frac{1}{R_{ct}} = \frac{1}{RT} [\alpha_1 k_1 (1 - \theta) + (1 - \alpha_1) k_{-1} \theta + \alpha_2 k_2 \theta + (1 - \alpha_2) k_{-2} (1 - \theta)] \quad (3b)$$

$$B = \frac{1}{RT\Gamma_{\max}} (-k_1 - k_{-1} + k_2 + k_{-2}) \times [\alpha_1 k_1 (1 - \theta) + (1 - \alpha_1) k_{-1} \theta - \alpha_2 k_2 \theta - (1 - \alpha_2) k_{-2} (1 - \theta)] \quad (3c)$$

and

$$G = \frac{1}{\Gamma_{\max}} (k_1 + k_{-1} + k_2 + k_{-2}) = \frac{F}{\sigma_1} (k_1 + k_{-1} + k_2 + k_{-2}) \quad (3d)$$

where the α_1 and α_2 are the symmetry coefficients, θ is the surface coverage and Γ_{\max} is maximal Gibbs adsorption.

It should be noted that the quantity $F\Gamma_{\max} = \sigma_1$ is the charge necessary for the total surface coverage by adsorbed intermediate. It is evident that R_{ct}^{-1} and G have always positive values but B may be positive or negative, depending on the values of the various

rate constants. Two general cases should be considered depending on the sign of the parameter B . If $B < 0$ then the faradic impedance Z_f is described as

$$Z_f = (Y_f)^{-1} = R_{ct} + \frac{R_{ct}^2 |B|}{j\omega + G - R_{ct} |B|} = R_{ct} + \frac{1}{R_{ad}^{-1} + j\omega C_{ad}}, \quad (4)$$

where the so-called adsorption resistance is expressed as $R_{ad} = R_{ct}^2 |B| / (G - R_{ct} |B|)$ and adsorption capacitance as $C_{ad} = (R_{ct}^2 |B|)^{-1}$. Eq.(4) characterizes a series connection of the charge transfer resistance R_{ct} with a parallel connection of R_{ad} and adsorption capacitance C_{ad} . The shape of the impedance complex plane ($-Z''$ vs. Z') plot depends on the sign of the denominator $(G - R_{ct} |B|)$ of R_{ad} [27].

Thus, reaction (2a) characterizes the formation of reaction intermediate and, depending on the chemical and crystallographic characteristics of the electrode metal, the formation of the adsorbed molecular hydrogen and evolution probably occur through the electrochemical desorption step for Bi electrodes [52, 53].

Experimental

The massive bismuth single crystal was grown by the modified Czochralski method (purity 99.9999 %) at the Institute of Problems of Microelectronics Technology and Superpure Materials, Russian Academy of Sciences. The Bi(001) plane orientation was obtained using X-ray diffraction method and the disorientation angle was smaller than 0.5° . The isolation of the surface area not interested was carried out by a thin polystyrene film prepared using the solution of polystyrene dissolved in toluene. After evaporation of toluene the electrode was placed into a Teflon holder [1, 34, 35]. The surface was polished mechanically to mirror finish, using standard metallographic procedure and thereafter electrochemically in the $KI + HCl$ aqueous solution at current density $\geq 1.5 \text{ A} \cdot \text{cm}^{-2}$ [1, 34, 35, 46, 47]. After electrochemical polishing the electrode was immediately rinsed with MilliQ+ water and submerged under constant electrode potential -0.64 V vs. $Hg|Hg_2Cl_2|4M \text{ KCl}$ (4M CE) into $x \text{ M HClO}_4$ aqueous solution (x from $1 \cdot 10^{-3}$ to $1 \cdot 10^{-2} \text{ M}$), deaerated with the pure argon (99.9995%).

The reference 4M KCl calomel electrode was connected to the impedance cell through the very long Luggin capillary [1, 34, 35, 46, 47] to avoid the contamination of $HClO_4$ solution with Cl^- anions. In this paper all electrode potentials are given vs. 4M CE and difference with saturated calomel electrode (SCE) is 4 mV. Current density values stabilized after at least two hours polarization were measured using Pine rotating electrode system. The aqueous $HClO_4$ solutions were prepared from the redistilled perchloric acid (Aldrich 99.999%) using MilliQ+ water ($> 18.2 \text{ M} \Omega \text{ cm}^{-1}$). The electrochemical impedance was measured at the rotating disk Bi(001) single-crystal electrodes (150 rev min^{-1}) to seclude the H_2 from surface with the exposed superficial area 0.1 cm^2 . For impedance measurements the electrolytic cell with a very large polycrystalline Pt counter electrode was used (flat cross section area $\sim 40 \text{ cm}^2$). Bi(001)

plane has been selected out because of the very good electrochemical stability in the wide potential region [1, 46, 47].

The electrochemical impedance data have been obtained using Autolab PGSTAT 30 with FRA2 (± 5 mV modulation) within the frequency region from 0.05 to $1 \cdot 10^4$ Hz. The Kramers - Kronig tests have been made to select out the frequency region free from systematic errors and it has been found that the data for $c_{\text{HClO}_4} = 0.001\text{M}$ and for 0.01M at $f \leq 2 \cdot 10^3$ Hz and $f \leq 7 \cdot 10^3$ Hz respectively, can be used for detailed kinetic analysis [27, 28, 54-60]. Based on the data presented in Figs. 1b, 2b and 3b, the provisional values of α_{CPE} can be calculated in a good agreement with the data obtained from the slope of $\log(-Z'')$ vs. $\log f$ plots. It should be noted that according to some works the impedance complex plane plots can be used in the wider high frequency region [27, 60] adding some elements into the equivalent circuit (very high frequency R_{hf} and C_{hf} elements). However based on the future equivalent circuit (EC) analysis, these elements (as well as an additional Pt wire electrode acting as a low impedance bypass to conventional reference electrode [27, 60]) have only very small influence on the fitting parameters for the medium and low frequency Nyquist plot region i.e. on the CPE fractional exponent α_{CPE} and coefficient Q , as well as R_{ad} and R_{ct} values, respectively.

Various equivalent circuits have been tested for fitting of the experimental impedance complex plane ($-Z''$ vs. Z'), Bode ($\log |Z|$ and phase angle ϕ vs. $\log f$ plots), $\log(-Z'')$ vs. $\log f$ plots using non-linear least-squares minimization program that minimizes the sum of $(Z_{\text{m}} - Z_{\text{c}})^2$ terms for all frequency points measured (Z_{m} and Z_{c} are the measured and calculated impedance values, respectively [62, 63]). The theoretical spectrum calculated (based on the arbitrarily chosen model) has been fitted to the experimental impedance data (spectrum) and the best-fitted case has been selected on the basis of the minimal χ^2 - function value. The standard deviation (SD) of the fit defined as, $SD = \sqrt{\chi^2 / 2l - p}$ (where l denotes the number of points and p denotes the number of parameters of the fitting model), is a general measure of the goodness of fit and therefore SD method [63] (only for ECs without distributed elements (CPE)) has been applied in this work too. Additionally, the weighted sum of squares Δ^2 , as well as errors of individual parameters obtained have been analyzed [27, 29, 62, 63] keeping the number of experimental points constant for all fittings made using various equivalent circuits.

Results and discussion

Impedance spectroscopy

Impedance complex plane and Bode plots as well as $\log(-Z'')$ vs. $\log f$ plots for the Bi(001) electrode measured in various HClO_4 aqueous solutions (c_{HClO_4} varies from $1 \cdot 10^{-}$

³ to $1 \cdot 10^{-2}$ M) at constant rotation velocity $\nu = 150 \text{ rev min}^{-1}$ and at various fixed electrode potentials are presented in Figs. 1-3, where $Z'' = (j\omega C_s)^{-1}$ and C_s is the series capacitance of the interface studied [27, 54-62]. Visual analysis of different kind of impedance spectra shows clearly a significant advantage of the Bode plots (Figs. 1c, d, 2c, d and 3c, d) over the impedance complex plane plots. Bode plots show clear impedance data over the total frequency range examined while the impedance complex plane data are very informative for the limited low frequency region ($f < 100 \text{ Hz}$) but higher frequency data at high extent are screened. The $\log(-Z'')$ vs. $\log f$ plots are very helpful for the analysis of reaction characteristics, i.e. to obtain the characteristic relaxation time(s) of low frequency process(es), as well as for CPE analysis of Bi(001) and other solid electrodes [27, 54-61, 64-76]. As can be seen in Figs. 1-3 an almost capacitive-resistive behavior is observed at medium frequency region. For all concentrations studied (Figs. 1d, 2d, 3d) the $\log |Z|$ vs. $\log f$ dependences show an almost resistive response at higher frequencies $f > 1000 \text{ Hz}$. The values of $\log |Z|$, given in Figs. 1d, 2d and 3d are independent of electrode potential at frequency $f > 1 \cdot 10^3 \text{ Hz}$, thus, there is no very quick faradaic processes at the Bi(001)| $\text{HClO}_4 + \text{H}_2\text{O}$ interface. At very high frequency the values of active resistance $R_{\text{el}} = Z(\omega \rightarrow \infty)$ depend nearly linearly on c_{HClO_4} , explained by the increase of the specific conductivity of the electrolyte resistance R_{el} with the rise of c_{HClO_4} .

The data in Figs. 1e, 2e and 3e show that for dilute HClO_4 solutions ($c_{\text{HClO}_4} \leq 1 \cdot 10^{-3} \text{ M}$) at small negative electrode potentials the $\log(-Z'')$ vs. $\log f$ plots have not very well expressed maxima even at very low f and, thus, the values of characteristic relaxation time $\tau_{\text{max}} = (2\pi f_{\text{max}})^{-1}$ (f_{max} is the frequency at the maximum of the $(-Z'' \text{ vs. } Z')$ plots) can not be calculated exactly, indicating the occurring of very slow kinetic process(es) at the Bi(001) surface. The values of total polarization resistance $R_p(\omega \rightarrow 0)$ at the electrode potentials E less negative than -0.75 V can not be determined exactly (Figs. 1a, 2a and 3a) and only at $E \leq -0.80 \text{ V}$ it is possible to calculate the values of $R_p(\omega \rightarrow 0)$, depending on c_{HClO_4} . For solutions with $c_{\text{HClO}_4} \geq 2 \cdot 10^{-3} \text{ M}$, the values of τ_{max} obtained (given in Fig. 4) depend on the electrode potential applied.

According to the data given in Figs. 1-3, the total polarization resistance decreases with increasing the negative electrode potential as well as c_{HClO_4} , (i.e. with the decrease of pH). The values of τ_{max} in Fig. 4, obtained using data in Figs. 1e, 2e and 3e, are in a good agreement with τ_{max} , obtained from impedance complex plane plots (Figs. 1a-3a). τ_{max} is practically independent of c_{HClO_4} at fixed potential if $E \geq -0.65 \text{ V}$, but τ_{max} depends noticeably on E , if $c_{\text{HClO}_4} = \text{const.}$

In the region of frequency from 1 to $3 \cdot 10^3 \text{ Hz}$ there is a noticeable dependence of $\log |Z|$ and phase angle ϕ values on $\log f$, indicating the comparatively slow electrical double-layer formation process. In this region, ϕ noticeably depends on c_{HClO_4} and only very

weakly on E (Figs. 1c, 2c and 3c). The analysis of ϕ vs. $\log f$ plots shows that, in the limited region of frequencies $1 < f < 100\text{Hz}$, the very high negative values of phase angle, practically independent of electrode potential applied, have been observed, characteristic of the nearly ideally flat capacitive electrode, caused by the high values of resistances (R_{ad} and R_{ct}) values in parallel with the double-layer impedance. Only at very low frequency the noticeable increase in absolute values of phase angle has been observed indicating the occurrence of the very slow charge transfer process (step) for HER at Bi(*hkl*). At frequency $f > 100\text{Hz}$, the values of phase angle are nearly independent of electrode potential applied. The influence of $c_{\text{H}_3\text{O}^+}$ on the position of the ϕ vs. $\log f$ plots is noticeable in the region $100\text{Hz} < f < 10^4\text{Hz}$, and with the dilution of HClO_4 solution, ϕ vs. $\log f$ plot is shifted toward lower frequencies being a simple consequence of relaxation between the resistance of electrolyte solution and electrical double-layer impedance of the Bi(001) electrode.

The analysis of the $\log(-Z'')$ vs. $\log f$ plots (Figs. 1e, 2e, 3e) shows that the deviation of the experimental system from the ideally flat surface toward constant phase element behaviour is very small [27, 54-61, 63-70] because the fractional exponent α_{CPE} for CPE with impedance $Z_{\text{CPE}} = Q^{-1}(j\omega)^{-\alpha_{\text{CPE}}}$, calculated from the slope of $\log(-Z'')$ vs. $\log f$ plots, is only somewhat lower than unity ($0.94 < \alpha_{\text{CPE}} < 0.98$), thus characteristic of the ideally flat capacitive interface [47, 54-62, 64-70].

Fitting results of impedance data

The number of experimental points in the impedance spectra has been kept constant if the various ECs have been tested. The good fitting ($\chi^2 < 7 \cdot 10^{-4}$, $SD \leq 2.7 \cdot 10^{-4}$, $\Delta^2 \leq 0.2$) at $c_{\text{HClO}_4} \leq 2 \cdot 10^{-3}\text{M}$ has been established if EC (i.e. model with one adsorbed intermediate species [27, 60], proposed by Armstrong and Henderson [61]), corresponding to the reaction steps given by Eqs. (2a) and (2b), has been applied. The very low SD values, calculated using method described in [63], nearly independent of the electrode potential applied, have been obtained. According to the fitting results the high frequency series resistance at $c_{\text{HClO}_4} = \text{const.}$ is independent of potential applied and thus, the calculated values of R_{el} correspond to the high frequency electrolyte resistance. In the C_{dl} vs. E curves for solutions with $c_{\text{HClO}_4} \leq 2 \cdot 10^{-3}\text{M}$ there are characteristic diffuse layer minima at the diffuse layer minimum potential $E_{\text{min}} = -0.65\text{V}$ (Fig. 6a), being in a good agreement with the zero charge potential $E_{\sigma=0}$ obtained for LiClO_4 solutions [34,35], and therefore the C_{dl} vs. E curves for dilute HClO_4 solutions ($c_{\text{HClO}_4} < 2 \cdot 10^{-3}\text{M}$) can be used for classical Frumkin ψ_1 potential correction analysis [34,34,47-53].

However, according to the detailed analysis in the case of solid electrodes [27, 34-36, 54-61, 64-71], the CPE element should be included into EC and therefore the double-layer capacitance C_{dl} valid for the ideally flat and energetically homogenous surface has

to be replaced with CPE, taking into account the geometrical surface roughness and energetic inhomogeneity of solid surface studied, to receive EC (Fig. 5). According to the data in Figs. 1-3 a very good fit ($\chi^2 < 5 \cdot 10^{-4}$, $\Delta^2 \leq 0.01$) has been observed if the modified Armstrong-Henderson EC has been established (solid lines - calculated impedance spectra using the model in Fig. 5; symbols - the experimental data). The results (Fig. 6 b) show that the Q depends very weakly on the electrolyte concentration and Q has minimal values in dilute HClO_4 solutions near $E_{\min} = -0.65 \text{ V}$, being in a very good agreement with C_{dl} values (Fig. 6a) obtained using Armstrong-Henderson EC. This is not surprising as the values of α_{CPE} at fixed E for dilute HClO_4 solutions are quite high ($\alpha_{\text{CPE}} \geq 0.97$) and depend weakly on c_{HClO_4} if $c_{\text{HClO}_4} \leq 2 \cdot 10^{-3} \text{ M}$. It should be mentioned that α_{CPE} decreases with the rise of c_{HClO_4} (Fig. 6c), contrary to the $\text{Bi(001)|LiClO}_4 + \text{H}_2\text{O}$ system, where α_{CPE} increases with the rise of c_{LiClO_4} [1, 34, 35]. Moreover, differently from LiClO_4 solutions, there is a very small minimum in the α_{CPE} vs. E dependence at $E = -0.65 \text{ V}$. The dependence of α_{CPE} on $c_{\text{HClO}_4} > 4 \cdot 10^{-3} \text{ M}$ indicates the very weak changes in surface energetic inhomogeneity caused by the adsorption of reaction intermediates. However $\alpha_{\text{CPE}} \geq 0.97$ for $1 \cdot 10^{-3} \text{ M HClO}_4$ aqueous solution indicates that the deviation of Bi(001)|HClO_4 interface from the classical conception of ideally flat interface [34, 35, 68-70] is very weak and the influence of replacing CPE with C_{dl} in EC on the values of other fitting parameters is comparatively small. At these conditions, to a first very rough approximation, the model of Brug et al. [64] can be used for calculation of the ideal C_{dl} values (Fig. 6a). This result can be explained by the fact that α_{CPE} for solutions with higher c_{HClO_4} ($\geq 2 \cdot 10^{-3} \text{ M}$) contains additional information concerning the influence of the weakly blocking adsorption of hydrogen on Bi(001) , but not only simply the surface roughness effect [34-36, 56-58]. According to the data (Fig. 7a), the charge transfer resistance decreases noticeably with increasing the negative potential, and R_{ct} is practically independent of c_{HClO_4} at $E_{\min} = -0.65 \text{ V}$, where the values of C_{dl} or Q are minimal [47-50].

The calculated values of current density

$$j_{\text{sum}} = \frac{RT}{nF(R_{\text{ct}} + R_{\text{ad}})} = (2.13 \pm 0.01) \cdot 10^{-6} \text{ A cm}^{-2} \text{ at } E_{\sigma=0} \text{ (} n \text{ is the number of electrons}$$

transferred) are in a good agreement with those obtained from the stationary Tafel measurements ($j_{\text{ct}} = 2 \cdot 10^{-6} \text{ A cm}^{-2}$ for 0.1 M HClO_4) [1]. At $E > E_{\min}$, there is only small decrease of R_{ct} with the rise of c_{HClO_4} caused by less pronounced classical Frumkin ψ_1 potential effect [1, 46-49]. The adsorption resistance R_{ad} (Fig. 7b) depends noticeably on the electrode potential, being maximal near the E_{\min} and the values of R_{ad} have a noticeable decrease with the rise of negative E . The decrease of R_{ad} with c_{HClO_4} is pronounced only in the region of small positive surface charge densities. The adsorption capacitance C_{ad} (Fig. 7c) is nearly independent of E and c_{HClO_4} at $E > -0.7 \text{ V}$. At more negative potentials (C_{ad} noticeably increases) which is more expressed for solutions with

lower pH. In concentrated HClO_4 solutions, C_{ad} is nearly 60 times higher than the values of Q at $E = -0.85$ V (Fig. 7c).

The attempts to use more complicated models like Ershler model (nowadays known as Frumkin-Melik-Gaikazyan-Randles circuit [58]) or the modified Grafov – Damaskin ECs, based on the multi-port impedance model for totally irreversible reaction discussed in detail in [71-73], did not give a better fit for the experimental data and the errors in R_{ad} and C_{ad} are very high. Thus, modified Armstrong-Henderson model (Fig. 5) is the only EC giving a good fit of the $\text{Bi}(001) | \text{HClO}_4 + \text{H}_2\text{O}$ interface data.

The so-called corrected Tafel plots (cTp) have been calculated according to the Eq. (5):

$$\log j + zF\psi_1(2.3RT)^{-1} = \text{const.} + (1 - \alpha)\log c + \alpha nF(2.3RT)^{-1}(E - E_{\sigma=0} - \psi_1) \quad (5)$$

where α is a transfer coefficient, z is charge number of particle, n is the number of electrons consumed [1]. For calculation of the cTp, ψ_1 potential has been taken equal to ψ_0 potential ($\psi_1 \approx \psi_0$), i.e. the reaction center has been taken to locate at the outer Helmholtz plane with the ψ_0 potential. The needful ψ_0 vs. E and surface charge density σ vs. E plots have been calculated using corresponding impedance data obtained for less concentrated HClO_4 solutions $c_{\text{HClO}_4} < 2 \cdot 10^{-3}$ M, where the influence of hydrogen adsorption on the values of C_{dl} or Q is weak. Calculated cTps are nearly linear for more concentrated HClO_4 solutions ($c_{\text{HClO}_4} > 6 \cdot 10^{-3}$ M) and corrected values of current density are nearly independent of c_{HClO_4} at $E - E_{\sigma=0} - \psi_0 < 0$. Thus, the cTps analysis method can be used for $\text{Bi}(001) | \text{HClO}_4$ interface data (Fig. 8) similarly to the systems with constant ionic strength [1, 42, 50]. It was found that the slope of cTp is equal to 0.117 V, giving the value of α equal to 0.51, in a good agreement with the data for $\text{Bi}(hkl) |$ constant ionic strength electrolyte interface [1]. If the corrected Tafel plots can be taken as representative of the kinetic mechanism [39, 41-43, 48-53] then, in a good agreement with the impedance data, the slow primary discharge is the slowest rate determining step. Of course, the same slope value would be observed for slow electrochemical desorption (Heyrovsky) step, i.e. $\text{H}_3\text{O}^+ + \text{MH}_{\text{ad}} + \text{e}^- \rightarrow \text{H}_2 + \text{H}_2\text{O} + \text{M}$ step, but then the surface coverage of $\text{Bi}(001)$ with adsorbed H_{ad} should be very high (and therefore $\theta_{\text{H}_{\text{ads}}} \rightarrow 1$) that is impossible in the case of $\text{Bi}(001)$ [1, 52, 53]. The electroreduction reaction of H_3O^+ cations is mainly limited by the very slow charge transfer step at the $\text{Bi}(001) | \text{HClO}_4 + \text{H}_2\text{O}$ interface.

Conclusions

Electrochemical impedance spectroscopy has been applied for investigation of the hydrogen evolution kinetics at the electrochemically polished $\text{Bi}(001)$ plane. The mixed kinetics reaction mechanism (slow adsorption and charge transfer steps) has been established for cathodic hydrogen evolution at $\text{Bi}(001) | \text{HClO}_4 + \text{H}_2\text{O}$ interface. The charge transfer resistance R_{ct} and adsorption capacitance C_{ad} depend noticeably on the electrode potential applied. The values of exchange current density calculated from the impedance data at zero charge potential are in a good agreement with those obtained

using stationary polarization method. The adsorption resistance R_{ad} value is maximal in the region of zero charge potential. The fractional exponent of the constant phase element CPE ($\alpha_{CPE} \geq 0.94$) only very weakly depends on the HClO_4 concentration and electrode potential, and therefore, the deviation of $\text{Bi}(001)|\text{HClO}_4 + \text{H}_2\text{O}$ interface from the classical conception of ideally flat electrode is weak and CPE coefficient Q is nearly equal to the high frequency electrical double-layer capacitance C_{dl} , if $c_{\text{HClO}_4} \leq 2 \cdot 10^{-3} \text{ M}$. Similarly to the stationary polarization measurements, the electrical double-layer structure, depending strongly on the effective Debye screening length of the electrolyte ions, has a very big influence on the cathodic hydrogen evolution kinetics at the $\text{Bi}(001)$ plane from HClO_4 aqueous solution.

Acknowledgement This work was supported in part by the Estonian Science Foundation under Projects Nos. 6696 and 5803.

References

1. Lust K, Perkson E, Lust E (2000) *Russ J Electrochem* 36:1257
2. Lasia A, Rami A (1990) *J Electroanal Chem* 294:123
3. Clavilier J, Rodes A, El Achi K, Zamarhchari MA (1991) *J Chem Phys* 88:1291
4. Morin S, Dumont H, Conway BE (1996) *J Electroanal Chem* 412:39
5. Barber J, Morin S, Conway BE (1998) *J Electroanal Chem* 446:125
6. Marković NM, Adžić RR, Cahan BD, Yeager EB (1994) *J Electroanal Chem* 377:249
7. Lucas CA, Marković NM (2003) In: Bard AJ and Stratmann M (ed) *Encyclopedia of Electrochem*, vol 2. Wiley VCH, pp 291
8. Bai L, Conway BE (1986) *Electrochim Acta* 32:1013
9. Bai L (1993) *J Electroanal Chem* 355:37
10. Schönfuss D, Müller L (1994) *Electrochim Acta* 39:2097
11. Harrington DA, Conway BE (1987) *Electrochim Acta* 32:1703
12. Bai L, Harrington DA, Conway BE (1987) *Electrochim Acta* 32:1713
13. Breiter MW (1961) In: Yeager E (ed) *Symposium on Electrode Processes*, The Electrochemical Society, Wiley, New York pp 307
14. Durand R (1979) *Electrochim Acta* 24:1095
15. Schuldinek S (1959) *J Electrochem Soc* 106:891
16. Seto K, Ianelli A, Love B, Lipkowski J (1987) *J Electroanal Chem* 226:351
17. Marković NM, Sarkaf ST, Gasteiger HA, Ross PN Jr (1996) *J Chem Soc, Faraday Trans* 92:3719
18. Breiter MW (1962) *J Electrochem Soc* 109:549
19. Losev VV (1981) *Elektrokhimija* 17:733
20. Duncan H, Lasia A (2007) *Electrochim Acta* 52:6195
21. Birry L, Lasia A (2006) *Electrochim Acta* 51:3356
22. Lim C, Pyun S-I (1993) *Electrochim Acta* 38:2695
23. Lim C, Pyun S-I (1994) *Electrochim Acta* 39:363
24. Yoon YG, Pyun S-I (1995) *Electrochim Acta* 40:999
25. Lasia A, Grégoire D (1995) *J Electrochem Soc* 142:3393
26. Chen JS, Diard J-P, Durand R, Montella C (1996) *J Electroanal Chem* 406:1
27. Lasia A (1999) In: Conway BE, Bockris JO'M, White RE (ed) *Modern Aspects of Electrochemistry*, vol 32. Kluwer Academic/Plenum Publishers, New York, pp 143
28. Lasia A (2006) *J Electroanal Chem* 593:159
29. Horvat-Radošević V, Kvastek K (2002) *Electrochim Acta* 48:311
30. Montella C (2001) *J Electroanal Chem* 497:3
31. Montella C (2000) *J Electroanal Chem* 480:150
32. Langkau T, Baltruschat H (1998) *Electrochim Acta* 44:909
33. Arold J, Tamm J (1989) *Elektrokhimija* 25:1417
34. Trasatti S, Lust E (1999) In: White RE, Conway BE and Bockris J O'M (ed) *Modern Aspects of Electrochemistry*, vol 33. Kluwer Academic/Plenum Publishers, New York, London, pp 1
35. Lust E (2002) In: Bard AJ, Stratmann M (ed) *Encyclopedia of Electrochemistry*, vol 1. Wiley, pp 188

36. Brug GJ, Sluyters – Rehbach M, Sluyters JH, Hemelin A (1984) *J Electroanal Chem* 181:245
37. Eberhardt D, Santos E, Schmickler W (1999) *J Electroanal Chem* 461:76
38. Jović VD, Parsons R, Jović BM (1992) *J Electroanal Chem* 339:327
39. Doubova LM, Trasatti S (1999) *J Electroanal Chem* 467:164
40. El-Halim AMAbd, Jüttner K, Lorenz WJ (1980) *J Electroanal Chem* 106:193
41. Trasatti S (1997) In: Gerischer H, Tobias CW (ed) *Advances in Electrochemistry and Electrochemical Engineering*, vol 10. Wiley Interscience, New York, pp 123
42. Trasatti S (1972) *J Electroanal Chem* 39:163
43. Trasatti S (1984) In: McIntyre JDE, Weaver MJ, Yeager EB (ed) *The Chemistry and Physics of Electrocatalysis*, vol 84-12. The Electrochemical Society, Pennington, pp 150
44. Kolb DM (1993) In: Lipkowski J, Ross PN (ed) *Structure of Electrified Interfaces*, VCH, New York, pp 65
45. Hamelin A (1995) In: Gewirth AA, Siegenthaler H (ed) *Nanoscale probes of the solid|liquid interface*, Kluwer, Dordrecht, pp 285
46. Härk E, Lust E (2008) Electroreduction of hexaamminecobalt(III) cations at electrochemically polished Bi(*hkl*) using impedance spectroscopy method (in prep.)
47. Jäger R, Härk E, Möller P, Nerut J, Lust K, Lust E (2004) *J Electroanal Chem* 566:217
48. Frumkin AN (1961) In: Delahay P (ed) *Ads Electrochem Sci Electrochem Eng*, vol 1. Intersci, New York, London, pp 1
49. Frumkin AN (1933) *Phys Chem A* 164:121
50. Petrii OA, Nazmutdinov RR, Bronshtein MD, Tsirlina GA (2007) *Electrochim Acta* 52:3493
51. Gileadi E, Kirowa-Eisner E (2005) *Corros Sci* 47:3068
52. Palm U, Tenno T (1973) *J Electroanal Chem* 42:457
53. Tenno TT, Palm UV (1972) *Elektrokhimiya* 18:1381
54. Orazem ME, Pèbère N, Tribollet B (2006) *J Electrochem Soc* 153:B129
55. Huang VM-W, Vivier V, Pèbère N, Orazem ME, Tribollet B (2007) *J Electrochem Soc* 154:C81
56. Huang VM-W, Vivier V, Frateur I, Orazem ME, Tribollet B (2007) *J Electrochem Soc* 154:C89
57. Huang VM-W, Vivier V, Pèbère N, Orazem ME, Tribollet B (2007) *J Electrochem Soc* 154:C99
58. Thomberg T, Nerut J, Lust E (2006) *J Electroanal Chem* 586:237
59. Macdonald JR (1987) (ed) *Impedance Spectroscopy: Emphasizing Solid Materials and Systems*, Wiley, New York
60. Lasia A (2002) In: Conway BE, White RE (ed) *Modern Aspects of Electrochemistry*, vol 35. Kluwer Academic / Plenum Publishers, New York, pp 1
61. Armstrong RD, Henderson M (1972) *J Electroanal Chem* 39:81
62. Zview for Windows (version 2.7) Fitting Program, Scribner, Southern Pines, NC, USA
63. Zoltowski P (2005) *Solid State Ionics* 176:1979
64. Brug GJ, Van der Eeden ALG, Sluyters-Rehbach M, Sluyters JH (1984) *J Electroanal Chem* 176:275

65. Mulder WH, Sluyters JH (1988) *Electrochim Acta* 33:303
66. Wang JC (1988) *Electrochim Acta* 33:707
67. de Levie R (1989) *J Electroanal Chem* 261:1
68. Zoltowski P (1998) *J Electroanal Chem* 443:149
69. Kerner Z, Pajkossy T (1998) *J Electroanal Chem* 448:139
70. Pajkossy T, Wandlowski Th, Kolb DM (1996) *J Electroanal Chem* 414:209
71. Stoyanov ZB, Grafov BM, Savova-Stoyanova BS, Elkin VV (1991) *Electrochemical Impedance*, Nauka, Moscow
72. Grafov BM, Damaskin BB (1992) *J Electroanal Chem* 329:129
73. Grafov BM, Damaskin BB (1994) *J Electroanal Chem* 366:29
74. Nurk G, Jänes A, Lust K, Lust E (2001) *J Electroanal Chem* 515:17
75. Lust E, Lust K, Jänes A, Väärtnõu M (1997) *Electrochim Acta* 42:771
76. Lust K, Väärtnõu M, Lust E (2002) *J Electroanal Chem* 532:303

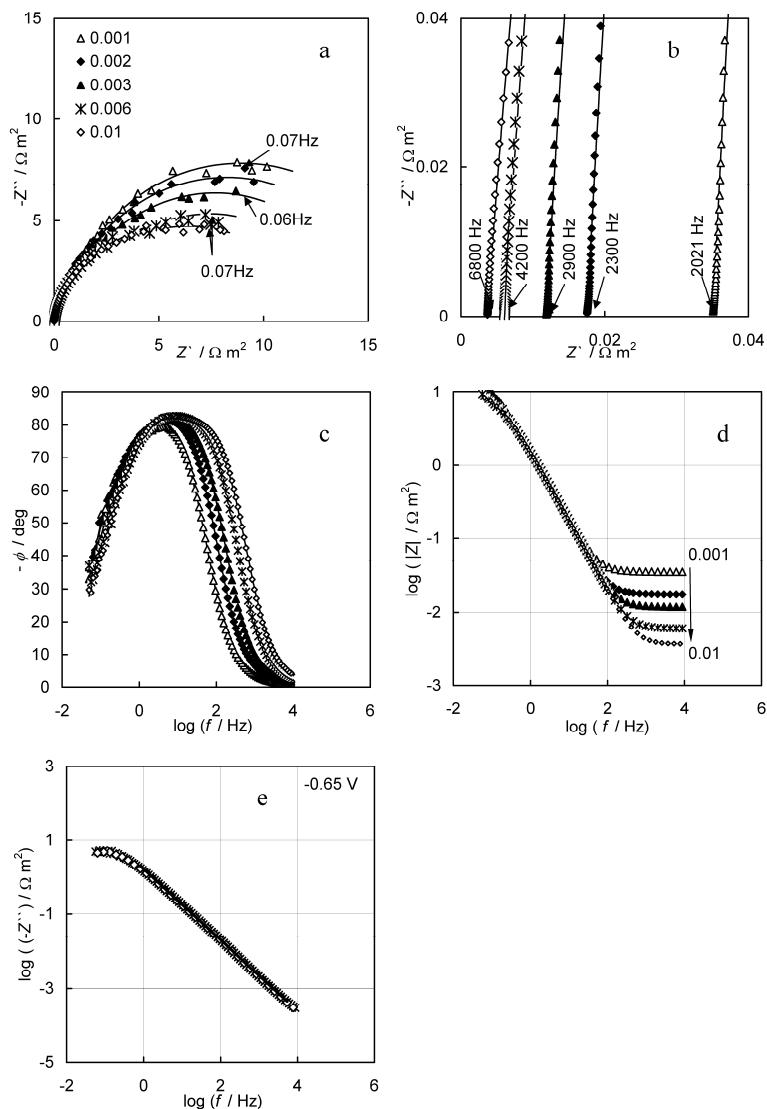


Fig.1. Plots of EIS spectra of EP Bi(001) at $\nu = 150 \text{ rev min}^{-1}$ and at the electrode potential $E = -0.65 \text{ V}$ in the case of HClO_4 aqueous solution with different concentrations (M) (noted in figure), in various coordinates: Impedance complex plane plots ($-Z''$ vs Z') (a), zoom of the high frequency part of plot a (b); phase angle (c), $\log|Z|$ (d) and $\log(-Z'')$ (e) vs. frequency dependences, (symbols – experimental data, solid lines – calculated data according to the circuit in Fig. 5).

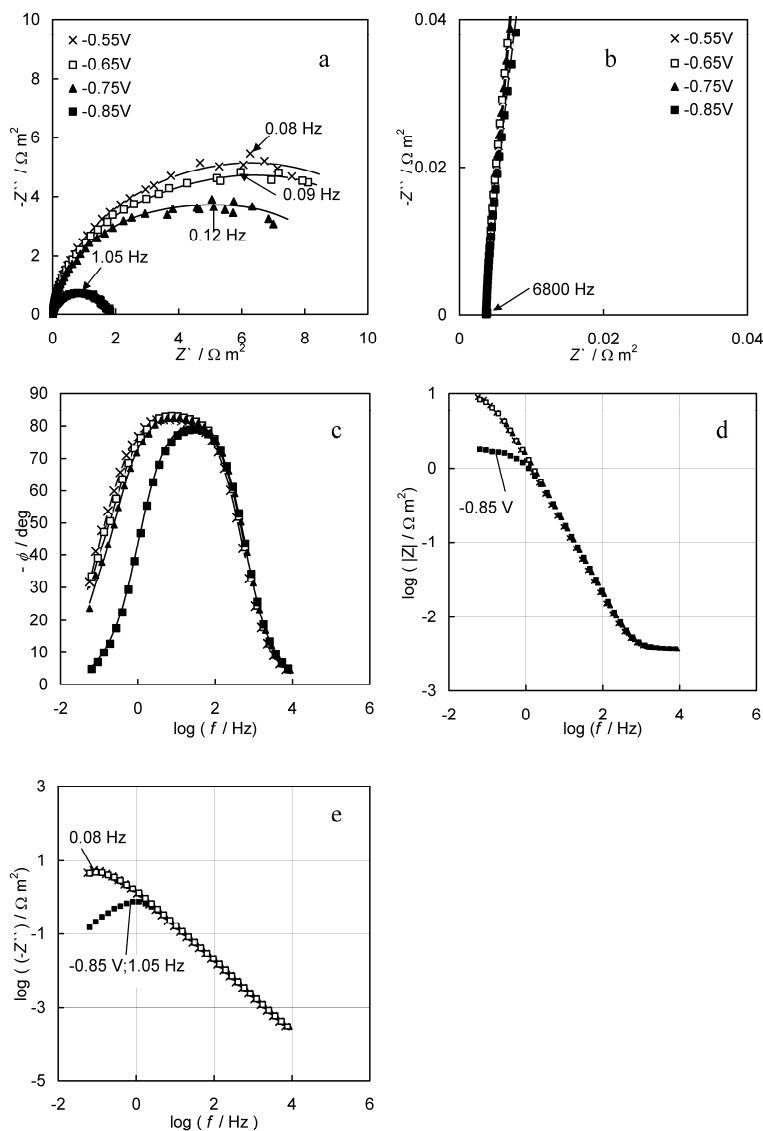


Fig.2. Plots of EIS spectra of EP Bi(001) at $\nu=150 \text{ rev min}^{-1}$ in the 0.01 M HClO_4 aqueous solution at different electrode potentials (V) (noted in figure), in various coordinates: Impedance complex plane plots ($-Z''$ vs. Z') (a); zoom of the high frequency part of plot a (b), phase angle (c), $\log |Z|$ (d) and $\log (-Z'')$ (e) vs. $\log f$ dependences, (symbols – experimental data, solid lines – calculated data according to the circuit in Fig. 5).

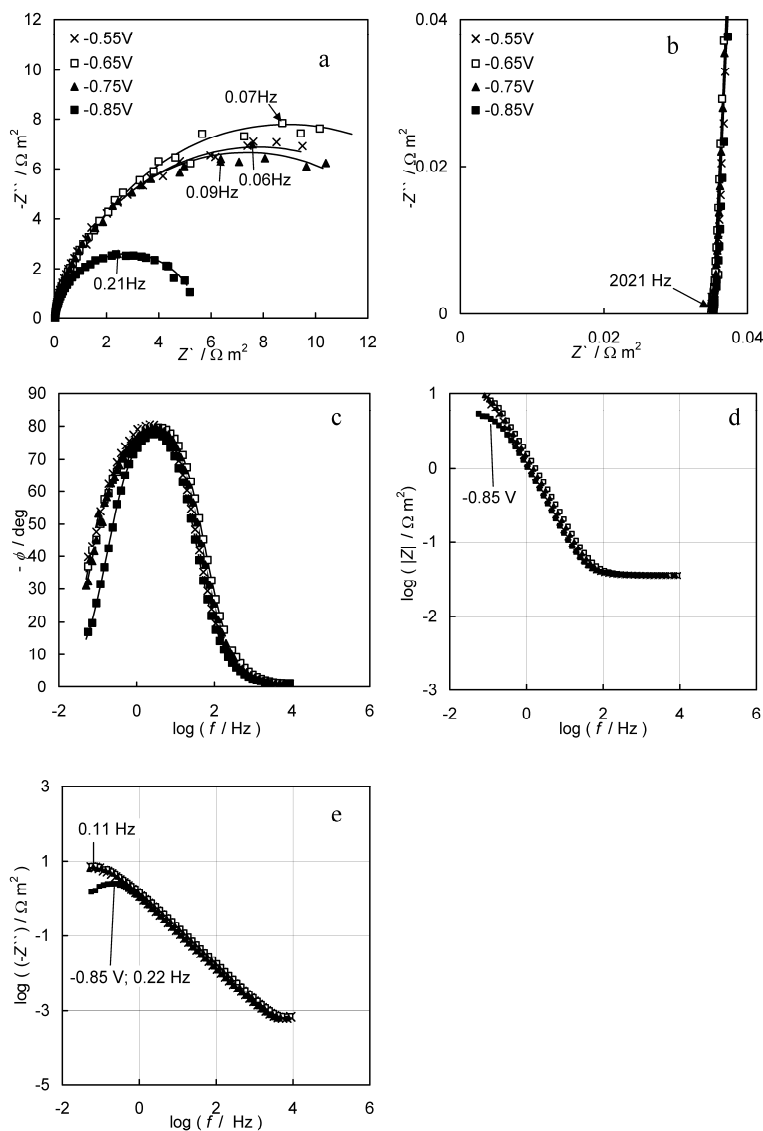


Fig.3. Plots of EIS spectra of EP Bi(001) at $\nu=150 \text{ rev min}^{-1}$ in the 0.001 M HClO₄ aqueous solution at different electrode potentials (V) (noted in figure), in various coordinates: Impedance complex plane plots ($-Z''$ vs. Z') (a); zoom of the high frequency part of plot a (b), phase angle (c), $\log |Z|$ (d) and $\log (-Z'')$ (e) vs. $\log f$ dependences, (symbols – experimental data, solid lines – calculated data according to the circuit in Fig. 5).

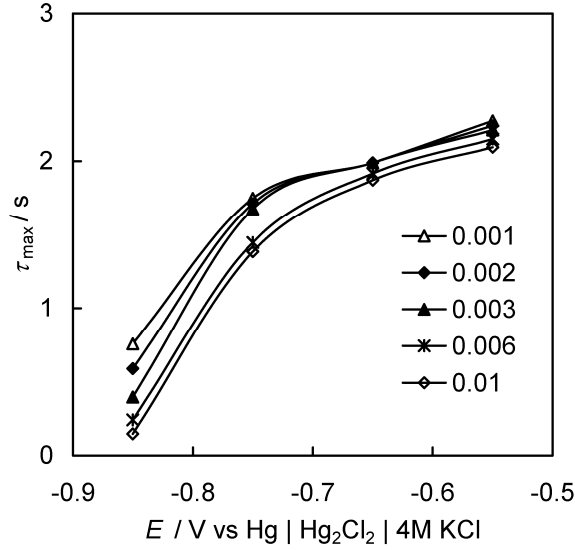


Fig.4. Characteristic relaxation time $\tau_{\max}=(2\pi f_{\max})^{-1}$ vs. electrode potential dependences for cathodic hydrogen evolution at Bi(001) in HClO_4 aqueous solution with concentrations (M), noted in figure.

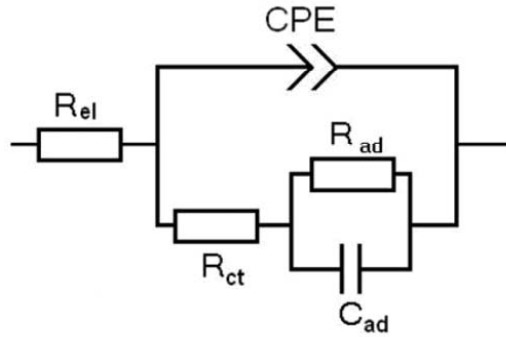


Fig.5. Modified Armstrong-Henderson model [61], where C_{dl} has been replaced by CPE, taking into account the adsorption of one intermediate particle used for fitting the experimental results: (R_{el} – high - frequency solution resistance; CPE – constant phase element; R_{ct} – charge transfer resistance; R_{ad} – adsorption or partial charge transfer resistance; C_{ad} – adsorption capacitance).

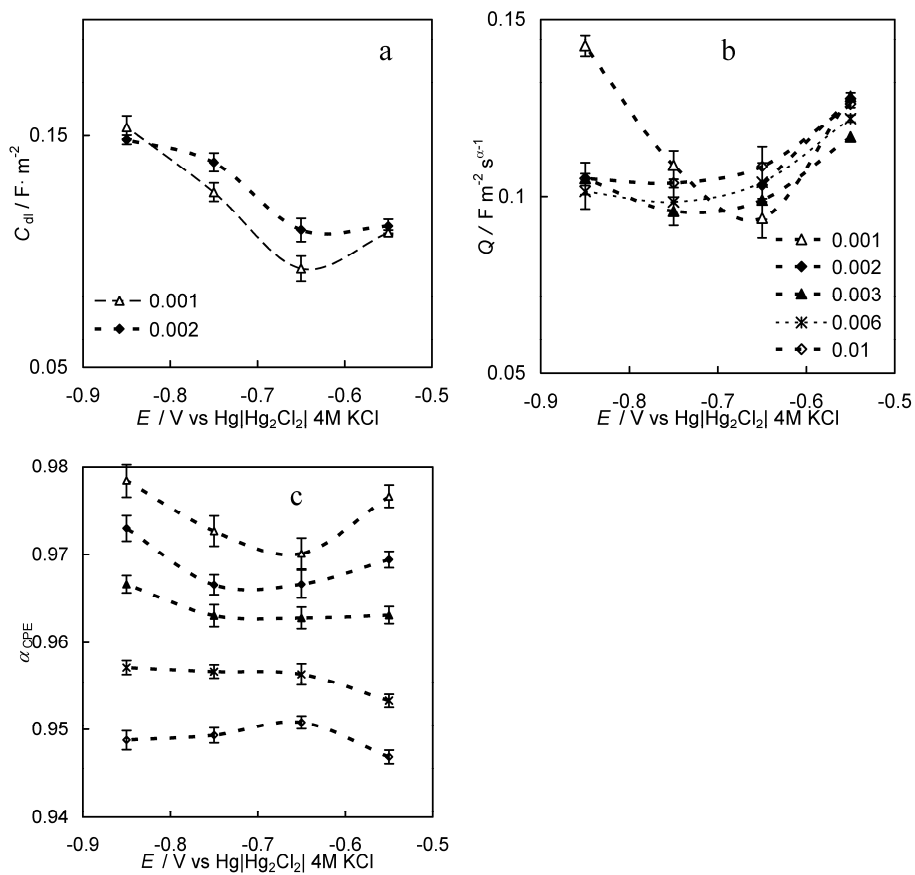


Fig.6. Dependences of C_{dl} (a) (calculated according to the Armstrong-Henderson circuit); CPE coefficient Q (b) and fractional exponent α_{CPE} (c) on the electrode potential (calculated according to the circuit in Fig. 5) for EP Bi(001) in HClO₄ aqueous solution with concentrations (M), noted in figure.

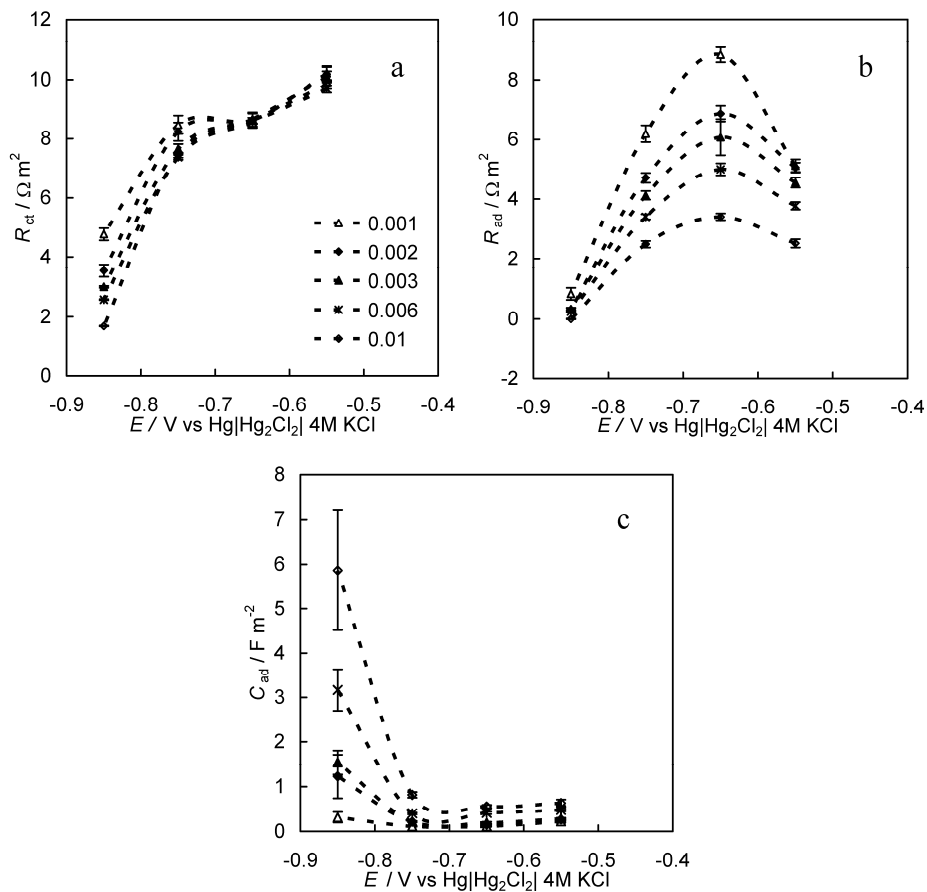


Fig.7. R_{ct} (a); R_{ad} (b) and C_{ad} (c) dependencies on the electrode potential (calculated according to the equivalent circuit in Fig. 5) for EP Bi(001) in HClO₄ aqueous solution with different concentrations (M), noted in figure.

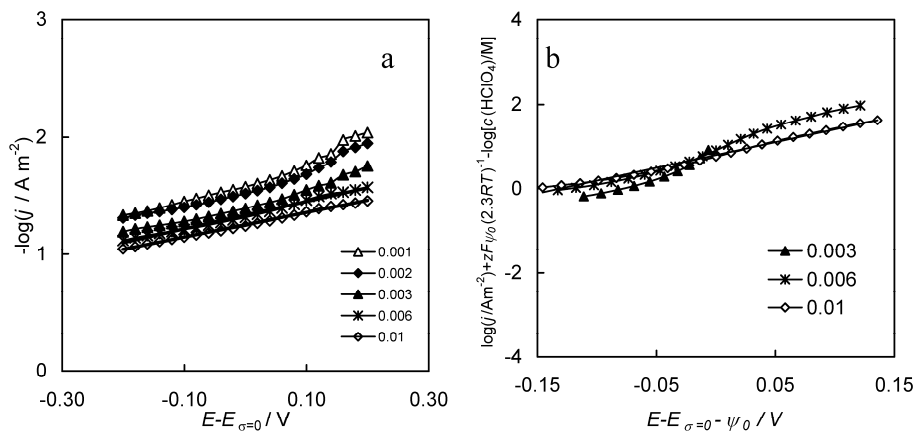


Fig.8. $-\log j$ vs. rational electrode potential ($E - E_{\sigma=0}$) plots (a) and corrected Tafel plots (b) for EP Bi(001) in HClO₄ aqueous solution with concentrations (M), noted in figure.

CURRICULUM VITAE

General data

Given name and surname: Eneli Härk
Date and place of birth: 26.01.1980, Valga
Citizenship: Estonian
Address: Institute of Chemistry
University of Tartu
2 Jakobi St., Tartu 51014, Estonia
e-mail address eneli.hark@ut.ee
Present employment: University of Tartu, Institute of Chemistry, extraordinary researcher (0.5)
University of Tartu, Doctoral School of Material Science and Material Technology, extraordinary researcher (0.08)

Education

2004– ... University of Tartu, *Ph.D.* student (physical and electrochemistry)
2002–2004 University of Tartu, *M. Sc.* in physical and electrochemistry
1998–2002 University of Tartu, *B. Sc.* in chemistry
...–1998 Valga Gymnasium

Professional employment

2007 – ... University of Tartu, Institute of Chemistry, extraordinary researcher (0.5)
2005–2008 University of Tartu, MMTDK, extraordinary researcher (0.1)
2006–2007 University of Tartu, Institute of Physical Chemistry, secretary (0.8)
2001–2006 University of Tartu, Institute of Physical Chemistry, laboratorian

Main scientific publications

1. R.Jäger, E.Härk, P.Möller, K.Lust and E.Lust, The kinetics of electro-reduction of hexaamminecobalt(III) cation on Bi planes in aqueous HClO_4 solutions, *Journal of Electroanalytical Chemistry*, 566 (2004) 217–226.
2. E.Härk, E.Lust, Electroreduction of Hexaamminecobalt(III) Cation on Bi(*hkl*) Electrodes from Weakly Acidified LiClO_4 Solutions. *Journal of the Electrochemical Society*, 153(6) (2006) E104–E110.
3. E.Lust, J.Nerut, E.Härk, R.Jäger, K.Lust, K.Tähnäs, S.Kallip, T.Thomberg, V.Grozovski, Electroreduction of Complex Ions at Bismuth and Cadmium Single Crystal Plane Electrodes. *ESC Transactions*, 1 (17) (2006) 9–17.
4. E.Härk, K.Lust, A.Jänes, E.Lust, Electrochemical impedance study of hydrogen evolution on Bi(001) electrode in the HClO_4 aqueous solutions. *Journal of Solid State Electrochemistry* (JSEL-D-08-00102)
5. E.Härk and E.Lust, Electroreduction of hexaamminecobalt(III) cation at electrochemically polished Bi(*hkl*) using impedance spectroscopy method. (in review)
6. E.Härk, E.Lust, Electroreduction of hexaamminecobalt(III) cations at electrochemically polished Bi single crystal electrodes using impedance spectroscopy method, Abstr. of the 209th Meeting of The Electrochemical Society, USA, Colorado, Denver 2006. (Oral Presentation)
7. E.Härk, E.Lust, Impedance spectroscopy of the cathodic hydrogen evolution reaction at Bi(001), Abstr. of EIS2007 Argles sur Mer 3–8.06.2007 France (Oral Presentation)

ELULOOKIRJELDUS

Ees- ja perekonnanimi: Eneli Härk
Sünniaeg ja koht: 26.01.1980, Valga
Kodakondsus: Eesti
Address: Keemia Instituut, Tartu Ülikool
Jakobi 2, Tartu 51014, Eesti
e-mail: eneli.hark@ut.ee
Praegune töökoht: Tartu Ülikool, Keemia Instituut, erakorraline teadur (0.5)
Tartu Ülikool, Materjaliteaduse ja materjalide tehnoloogia doktorikool, erakorraline teadur (0.08)

Haridus

2004– ...	Tartu Ülikool, Loodus- ja tehnoloogiateaduskond, doktorant füüsikalise ja elektrokeemia erialal
2002–2004	Tartu Ülikool, Füüsika-keemiateaduskond, M. Sc. füüsikalise ja elektrokeemia erialal
1998 – 2002	Tartu Ülikool, Füüsika-keemiateaduskond, B. Sc. Keemia erialal
...–1998	Valga Gümnaasium

Teenistuskäik

2007 – ...	Tartu Ülikool, Keemia Instituut, erakorraline teadur (0.5)
2005 – 2008	Tartu Ülikool, MMTDK, erakorraline teadur
2006 – 2007	Tartu Ülikool, Füüsikalise keemia Instituut, vastutav sekretär (0.8)
2001 – 2006	Tartu Ülikool, Füüsikalise keemia Instituut, laborant

Tähtsamad teaduspublikatsioonid

1. R.Jäger, E.Härk, P.Möller, K.Lust and E.Lust, The kinetics of electroreduction of hexaamminecobalt(III) cation on Bi planes in aqueous HClO_4 solutions, *Journal of Electroanalytical Chemistry*, 566 (2004) 217–226.
2. E.Härk, E.Lust, Electroreduction of Hexaamminecobalt(III) Cation on Bi(*hkl*) Electrodes from Weakly Acidified LiClO_4 Solutions. *Journal of the Electrochemical Society*, 153(6) (2006) E104–E110.
3. E.Lust, J.Nerut, E.Härk, R.Jäger, K.Lust, K.Tähnas, S.Kallip, T.Thomberg, V.Grozovski, Electroreduction of Complex Ions at Bismuth and Cadmium Single Crystal Plane Electrodes. *ESC Transactions*, 1 (17) (2006) 9–17.
4. E.Härk, K.Lust, A.Jänes, E.Lust, Electrochemical impedance study of hydrogen evolution on Bi(001) electrode in the HClO_4 aqueous solutions. *Journal of Solid State Electrochemistry (JSEL-D-08-00102)*
5. E.Härk and E.Lust, Electroreduction of hexaamminecobalt(III) cation at electrochemically polished Bi(*hkl*) using impedance spectroscopy method. (in review)
6. E.Härk, E.Lust, Electroreduction of hexaamminecobalt(III) cations at electrochemically polished Bi single crystal electrodes using impedance spectroscopy method, Abstr. of the 209th Meeting of The Electrochemical Society, USA, Colorado, Denver 2006. (Suuline ettekanne)
7. E.Härk, E.Lust, Impedance spectroscopy of the cathodic hydrogen evolution reaction at Bi(001), Abstr. of EIS2007 Argles sur Mer 3–8.06.2007 France (Suuline ettekanne)

DISSERTATIONES CHIMICAE UNIVERSITATIS TARTUENSIS

1. **Toomas Tamm.** Quantum-chemical simulation of solvent effects. Tartu, 1993, 110 p.
2. **Peeter Burk.** Theoretical study of gas-phase acid-base equilibria. Tartu, 1994, 96 p.
3. **Victor Lobanov.** Quantitative structure-property relationships in large descriptor spaces. Tartu, 1995, 135 p.
4. **Vahur Mäemets.** The ^{17}O and ^1H nuclear magnetic resonance study of H_2O in individual solvents and its charged clusters in aqueous solutions of electrolytes. Tartu, 1997, 140 p.
5. **Andrus Metsala.** Microcanonical rate constant in nonequilibrium distribution of vibrational energy and in restricted intramolecular vibrational energy redistribution on the basis of Slater's theory of unimolecular reactions. Tartu, 1997, 150 p.
6. **Uko Maran.** Quantum-mechanical study of potential energy surfaces in different environments. Tartu, 1997, 137 p.
7. **Alar Jänes.** Adsorption of organic compounds on antimony, bismuth and cadmium electrodes. Tartu, 1998, 219 p.
8. **Kaido Tammeveski.** Oxygen electroreduction on thin platinum films and the electrochemical detection of superoxide anion. Tartu, 1998, 139 p.
9. **Ivo Leito.** Studies of Brønsted acid-base equilibria in water and non-aqueous media. Tartu, 1998, 101 p.
10. **Jaak Leis.** Conformational dynamics and equilibria in amides. Tartu, 1998, 131 p.
11. **Toonika Rinken.** The modelling of amperometric biosensors based on oxidoreductases. Tartu, 2000, 108 p.
12. **Dmitri Panov.** Partially solvated Grignard reagents. Tartu, 2000, 64 p.
13. **Kaja Orupõld.** Treatment and analysis of phenolic wastewater with microorganisms. Tartu, 2000, 123 p.
14. **Jüri Ivask.** Ion Chromatographic determination of major anions and cations in polar ice core. Tartu, 2000, 85 p.
15. **Lauri Vares.** Stereoselective Synthesis of Tetrahydrofuran and Tetrahydropyran Derivatives by Use of Asymmetric Horner-Wadsworth-Emmons and Ring Closure Reactions. Tartu, 2000, 184 p.
16. **Martin Lepiku.** Kinetic aspects of dopamine D_2 receptor interactions with specific ligands. Tartu, 2000, 81 p.
17. **Katrin Sak.** Some aspects of ligand specificity of P2Y receptors. Tartu, 2000, 106 p.
18. **Vello Pällin.** The role of solvation in the formation of iotsitch complexes. Tartu, 2001, 95 p.

19. **Katrin Kollist.** Interactions between polycyclic aromatic compounds and humic substances. Tartu, 2001, 93 p.
20. **Ivar Koppel.** Quantum chemical study of acidity of strong and superstrong Brønsted acids. Tartu, 2001, 104 p.
21. **Viljar Pihl.** The study of the substituent and solvent effects on the acidity of OH and CH acids. Tartu, 2001, 132 p.
22. **Natalia Palm.** Specification of the minimum, sufficient and significant set of descriptors for general description of solvent effects. Tartu, 2001, 134 p.
23. **Sulev Sild.** QSPR/QSAR approaches for complex molecular systems. Tartu, 2001, 134 p.
24. **Ruslan Petrukhin.** Industrial applications of the quantitative structure-property relationships. Tartu, 2001, 162 p.
25. **Boris V. Rogovoy.** Synthesis of (benzotriazolyl)carboximidamides and their application in relations with *N*- and *S*-nucleophiles. Tartu, 2002, 84 p.
26. **Koit Herodes.** Solvent effects on UV-vis absorption spectra of some solvatochromic substances in binary solvent mixtures: the preferential solvation model. Tartu, 2002, 102 p.
27. **Anti Perkson.** Synthesis and characterisation of nanostructured carbon. Tartu, 2002, 152 p.
28. **Ivari Kaljurand.** Self-consistent acidity scales of neutral and cationic Brønsted acids in acetonitrile and tetrahydrofuran. Tartu, 2003, 108 p.
29. **Karmen Lust.** Adsorption of anions on bismuth single crystal electrodes. Tartu, 2003, 128 p.
30. **Mare Piirsalu.** Substituent, temperature and solvent effects on the alkaline hydrolysis of substituted phenyl and alkyl esters of benzoic acid. Tartu, 2003, 156 p.
31. **Meeri Sassian.** Reactions of partially solvated Grignard reagents. Tartu, 2003, 78 p.
32. **Tarmo Tamm.** Quantum chemical modelling of polypyrrole. Tartu, 2003. 100 p.
33. **Erik Teinemaa.** The environmental fate of the particulate matter and organic pollutants from an oil shale power plant. Tartu, 2003. 102 p.
34. **Jaana Tammiku-Taul.** Quantum chemical study of the properties of Grignard reagents. Tartu, 2003. 120 p.
35. **Andre Lomaka.** Biomedical applications of predictive computational chemistry. Tartu, 2003. 132 p.
36. **Kostyantyn Kirichenko.** Benzotriazole — Mediated Carbon–Carbon Bond Formation. Tartu, 2003. 132 p.
37. **Gunnar Nurk.** Adsorption kinetics of some organic compounds on bismuth single crystal electrodes. Tartu, 2003, 170 p.
38. **Mati Arulepp.** Electrochemical characteristics of porous carbon materials and electrical double layer capacitors. Tartu, 2003, 196 p.

39. **Dan Cornel Fara.** QSPR modeling of complexation and distribution of organic compounds. Tartu, 2004, 126 p.
40. **Riina Mahlapuu.** Signalling of galanin and amyloid precursor protein through adenylate cyclase. Tartu, 2004, 124 p.
41. **Mihkel Kerikmäe.** Some luminescent materials for dosimetric applications and physical research. Tartu, 2004, 143 p.
42. **Jaanus Kruusma.** Determination of some important trace metal ions in human blood. Tartu, 2004, 115 p.
43. **Urmas Johanson.** Investigations of the electrochemical properties of polypyrrole modified electrodes. Tartu, 2004, 91 p.
44. **Kaido Sillar.** Computational study of the acid sites in zeolite ZSM-5. Tartu, 2004, 80 p.
45. **Aldo Oras.** Kinetic aspects of dATP α S interaction with P2Y₁ receptor. Tartu, 2004, 75 p.
46. **Erik Mölder.** Measurement of the oxygen mass transfer through the air-water interface. Tartu, 2005, 73 p.
47. **Thomas Thomberg.** The kinetics of electroreduction of peroxodisulfate anion on cadmium (0001) single crystal electrode. Tartu, 2005, 95 p.
48. **Olavi Loog.** Aspects of condensations of carbonyl compounds and their imine analogues. Tartu, 2005, 83 p.
49. **Siim Salmar.** Effect of ultrasound on ester hydrolysis in aqueous ethanol. Tartu, 2006, 73 p.
50. **Ain Uustare.** Modulation of signal transduction of heptahelical receptors by other receptors and G proteins. Tartu, 2006, 121 p.
51. **Sergei Yurchenko.** Determination of some carcinogenic contaminants in food. Tartu, 2006, 143 p.
52. **Kaido Tamm.** QSPR modeling of some properties of organic compounds. Tartu, 2006, 67 p.
53. **Olga Tšubrik.** New methods in the synthesis of multisubstituted hydrazines. Tartu. 2006, 183 p.
54. **Lilli Sooväli.** Spectrophotometric measurements and their uncertainty in chemical analysis and dissociation constant measurements. Tartu, 2006, 125 p.
55. **Eve Koort.** Uncertainty estimation of potentiometrically measured pH and pK_a values. Tartu, 2006, 139 p.
56. **Sergei Kopanchuk.** Regulation of ligand binding to melanocortin receptor subtypes. Tartu, 2006, 119 p.
57. **Silvar Kallip.** Surface structure of some bismuth and antimony single crystal electrodes. Tartu, 2006, 107 p.
58. **Kristjan Saal.** Surface silanization and its application in biomolecule coupling. Tartu, 2006, 77 p.
59. **Tanel Tätte.** High viscosity Sn(OBu)₄ oligomeric concentrates and their applications in technology. Tartu, 2006, 91 p.

60. **Dimitar Atanasov Dobchev.** Robust QSAR methods for the prediction of properties from molecular structure. Tartu, 2006, 118 p.
61. **Hannes Hagu.** Impact of ultrasound on hydrophobic interactions in solutions. Tartu, 2007, 81 p.
62. **Rutha Jäger.** Electroreduction of peroxodisulfate anion on bismuth electrodes. Tartu, 2007, 142 p.
63. **Kaido Viht.** Immobilizable bisubstrate-analogue inhibitors of basophilic protein kinases: development and application in biosensors. Tartu, 2007, 88 p.
64. **Eva-Ingrid Rõõm.** Acid-base equilibria in nonpolar media. Tartu, 2007, 156 p.
65. **Sven Tamp.** DFT study of the cesium cation containing complexes relevant to the cesium cation binding by the humic acids. Tartu, 2007, 102 p.
66. **Jaak Nerut.** Electroreduction of hexacyanoferrate(III) anion on Cadmium (0001) single crystal electrode. Tartu, 2007, 180 p.
67. **Lauri Jalukse.** Measurement uncertainty estimation in amperometric dissolved oxygen concentration measurement. Tartu, 2007, 112 p.
68. **Aime Lust.** Charge state of dopants and ordered clusters formation in $\text{CaF}_2\text{:Mn}$ and $\text{CaF}_2\text{:Eu}$ luminophors. Tartu, 2007, 100 p.
69. **Iiris Kahn.** Quantitative Structure-Activity Relationships of environmentally relevant properties. Tartu, 2007, 98 p.
70. **Mari Reinik.** Nitrates, nitrites, N-nitrosamines and polycyclic aromatic hydrocarbons in food: analytical methods, occurrence and dietary intake. Tartu, 2007, 172 p.
71. **Heili Kasuk.** Thermodynamic parameters and adsorption kinetics of organic compounds forming the compact adsorption layer at Bi single crystal electrodes. Tartu, 2007, 212 p.
72. **Erki Enkvist.** Synthesis of adenosine-peptide conjugates for biological applications. Tartu, 2007, 114 p.
73. **Svetoslav Hristov Slavov.** Biomedical applications of the QSAR approach. Tartu, 2007, 146 p.